Mechanics and Thermal Modeling of Micro Milling

by

Ali MAMEDOV

A Thesis Submitted to the

Graduate School of Engineering

in Partial Fulfillment of the Requirements for

the Degree of

Doctor of Philosophy

in

Mechanical Engineering

Koc University

November 2015

Koc University

Graduate School of Sciences and Engineering

This is to certify that I have examined this copy of a doctoral thesis by

Ali MAMEDOV

and have found that it is complete and satisfactory in all respects,

and that any and all revisions required by the final

examining committee have been made.

Committee Members:

Ismail Lazoglu, Ph. D. (Advisor)

Erhan Budak, Ph. D.

Demircan Canadinç, Ph. D.

Mustafa Bakkal, Ph. D

Ugur Unal, Ph. D.

Date: 26.11.2015

ABSTRACT

Micro milling is widely used in high-tech industries such as biomedical, aerospace, optics, electronics and die-mold with the increasing demand for precisely manufactured miniature parts. In today's competitive industrial world, the manufacturing of high quality miniature parts having complex free form geometry with very tight tolerances is required. Therefore, surface and subsurface integrities, accuracy and repeatability of the micro machining process are critical.

The main aim of this research thesis is to shed light on the mechanics and thermal aspects of micro milling in order to increase the efficiency and effectiveness of the process in industrial applications by understanding the micro milling physics. The contribution of this research is in the investigation of uncut chip thickness models and developing a cutting force model for micro milling. In this thesis, it is shown that based on the developed cutting force model, the cycle time of the process can be improved by scheduling the feedrate. Understanding and modeling the micro milling mechanics also helps to predict the micro tool deflection. Thermal modelling also allows predicting the temperature fields and machining induced micro thin part distortions.

There are different chip thickness models derived from various kinematic analyzes for the micro milling in the literature. The most accurate chip thickness model for micro milling is selected by examining their direct effect on predictions of cutting forces.

Using selected uncut chip thickness model and mechanistic cutting force coefficients a novel cutting force model is developed considering cutting forces formed due to shearing and ploughing dominant regimes. The geometry of the cutting flute is precisely modeled by scanning the tool using a laser sensor for determining the helix angle and using White Light Interferometer for determining edge radius. In order to validate the force model, the set of cutting experiments under different cutting conditions is performed.

A new mathematical model for estimation of tool deflection in micro milling process using the FEM method is proposed. The tool is considered as a cantilever beam supported in the tool holder. The Timoshenko element beam is used for FEM analysis of the tool under distributed cutting force load. Specially designed setup with two laser displacement sensors is attached to the spindle of the machine to monitor the instantaneous tool deflection and to validate the mathematical model of tool deflection.

In order to increase the productivity by decreasing the machining cycle time, an offline force based feedrate scheduling algorithm is proposed. This algorithm is tested on both flat and ball end mill for complex freeform geometries. Using the proposed model, the feedrate can be defined offline for each cutter location (CL) point accordingly.

Prediction of the workpiece and tool temperature fields in micro milling of Titanium is important, due to the fact that not only the temperature in machining affects the tool wear, but also the temperature fields have direct influence on the residual stresses, the 3D distortions, dimensional and geometrical accuracy of micro parts. The cutting temperatures are predicted by new hybrid finite element model. Temperature simulations are validated by the thermocouple measurements in micro milling of Ti-6Al-4V.

Finally, modeling micro milling induced distortions during thin wall machining is thoroughly investigated. A new strategy is proposed to estimate deflection of the thin wall. The novelty of the proposed strategy lies in combining thermal and mechanical effects during distortion modeling. The presented approach is validated experimentally through micro milling cutting experiments and White Light Interferometer measurements.

ÖZET

Mikro frezeleme hassas üretilmiş minyatür parçalara artan taleple birlikte biyomedikal, havacılık, optik, elektronik ve mikro kalıplar gibi ileri teknoloji endüstrilerinde yaygın olarak kullanılmaktadır. Bugünkü rekabetçi sanayi dünyasında, karmaşık geometriye sahip yüksek kaliteli mikro parçaların istenilen toleranslarda üretilmesini gerektirmektedir. Bu yüzden mikro frezeleme işleminin doğruluğu ve tekrarlanabilirliği son derece önemlidir.

Bu tezin temel amacı mikro frezeleme işleminin fiziğini anlayarak endüstriyel uygulamalarda sürecin verimliliğini ve etkinliğini arttırmak amacıyla süreç mekaniğini modellemek, ısı modellemesini incelemek ve süreç en iyileştirmesini gerçekleştirmektir. Gerçekleştirilen araştırmanın esas katkısı kinematik analizde kullanılacak talaş kalınlık modellerinin incelenmesi ve mikro frezeleme için yeni bir kesme kuvveti modelinin geliştirilmesidir. Geliştirilmiş kesme kuvveti modeli kullanılarak ilerleme hızına dayalı süreç en iyileştirilmesi, takım deformasyonu, kesme sıcaklıkları ve iş parçası çarpılmaları modellemesi yapılmıştır.

Literatürde çeşitli kinematik analizlerden türetilmiş mikro frezeleme için talaş kalınlığı modelleri mevcuttur. Geliştirilmiş modeller arasında mikro frezelemeye en uygun olanı kuvvet modellemesi üzerindeki etkisi doğrudan incelenerek seçilmiştir.

Seçilen talaş kalınlığı modeli ve mekanistik kesme katsayıları kullanılarak, kesme ve kazımadan doğan kuvvetleri dikkate alan yeni kuvvet modeli geliştirilmiştir. Helis açısını ölçmek için lazer ve kesici ağız yarıçapını ölçmek için Beyaz Işık İnterferometresi kullanılarak kesme ağzı geometrisi detaylı modellenmiştir. Geliştirilen kuvvet modelini doğrulamak için farklı kesme koşullarında kesme deneyleri gerçekleştirilmiştir.

FEM yöntemi kullanılarak takım deformasyonunu ölçmek için yeni matematiksel model geliştirilmiştir. Takım, tutucuda sabitlenen kiriş olarak kabul edilmiş ve yayılı yük altında takımın FEM analizi için Timoşenko çubuk teorisi kullanılmıştır. Kesme sırasında takım deformasyonunu ölçmek ve geliştirilen matematiksel modeli doğrulamak için iki lazerli özel düzenek tezgâh ana miline bağlanmıştır.

Süreç verimliliğini artırmak ve işleme zamanını azaltmak için kesme kuvvet esaslı ilerleme hızı zamanlama algoritması geliştirilmiştir. Bu algoritma, basit ve karmaşık yüzeylerde hem düz hem de küresel uçlu frezeleme takımlarıyla test edilmiştir. Önerilen model kullanılarak, her kesme noktası için ilerleme hızı çevrim dışı olarak hesaplanabilmektedir.

Takım aşınmasını, artık gerilmelerin oluşumunu, üç boyutlu iş parçası çarpılmalarını, geometrik ve ölçü hassasiyetlerini doğrudan etkiledikleri için mikro frezeleme esnasında takım ve iş parçası sıcaklıkların modellenmesi önemlidir. İşleme esnasında oluşan kesme sıcaklıkları yeni hibrid sonlu elemanlar modeli ile öngörülmektedir. Sıcaklık simülasyonları Ti-6Al-4V iş parçasının mikro frezelemesi esnasında termokupl ölçümlerle doğrulanmıştır.

Son olarak, mikro frezeleme esnasında oluşan ince duvar çarpılmaları incelenmiştir. İnce duvar çarpılmalarını modellemek için yeni strateji geliştirilmiştir. Önerilen stratejinin yeniliği çarpılma modellemesi esnasında ısıl ve mekanik yüklerin etkilerini birleştirmesidir. Geliştirilen model mikro frezeleme deneyleri ve Beyaz Işın İnterferometresi ölçümleri ile doğrulanmıştır.

ACKNOWLEDGEMENTS

I would like to thank my supervisor Prof. Dr. İsmail Lazoğlu for his guidance and support. This dissertation would not have been possible without his valuable advices, feedback, encouragement, moral and financial supports.

I would like to express sincere gratitude to my parents Mamedov Ramis, Mamedova Nailya and my sister Mamedova Sabina for their love and support, that always kept me making progress during my Ph.D.

Special thanks to my friend and colleague Dr. Seyed Ehsan Layegh Khavidaki and our technician Muzaffer Bütün for their willingness to assist me throughout my studies in MARC laboratory.

I also want to thank all my colleagues in MARC laboratory for being friendly and always willing to help. Especially, I appreciate Suat Cömert, Bircan Buğdaycı, İsmail Enes Yiğit, Adnan Hassan, Armin Bijanzad, Çağlar Öztürk and Başar Aka. I have been enjoying studying and working with them.

I want to acknowlegde the Scientific and Technological Research Council of Turkey (TUBITAK Grant No. MAG110M697) for their financial support. I also would like to thank Koc University Surface Science and Technology Center for providing their facilities. Sandvik Coromant, Toolex and Nikken companies are also acknowledged for their kind supports for the research.

TABLE OF CONTENTS

LIST OF TABLES

LIST OF FIGURES

NOMENCLATURE

A	Cross section area of Timoshenko beam element
A_p	Ploughing area
a	Depth of cut
dz	Differential axial depth of cut
dA_c	Differential chip load
dF_{xs}, dF_{ys}, dF_{zs}	Shearing components of differential forces in X, Y and Z directions
dF_{xp}, dF_{yp}, dF_{zp}	Ploughing components of differential forces in X, Y and Z directions
E	Modulus of elasticity
$[ETM]$	Element Transformation Matrix
$\bar{F}$	Average cutting force
F_{eq}	Equivalent force
$F_{1,i}$	Estimated resultant force at point I for feed f_1
F_{lim}	Threshold value of resultant cutting force
F_R	Planar resultant cutting force
F_s	Shear force on the shear plane
F_u	Friction force on the rake face
F_x, F_y, F_z	Cutting Force in X, Y and Z directions
F_r, F_t, F_a	Cutting Force in radial, tangential and axial directions
f	Feedrate
G	Shear modulus
h	Undeformed chip thickness
h_e	Height of elastically recovered material
h_{min}	Minimum uncut chip thickness
h_t	The convective heat transfer coefficient for rotating cutting tool

h_w	Convective heat transfer coefficient for workpiece
I	Moment of inertia
$[K]$	Stiffness matrix
K_e	Element stiffness matrix
K_{rc}, K_{tc}, K_{ac}	Cutting Force coefficients in radial, tangential and zenith directions
K_{re}, K_{te}, K_{ae}	Edge Force coefficients in radial, tangential and zenith directions
K_{rp}, K_{tp}, K_{ap}	Ploughing coefficients in radial, tangential and zenith directions
K_s	Correction factor
L	Element length
l_c	Chip contact length
l_{sh}	Shear plane length
MSE	Mean square error
N	Number of cutting flutes
n	Number of elements
nel	Number of elements
$ndof$	Number of degrees of freedom
P_f	Friction power
P_s	Shearing power
R	Tool radius
R_i	Rotation radius of arbitrary element of i^{th} cutting flute
R^2	Coefficient of determination
$RMSD$	Root mean square deviation
r_e	Edge radius of the tool
SS_R	Regression sum of squares
SS_T	Total sum of squares
t_x	Feed per tooth

U1, U2, U4, U5	Translation components of Timoshenko beam element
U3, U6	Rotational components of Timoshenko beam element
V	Cutting velocity
V_c	Chip velocity
V_s	Shear velocity
Y	Vector of true values
$\hat{Y}$	Vector of estimates
$\bar{Y}$	Mean value of true values
α	Rake angle
α_n	Normal rake angle
β	Helix angle
β_a	Friction angle
β_n	Normal friction angle
λ	Run-out angle
ϕ_c	Shear angle
ϕ_n	Normal shear angle
θ	Immersion Angle
θ_{ex}	Engagement exit angle
θ_i	Angular position of the reference flute
θ_{st}	Engagement entrance angle
ρ	Run-out amplitude
τ_s	Average shear flow stress
ν	Poisson ratio
ψ_e	Clearance angle

Chapter 1
INTRODUCTION

1.1 Overview

Micro milling is widely used in high-tech industries such as biomedical, aerospace, optics, electronics and die-mold with the increasing demand for precisely manufactured miniature parts. These industries have a high demand for tight manufacturing tolerances, surface quality and usually have complex geometries requiring micron level accuracy.

The demand for smaller and durable components with high number of functions has imposed strong requirements on manufacturing processes. Mainly micro manufacturing processes can be categorized in two groups: surface micro manufacturing (2D components) and mechanical micro manufacturing (3D components). The surface micro manufacturing consists of additive technique, lithography technique, laser, ultrasonic, ion beam and micro electro discharge machining methods. Despite geometrical and material restrictions it is possible to manufacture relatively complex geometries, but this process is expensive, tedious and requires a lot of engineering job like the design of the substrate masks. Due to this reason surface micro manufacturing is assumed to be costly, time consuming and not an efficient micro fabrication method, which is generally used for manufacturing of simple 2D components.

Compared to surface manufacturing techniques, mechanical micro manufacturing, well known as micro cutting, has the advantage of manufacturing 3D complex parts with free form geometry and at the same time satisfy required dimensional tolerances. With recent advances in manufacturing field production of the ultra-precise micro components for engineering products has become possible. At the same time, ultra-precise manufacturing requires understanding of the fundamentals of the micro cutting process like chip formation, kinematics, dynamics, thermal aspects and surface integrity. Due to this reason academic and industrial researchers work on these fundamentals to understand how they differ from macro scale machining. In comparison to macro milling, micro cutting tools are typically smaller in diameter, which varies from 10 μm to 1 mm. This requires accurate selection of the cutting parameters like cutting speed, depth of cut and feedrate in order to prevent premature tool wear and failure. Micro milling can be implemented in a large spectrum of materials. However, due to their superior properties such as high strength to weight ratios and low thermal conductivities, biocompatibilities, etc., Titanium alloys are very commonly used advanced engineering materials. Most of the small-sized freeform Titanium parts are machined using micro ball-end milling before polishing and other surface treatments. Some case studies manufactured from different engineering material like Ti-6Al-4V and Al-7050 are shown below in Figure 1-1.

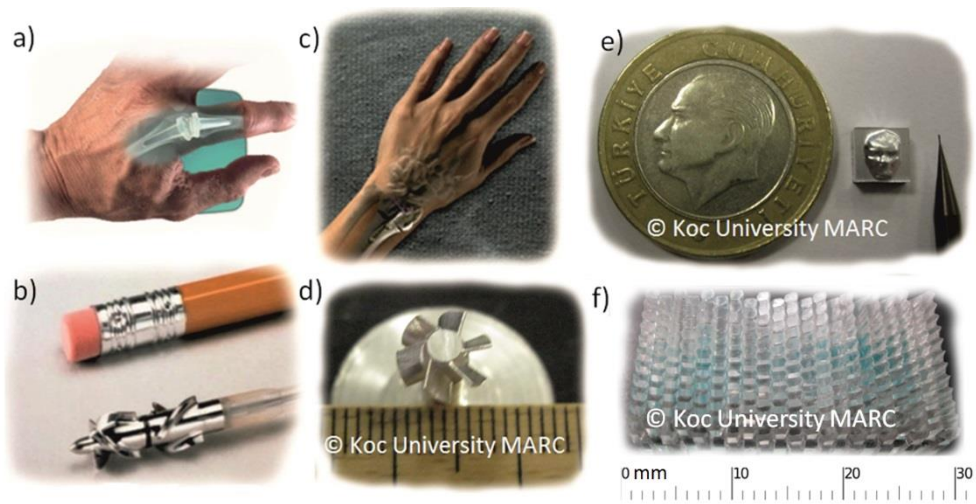

Figure 1-1 - a) Finger joint implants from DePuySynthes Joint Reconstruction Inc., b) Impeller of the blood pump from Jarvik Heart, c) Reconstructive joint implants from Wright Medical Technology Inc., d) Miniature impeller, e) Miniature freeform surface, f) Mold of special focusing lens

1.2 Thesis Outline

The objective of this thesis is to shed a light on the mechanics and thermal aspects of micro milling in order to increase the efficiency of the process. It is achieved through the scientific approach to modeling of the cutting process and validation of it through series of micro cutting experiments. The structure of the thesis is organized as follows: A detailed literature review of micro scale machining is provided in Chapter 2. Chapter 3 presents an evaluation of micro milling chip thickness models. Chapter 4 proposes a new cutting force model developed for micro milling. Shearing and ploughing effects are considered during estimation of cutting forces. Based on proposed cutting force model a new mathematical model for estimation of tool deflection is presented in Chapter 5. The Timoshenko element beam is used for FEM analysis of the tool under distributed cutting force load. Chapter 6 presents a force based feedrate scheduling technique developed for micro milling in order to increase productivity of the process. The proposed technique is experimentally validated for flat and ball end mills. Using the proposed model, the feedrate through entire cutting path can be defined offline. A newly developed hybrid finite element model for estimation of the tool and workpiece temperature fields during micro milling is presented in Chapter 7. The hybrid model combines analytical calculation of cutting powers, generated during cutting and FE model that estimates temperature distribution in accordance with heat inputs. A new strategy for estimation of micro milling induced distortions is proposed in Chapter 8. The presented finite element model combines mechanical and thermal effects applied to the workpiece during machining and estimates distortion of the machined thin wall. All presented analytical and finite element models are validated through the sets of the experiments for different cutting conditions.

Chapter 2
LITERATURE REVIEW

2.1 Overview

Nowadays, virtual simulation of machining operations plays very critical role in global industrial competition [1]. This thesis project aims to virtually simulate the process of micro milling. This simulation includes cutting force, cutting temperature, tool deflection and workpiece deflection estimation. The process optimization is performed based upon simulated data, validated through experimental tests. The best cutting parameters are suggested to improve the efficiency of the machining operation considering cycling time, tool and workpiece deflection. In this chapter, a review of previous researches conducted on kinematic analysis, mechanical and thermal simulation of the micro milling is provided.

2.2 Chip Thickness Modeling and Minimum Chip Thickness

Research results show that micro milling is not exactly the scaled down version of conventional milling, but it differs from conventional milling in several aspects such as chip thickness, critical depth of cut, and the cutting mechanisms, etc. As the result a deep investigation of the cutting process is required. An accuracy of cutting force estimations is very much dependent on the accuracy of the chip thickness model. Hence, the integration of the most accurate chip thickness model is always desired in the estimation of cutting forces to the micro milling mechanics models.

There are different chip thickness models available in the literature developed from various kinematic analyzes of micro milling process based on the fact that micro milling requires higher feed per tooth to tool radius ratios and differs from conventional milling. Integration of different chip thickness models in the micro milling mechanics model will result in differences in the predicted cutting forces. Four major chip thickness models for micro milling used in the literature were presented by Martellotti, Bao, Li, Kang and Zheng.

The chip thickness model presented by Martellotti [2] is the oldest and the most widely used model, especially employed for modeling conventional milling operations. In his work, Martellotti showed that the milling cutter is following a trochoidal path. However, the approximated version of his model was commonly used due to the simplicity. This model assumes that the toolpath is circular, tool and machine geometries are ideal. In the most conventional milling operations feed per tooth to tool radius ratio is small and due to this reason model presented by Martellotti is giving acceptable results and widely used. However, a traditional model cannot satisfy accuracy demands of micro milling, because simplifications made during the analyses bring an error to the solution and presented model is no longer valid for high feed per tooth to tool radius ratios.

Bao [3,4] developed a chip thickness model that considers a trochoidal motion of the tool and tool run-out for suitable micro milling cutting conditions. Presented chip thickness model, considers trochoidal tool motion, a difference between up and down milling and an additional chip thickness term. Bao stated that an additional chip thickness term is important in micro milling simulations, because it calculates chip thickness at immersion angles close to 0 or 180 degrees.

Later, Li et al. [5,6] proposed a numerical chip thickness model, with and without run-out. Presented a chip thickness model which uses true tool path, where undeformed chip thickness is calculated by finding the intersection point of the path curve left by the previous tooth and the line passing through the current tooth tip as well as the cutter axis.

Kang and Zheng [7] developed a chip thickness model that sums conventional chip component with additional chip component and is expressed in terms of Fourier series. Authors stated that in the expanded Martellotti's model estimation accuracy increases, while cutting flute approaches $\pi/2$ angular position and they have extended the expanded Martellotti's model to micro milling by calculating true chip thickness between two consecutive cutting paths. The available micro chip thickness models are based on certain assumptions in the kinematic analysis, which results in differences in the simulated cutting force amplitudes.

An understanding of chip formation during micro milling is important for accurate force prediction. Kim et al. [8] showed that chip formation in micro machining differs from conventional machining. Different from macro scale machining sharp edge cutting edge model is not valid for micro milling and chip occurs along rounded tool edge. Since, in conventional machining feed per tooth is higher than tool edge radius, the material is assumed to be removed by a sharp edge. However, due to small feedrate, depth of cut and relatively high tool edge radius a large negative rake angle is formed, which cause elastic recovery of the workpiece material and rough surface. This phenomenon is called ploughing. Several research groups conducted research on a presence of these two cutting mechanisms in the micro milling process and investigated the factors affecting them.

Jin and Altintas [9] developed a finite element model for orthogonal cutting operation. Presented model estimates cutting forces considering chip size, tool edge radius effect, tool run-out and dynamometer dynamics. From estimated cutting forces cutting coefficients are expressed as a non-linear function of tool edge radius and uncut chip thickness. The model considers strain rate, strain hardening and temperature effects as well.

Malekian et al. [10] developed a cutting force model considering cutting forces generated due to shearing and ploughing. In order to accurately model micro milling operation receptance coupling of the machining center, spindle and a micro tool is employed to extract the dynamics of the tool tip. Presented receptance coupling method allows predicting overall assembled system dynamics and its effect on uncut chip thickness and cutting force variations.

Wang and Zheng [11] developed an analytical force model with dual shearing and ploughing mechanism in the frequency domain. The presented model has Fourier coefficients of milling forces. These coefficients contain milling parameters and cutting constants for both shearing and ploughing mechanisms.

Lucca et al. [12] stated that ploughing mechanism is more dominant than cutting mechanism when undeformed chip thickness is less than minimum chip thickness. The minimum chip thickness is the concept where feed per tooth or depth of cut must be over this critical limit for chip formation. The minimum chip thickness depends on cutting edge radius of the tool and workpiece material properties. Vogler et al. [13] investigated minimum chip thickness for micro milling of steel by finite element model and reported that it differs between 20 – 30 % of tool edge radius for different phase steels.

Liu et al. [14] analyzed minimum chip thickness from experimentally measured cutting forces and related a sudden change in thrust force to shift from ploughing to shear dominant cutting regime. Later, Son et al. [15] investigated the effect of friction coefficient on minimum chip thickness and analytically formulated minimum chip thickness, relating it to tool edge radius and friction coefficient of workpiece material.

Chapter 3 presents a comparative evaluation of chip thickness models for micro milling by examining their direct effects on the prediction of cutting forces. Performances of four different and major chip thickness models for micro milling available in the literature are tested and compared with the experimental force measurements. The micro milling chip thickness models are evaluated by simulating micro milling forces for different feed per tooth to tool radius ratios.

2.3 Force Model for Micro Milling

In order to improve machining quality, control and understand cutting process modeling of the micro milling forces is studied by many researchers. From the prior research, it is now clear that micro milling is different from conventional machining operations and besides scaling down of the process, presences of specific phenomena were found. Kim et al. [8] analytically calculated the difference between conventional and micro milling.

In foregoing research Waldorf et al. [16] presented shear plane plasticity model, where three turning force components with a rounded cutting edge can be predicting using machining conditions, material shear stress and hone radius. The author also investigated the effect of ploughing on process damping and stated that increasing edge radius increases damping ratio.

Later, Jun [17] developed a model for micro milling that predicts dynamic cutting forces and micro end mill vibrations. The model employs chip thickness configuration that considers the elastic-plastic nature of the ploughing/rubbing and elastic recovery. The slip-line field modeling approach for the two cutting mechanisms considering variations in the dead metal cap size and effective rake angle is employed in force estimations.

Fang et al. [18,19] performed a more detailed study on plasticity model and investigated elastic recovery of ploughed material. Authors utilized a slip-line field model to model shearing and ploughing forces. The presented model consists of slip-line sub-regions, each having its own physical meaning. The model accounts for the effects like shear zone effect, size effect, ploughing force and chip up-curl radius.

Rodrigues and Labarga [20] developed an analytical force model for micro end milling based on process geometry and considering the size effect and eccentric deviation of the tool path. These factors provide a linear equation system that should be solved in order to obtain cutting force estimations.

Park and Malekian [21] developed a mechanistic cutting force model for micro milling operation which estimates forces for two cutting regimes, shearing and ploughing dominant regimes. The conventional mechanistic model is used for force estimation during shearing dominant regime and newly developed mechanistic model is used for force estimation during ploughing dominant regime. This model is based on interference volume between a tool and flank face of the workpiece and considers elastic recovery of the workpiece material.

Jing et al. [22] proposed a hybrid force model for predicting cutting forces for micro end milling, where cutting force coefficients are obtained from finite element model of orthogonal micro cutting and then integrated into mechanistic force model which can predict cutting forces for required cutting conditions.

Budak et al. [23] proposed thermo-mechanical model where sticking and sliding zones are implemented in the third deformation zone in order to investigated the effect of hone radius and flank contact on cutting forces.

A comparison between mechanistic force model and material based force model with orthogonal to oblique transformation was performed and it was seen that the mechanistic force model gives more precise estimations. Due to this reason force model presented in Chapter 4 is developed as a mechanistic force model.

In Chapter 4 of the current research thesis, a new mathematical modeling of micro cutting process by considering tool edge radius effect and tool run-out is proposed to estimate cutting forces. Estimated cutting forces are presented as a function of cutting coefficients in both shearing and ploughing zones. A comprehensive chip thickness model developed by Li for micro milling is used for precise estimation of cutting forces. Ploughing force is modeled as the function of ploughed area and related to the height of elastically recovered material.

2.4 Tool Deflection in Micro Milling

Cutting forces during micro milling process result in tool deflection and form error of machined surface. Therefore, many researchers have worked on modeling of tool deflections in order to improve the quality of final machined parts. Kim et al. [24] considered a tool as a cantilever beam and estimated deflection and dimensional error. Presented model analyses three-dimensional form error of a ball-end milled surface due to tool deflection during cutting operation.

Depince et al. [25] utilized the mirror method to compensate deflection of the tool. Presented method takes into account tool deflection during toolpath generation and compensates machining errors due to tool deflection. The model performs optimization of the tool path trajectory in order to perform machining with specified tolerances.

Kaymakci and Lazoglu [26] developed a mathematical model to simulate tool contact region and developed advanced process simulator, which was used with CAM software to predict cutting forces, surface topographies, machining errors and cycle time precisely.

Larue [27,28] worked on the prediction of form errors in the side wall machining. The geometric model was developed in order to calculate intersection boundaries between tool and workpiece. Later based on calculated intersection boundaries cutting forces and tool deflections were estimated.

Ryu [29] developed an effective model for form error prediction during side wall machining due to tool deflection. The presented model estimated cutting forces and tool deflection considering tool geometry, tool setting error and machine tool stiffness. The characteristics of generated surfaces depending on machining conditions are discussed.

Ratchev et al. [30] studied methodologies of machining of low-rigidity parts. The theoretical flexible force model is employed to estimate cutting forces acting on thin wall. The proposed deflection prediction methodology accurately models the flexible cutting forces and deflection in machining of low-rigidity components.

Rao and Rao [31] modeled a compensation of surface error caused by cutting forces for peripheral milling of curved geometry. The mechanistic model for force estimation and cantilever beam model for deflection estimation are used. The differences in a surface generation while machining straight and curved surfaces and different error compensation strategies are discussed.

Zeroudi et al. [32] presented an analytical FE model for compensation of tool deflection error. A mirror correction based compensation method is employed for tool deflection calculations. Later, by coupling deflection model with the cutting forces model, an optimum trajectory can be found after several interactions of tool path lagging and forces recalculation.

Rodriguez and Labarga [33] investigated the effect of tool deflection on cutting forces in micro milling by adding calculated deflection of the tool to instantaneous chip thickness. The developed model is based on tool geometry and theory of elasticity of materials, where a tool was considered as a cantilever beam under an action of distributed loads.

Modeling of tool deflection in micro milling is important, because it affects machining accuracy and tool life. Another parameter affecting machining accuracy is burr formation. The burr formation during micro milling is a major problem. Several groups of researchers investigated this problem. Lekkala et al [34] investigated effect of process parameters on surface finish and formation of burr free surface. Aurich et al. [35] presented a research paper on general burr classification, burr formation mechanisms and corresponding measurement techniques. Piquard et al. [36] presented an experimental design approach to study effect of cutting parameters on burr formation during micro milling of nickel-titanium shape memory alloys. As the result, author stated that burr formation is deeply influenced by feed per tooth and width of cut.

In Chapter 5 of this thesis, a new FE model is employed to estimate instantaneous deflection of the tool during cutting. Unlike applying the total forces at the tool tip as in the existing models in the literature, the newly presented micro tool deflection model considers cutting forces as distributed loads along cutting flutes in the workpiece tool contact zone. Specially designed setup with two laser displacement sensors is used to validate estimated deflections of the micro end mill. In presented thesis burr formation was not investigated.

2.5 Feedrate Scheduling

Most of the small-sized Titanium parts with freeform geometries are machined using micro ball-end milling before polishing and other surface treatments. As the demand for parts with complex geometries increases, the need for increasing efficiency also increases. Decreasing the cycle time of the machining parts is important for the productivity. One of the potentials to decrease cycle time is the optimization of feedrate during the cutting process. There are several methods of feedrate scheduling. The most popular ones are material removal rate based and cutting force based technique.

Merdol and Altintas [37] presented a constraint-based feedrate scheduling technique that adjusts feedrates to maximize material removal rate. Maximum allowed feedrate and spindle speed for each CL point are calculated. Later NC program is updated with optimized values. During feedrate calculations, bandwidths of feed drive systems and acceleration limits are considered to avoid frequent fluctuation in feedrate.

Erdim et al. [38] investigated different techniques and stated that force based technique, where feedrate is set to a value which keep value of average or maximum machining force at desired limit is more applicable rather than material removal rate based scheduling technique, where feedrate is inversely proportional to average or maximum volumetric removal rate.

Ko and Cho [39] investigated feedrate scheduling for 3D ball-end milling. The presented analytical offline feedrate scheduling model accounts changes in the uncut chip thickness due to run-out and cutter deflection. Transverse rupture strength of the cutting tool is used to determine reference cutting force at which resultant cutting forces are regulated.

Layegh and Lazoglu [40] presented an offline force control and feedrate scheduling method for 5-axis milling operations, where they optimize feed by keeping resultant cutting force below a constant value. An enhanced solid modeler kernel is developed to find an engagement between tool and workpiece for complicated 5-axis machining operations.

Altintas and Erkorkmaz [41] introduced an algorithm for feedrate optimization of spline interpolation in high speed machine tools, where they reduce cycle time while keeping axis velocity, torque and jerk below the constraints of the servo drivers with minimal tracking error. The optimized feed profiles allow non-zero acceleration and jerk values at segmented connections, which results in smooth and continues motion.

Sun et al. [42] developed a guide spline based feedrate scheduling technique for machining along curvilinear paths with acceleration and chord error constraints. The proposed model schedules feedrate along a guide spline associated with modified curvature radius of tool paths.

Erkorkmaz et al. [43] presented an enhanced force based feedrate scheduling technique for 5-axis milling, where the feedrate is modulated to keep resultant cutting forces below a desired threshold without violating the constraints of the feed drive system. The drive constraints are considered by limiting the velocity, acceleration, and jerk magnitudes commanded to each actuator. Feed profiling is realized with uninterrupted acceleration transitions, capable of spanning multiple toolpath segments.

In Chapter 6 of this thesis, a force based feedrate scheduling technique for micro milling is presented. Presented model considers mechanical effects of machining parameters in flat and ball-end milling. The force based feedrate scheduling technique is implemented on the Titanium part with a freeform surface geometry.

2.6 Thermal Modeling of Micro Milling

The temperature in micro machining of advanced engineering materials like Titanium alloys is one of the critical factors affecting an accuracy of parts, thermal and residual stresses, part distortions and tool wear. Due to these reasons, modeling of temperature is becoming essential for machining alloys with difficult thermo-mechanical properties like Ti-6Al-4V. Several groups of researchers worked on modeling of the temperature for the machining processes.

Komanduri and Hou [44] described temperature fields in workpiece and chip due to heat sources formed at the shear plane and in the friction zone at tool-chip interface using different heat source models like Hahn’s moving oblique band heat source and Jaeger’s moving band heat source.

Molinari and Moufki [45] presented a thermo-mechanical model for turning operations. Presented model is predicting chip flow direction, an interaction between chip and tool and temperature distribution on the rake face of cutting tool.

Lazoglu and Altintas [46] developed temperature model for continuous and interrupted machining operations considering shear energy formed in the primary zone, friction energy created at the chip-tool interface and the heat balance between chip and cutting tool. The temperature distribution is solved using finite difference method. The temperature field is modeled as first-order dynamic system and time constant is identified based on tool and workpiece material properties.

Ulutan et al. [47] used a finite difference-based technique to solve heat balance equations for determining the thermal fields of the tool, chip and workpiece. The model was validated with infrared thermal measurements from machining of AISI 1050 and AISI H13 materials.

Lazoglu and Islam [48] developed a 3D temperature model for oblique machining operations. Finite difference method was used to solve heat transfer problems and a general oblique cutting process model was employed for the prediction of the temperatures of turning operation.

Lazoglu and Bugdayci [49] introduced a new thermal model for the milling processes for determining the temperature fields of the tool. They also investigated effects of the temperature on wear for various carbide tool compositions in the machining of Aerospace-grade Aluminum alloys.

Recently, Lin et al. [50] proposed a temperature model for end milling process, which predicts cyclic temperature variation in the workpiece and considers the movement of the cutting tool.

Yang et al. [51] modeled the effect of tool edge radius on cutting force, effective stress and mean temperature for micro end milling of an Al2024-T6 alloy. Richardson et al. [52] modeled workpiece temperature during dry milling by implementing moving heat source.

Wissmiller and Pfefferkorn [53] presented modeling and measurement techniques for temperature measurement and discussed cooling strategies for the micro milling process. A two-dimensional transient heat transfer model is employed for temperature estimations during the cutting process. The heat input is estimated by applying Loewen and Shaw's heat partition method.

Ozel et al. [54] investigated on effects of machining parameters on surface roughness and tool wear for uncoated and cBN coated micro tools. A finite element model is employed to predict cutting forces, temperatures and wear rate of uncoated and cBN coated tool. Simulation results reveal advantages of cBN coating on tool wear. Chen et al. [55] employed fast response self-renewing thermocouple to validate steady state temperatures of tool and workpiece modeled using finite element method simultaneously.

Pittala and Monno [56] presented an FEM model to estimate thermal field due to the cutting of Ti-6Al-4V workpiece and used an infrared camera to measure the average temperature of the workpiece during cutting.

Molinari et al. [57] presented a comprehensive FEM analysis of contact problem, which investigates contact variables and thermal effects at the tool chip interface. The developed numerical model employs an Arbitrary Langrangian Eulerian finite element technique. The contact variables are mostly determined by flow stress of workpiece material.

Kim et al. [58] presented a finite element model to predict cutting force, cutting temperature, chip shape and stress distribution during micro milling process. By considering the effect of tool edge radius, presented finite element model can analyze micro machining with a very small depth of cut and can observe size effect characteristics.

Recently, Islam et al. [59] presented a new three-dimensional finite difference model for transient thermal modeling of machining processes. A finite difference technique with implicit time discretization is used for the solution of partial differential equations to simulate cutting temperatures.

In Chapter 7 of this thesis, an analysis for micro milling of titanium alloy using finite element modeling and experimental approaches is presented. In this approach, energy formed in the primary zone and friction energy created at the chip - tool interface is estimated using analytical thermo-mechanical model. A finite element model of micro milling process is developed in multi-physics simulation software. The temperature distribution in the tool and the workpiece is estimated using heat generated in primary and secondary deformation zones, previously calculated in the mechanical model. The cutting process is simulated as the time-dependent heat transfer model. Simulation results are validated through temperature measurement experiments on the workpiece using a specially designed set-up with thermocouples.

2.7 Machining Induced Distortions during Micro Milling

Simulation of the machining-induced distortions is important since it directly affects the accuracy of manufactured micro parts. Due to this reason, it is crucial to predict distortions of the thin wall and develop strategies to prevent geometrical errors. Several groups of researchers worked on modeling of the cutting forces, temperature, residual stresses and surface integrity that affect machining-induced distortions.

Jawahir et al. [60] published a comprehensive work on recent progress in experimental and theoretical investigations of residual stresses, where they investigated and compared main residual stress modeling techniques available in the literature.

Denkena et al. [61] investigated the effect of cutting parameters and cutting edge geometry on residual stresses and subsurface material changes in Aluminum alloys. The results of the model showed a clear influence of machining parameters, cutting edge geometry and tool wear on residual stresses.

Lazoglu et al. [62] developed an analytical elasto-plastic model to estimate machining induced residual stresses and validated their model via X-ray residual stress measurements on Waspaloy material.

Arrazola et al. [63] developed a finite element model to estimate residual stresses during turning operation of Nickel based supper alloy, where they related residual stresses to material properties like yield stress and friction angle.

Smith and Dvorak [64] proposed a model based on tool path optimization strategy that aims to increase the accuracy of machined thin webs. Wang et al. [65] developed an FEM based model to simulate the deformation of thin wall workpiece during milling operation, where they investigated the effect of cutting forces on deformation of the thin wall.

Schulze et al. [66] modeled deflection of the T-profile thin wall made of Aluminum alloy. The influence of different initial stress states and different machining parameters on the amount of distortion is examined using FEM simulations and experimental results. As the result, it was stated that amount of initial stress state has a significant effect on distortion potential.

Chapter 8 of this thesis presents an investigation of micro milling induced distortions of thin wall workpiece made of Titanium alloy using finite element modeling approach. The factors affecting distortions – thermal and mechanical effects are considered in proposed model. The results from developed thermal and force models, presented in Chapter 4 and Chapter 7, are used as inputs for the distortion simulations. The effects of the cutting parameters, forces and cutting temperatures are investigated. The model is validated through micro milling experiments and White Light Interferometer (WLI) measurements.

Chapter 3
AN EVALUATION OF MICRO MILLING CHIP THICKNESS MODELS

3.1 Overview

The chip thickness model is one of the most important issues in the development of any machining process model for accurate prediction of cutting forces, tool deflections, machined surface quality, tool life, process stability, etc. In this section, four different major chip thickness models available in the literature are evaluated from the perspective of micro milling mechanics.

There are different chip thickness models available in the literature developed from various kinematic analyzes of micro milling process based on the fact that micro milling requires higher feed per tooth to tool radius ratios and differs from conventional milling. Integration of different chip thickness models in the micro milling mechanics model will result in differences in the predicted cutting forces. Four major chip thickness models for micro milling used in the literature were presented by Martellotti, Bao, Li, Kang and Zheng. Martellotti [2] showed that true toolpath of cutting tool due to rotational and translational motion is trochoidal. Bao [3,4] developed a chip thickness model that considers a trochoidal motion of the tool and tool run-out for suitable micro milling cutting conditions. Later, Li et al. [5,6] proposed a numerical chip thickness model, with and without run-out, which analyzes true tool path of the micro milling tool. Kang and Zheng [7] developed a chip thickness model that sums conventional chip component with additional chip component and is expressed in terms of Fourier series.

The available chip thickness models are based on certain assumptions, but there is no comparative evaluation of these models from the perspective of micro milling mechanics in the literature, yet. Here, the performance of four different and major chip thickness models for micro milling available in the literature is tested and compared with the experimental force measurements. The micro milling chip thickness models are evaluated by simulating micro milling forces for different feed per tooth to tool radius ratios. The Root Mean Square Deviation (RMSD) and the coefficient of determination (R^2) values between the estimated and measured micro milling forces are presented for the comparative evaluation of all the chip thickness models at various feed-per-tooth to tool diameter ratios.

3.2 Chip Thickness Models

An accurate chip thickness model is one of the most critical requirements for the modeling of micro milling mechanics. An accuracy of the chip thickness models used in the micro milling mechanics models directly affects the accuracy of the cutting force predictions. In this section, four different major chip thickness models available in the literature and utilized in the force validation tests are presented in their closed-forms.

One of the commonly used chip thickness model is based on trochoidal toolpaths during milling process was presented by Martellotti [2] as the following:

$$h = R + t_x \, sin\theta - \sqrt{R^2 - t_x^2 cos^2\theta} \tag{3-1}$$

Here, h is the undeformed chip thickness, R is the radius of the milling tool, t_x is the feed-per-tooth and θ is the angular position of the tool. However, the equation given above is approximated for cutting process with small t_x over R ratio and is employed for the most of conventional milling processes as:

$$h = t_x \, sin\theta \qquad (3\text{-}2)$$

In micro milling due to the small tool diameter and relatively higher chip thickness to tool radius ratio, chip thickness model becomes very important. Bao [3] developed a chip thickness model for trochoidal tool path, which considered the nature of chip thickness formation in micro milling at high feed per tooth to tool radius ratios. The obtained chip thickness model is given below in Equation (3-3).

$$h = t_x \, sin\theta - \frac{N}{2\pi R} t_x^2 sin\theta cos\theta + \frac{1}{2R} t_x^2 cos^2\theta \qquad (3\text{-}3)$$

Here, N is the number of cutting flutes. The physical meaning of each term in Equation (3-3) is as following: the first term in the equation is a major contributor to the chip thickness, the second term is the difference between up and down milling and the third term is the additional chip thickness.

Kang and Zheng [7] developed a chip thickness model which is the sum of conventional chip thickness and additional chip thickness. Presented model is expressed in terms of Fourier series and closed form of the model demonstrated in Equation (3-4).

$$h = t_x sin\theta - \frac{N t_x^2 cos\theta sin\theta}{2\pi R + N t_x cos\theta} + R - \sqrt{R^2 - \left(\frac{2\pi R t_x cos\theta}{2\pi R + N t_x cos\theta}\right)^2} \qquad (3\text{-}4)$$

Li et al. [5] developed a numerical method to calculate undeformed chip thickness, which calculates undeformed chip thickness for engaged cutting tooth through finding the intersection point of the path curve left by proceeding tooth and the line passing through the current tool tip and tool axis. The closed-form of the chip thickness proposed by Li is given below in Equation (3-5).

$$h = R\left[1 - \sqrt{1 - \frac{2t_x sin\theta}{R + \frac{Nt_x}{2\pi}cos\theta} - \frac{t_x^2\,cos(2\theta)}{(R + \frac{Nt_x}{2\pi}cos\theta)^2} + \frac{t_x^3 sin\,\theta\,cos^2\theta}{(R + \frac{Nt_x}{2\pi}cos\theta)^3}}\right] \tag{3-5}$$

The mechanistic model for estimating cutting forces during the micro milling process is established using chip thickness models mentioned above. The instantaneous differential chip load for k^{th} disk having a differential height of dz can be written as the following:

$$dA_c = (h)_k \cdot (dz)_k \tag{3-6}$$

The mechanistic cutting force model can be represented using following formula:

$$F_i = K_{ic}A_c + K_{ie} \tag{3-7}$$

Above, F_i represents F_t, F_r and F_a are forces in tangential, radial and axial directions, respectively. K_{ic} and K_{ie} stand for K_{tc}, $K_{rc}, K_{ac}, K_{te}, K_{re}$ and K_{ae} that are specific cutting coefficients and specific edge coefficients in tangential, radial and axial directions, respectively. Tangential, radial and axial forces are transformed to forces in three Cartesian directions in mini dynamometer coordinate frame (X, Y and Z) shown in Figure 3-1 as the following:

$$\begin{bmatrix} dF_x \\ dF_y \\ dF_z \end{bmatrix} = \begin{bmatrix} cos(\theta) & sin(\theta) & 0 \\ -sin(\theta) & cos(\theta) & 0 \\ 0 & 0 & 1 \end{bmatrix} \times \begin{bmatrix} dF_t \\ dF_r \\ dF_a \end{bmatrix} \tag{3-8}$$

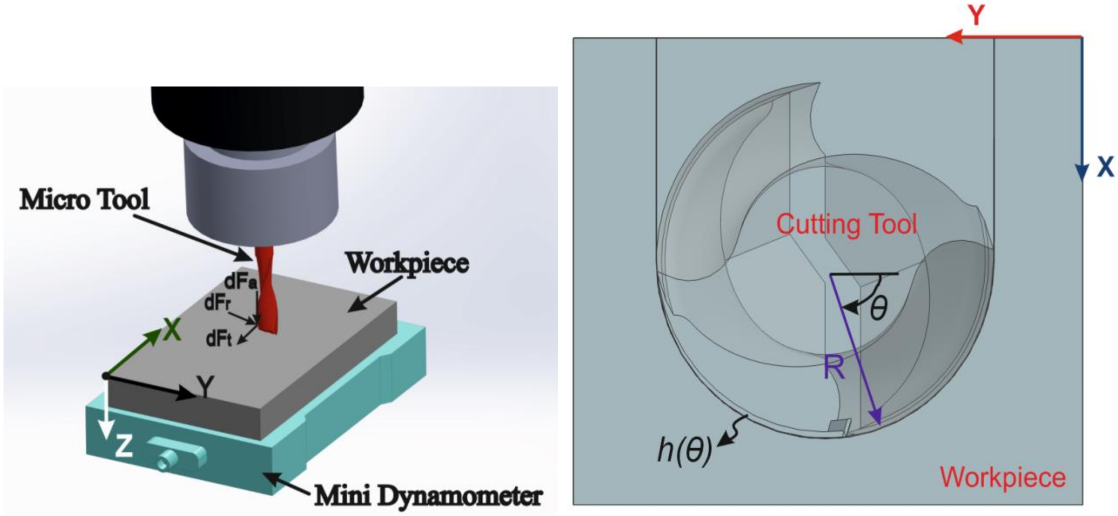

Figure 3-1 – a) An illustration of experimental setup and coordinate frame for force measurements, b) An illustration of uncut chip thickness

In Section 3.3, the effect of presented chip thickness models for the force estimation is analyzed and predicted forces for different feed per tooth to tool radius ratios are compared with the experimental results.

3.3 Force Simulations for Chip Thickness Models and Experimental Validations

Experiments are performed on aerospace grade Aluminum alloy Al7050 using 500 μm diameter two fluted Tungsten Carbide micro end mill on Mori Seiki NMV5000DCG 5-axis CNC milling machine and cutting forces are measured with a table type mini dynamometer. The experimental setup used for validation of chip thickness models is shown below in Figure 3-2.

Figure 3-2 - Experimental setup used in the validation tests

Slot cutting experiments are performed on aerospace grade Aluminum alloy Al7050 at 20.000 rpm spindle speed with various feed per tooth to tool radius ratios at 50 µm depth of cut. Run-out of the tool was measured as 5 µm and was considered in the model for the simulations. Table 3-1 presents the cutting conditions and tool specifications used for micro milling simulation and experiments. Cutting coefficients for the micro end mill are estimated according to technique presented by Altintas [67], force measurements used during calibrations are presented in Figure 3-3 and cutting coefficients are given in Table 3-2.

Table 3-1 – Cutting conditions and tool specifications

Tool Diameter	500 [μm]
Number of flutes	2
Tool edge radius	4 [μm]
Measured helix angle	27.5˚
Spindle Speed	20000 rpm
Feedrate	1000-5000 [mm/min]
Depth of cut	50 [μm]

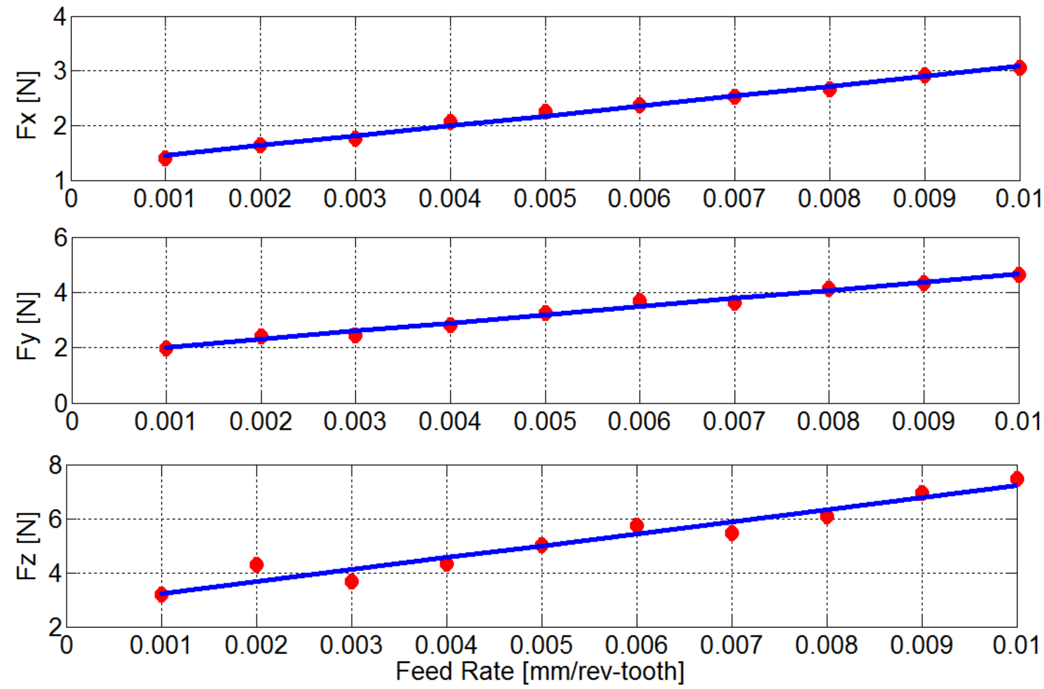

Figure 3-3 - Experimentally measured average cutting forces for n=20.000 rpm spindle speed and a=200 μm depth of cut with 500 μm diameter micro end mill

Table 3-2 – Cutting coefficients for Al7050 with Tungsten Carbide cutting tool

K_{tc} [N/mm^2]	K_{te} [N/mm]	K_{rc} [N/mm^2]	K_{re} [N/mm]	K_{ac} [N/mm^2]	K_{ae} [N/mm]
2959.0	13.41	1809.80	9.98	3495.30	13.87

Cutting experiments and chip thickness model comparisons are performed at five different feed per tooth to tool radius ratios suitable for micro milling. The simulated forces with different chip thickness models are given in Equation (3-1) – Equation (3-5) and their comparison with experimentally measured forces in feed direction are presented in Figure 3-4 – Figure 3-8.

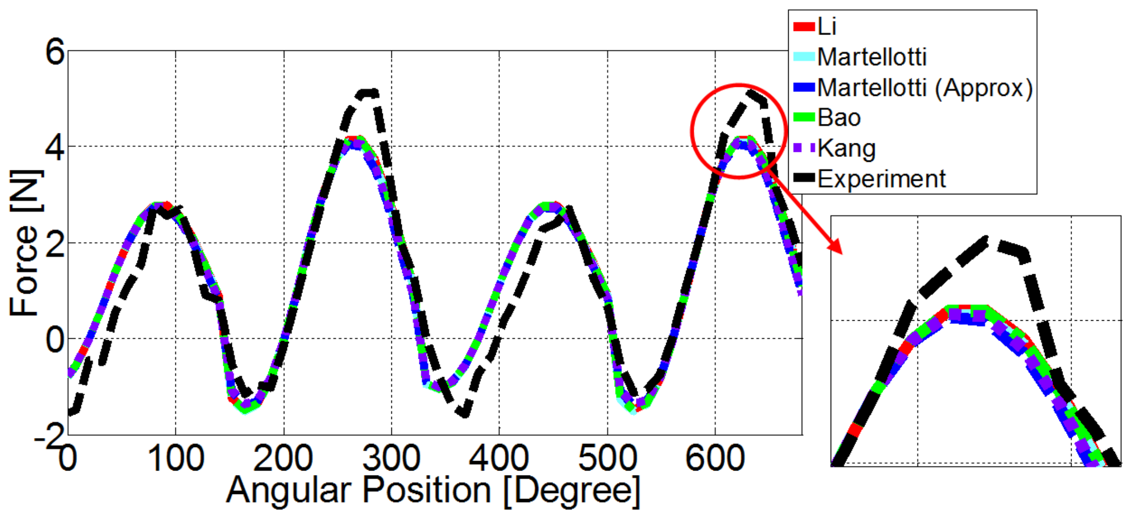

Figure 3-4 - Comparison of force estimation of chip thickness models for the feed per tooth to tool radius ratio 0.1

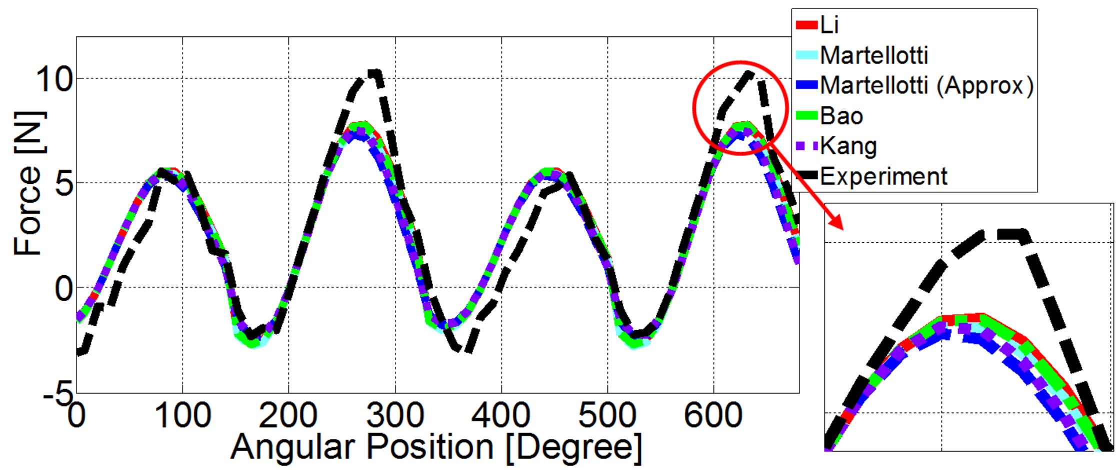

Figure 3-5 - Comparison of force estimation of chip thickness models for the feed per tooth to tool radius ratio 0.2

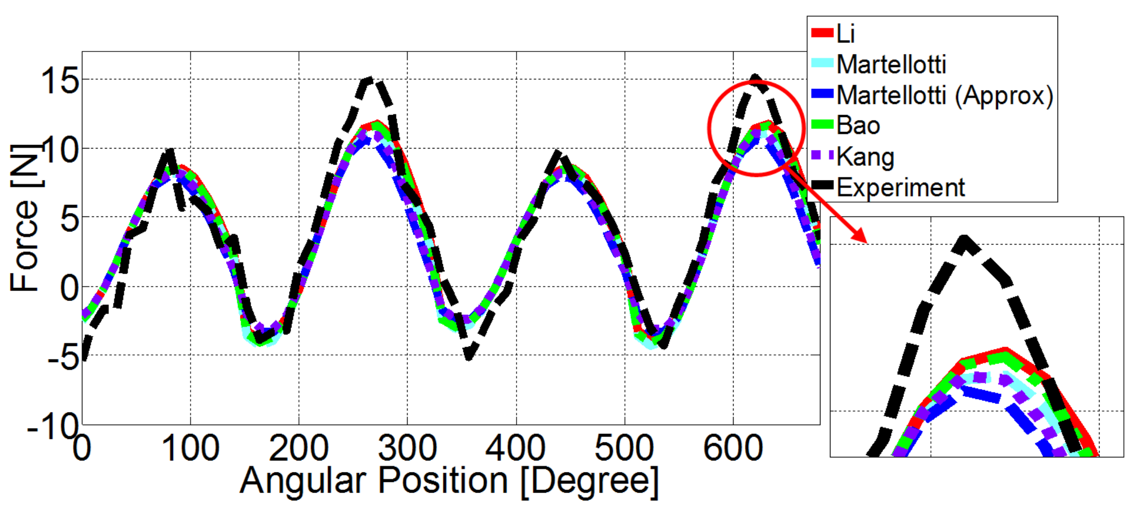

Figure 3-6 - Comparison of force estimation of chip thickness models for the feed per tooth to tool radius ratio 0.3

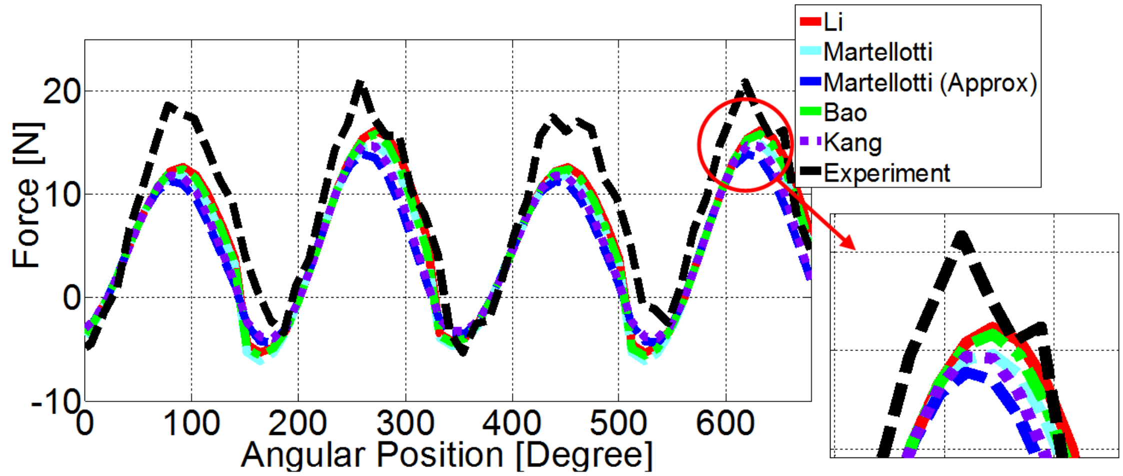

Figure 3-7 - Comparison of force estimation of chip thickness models for the feed per tooth to tool radius ratio 0.4

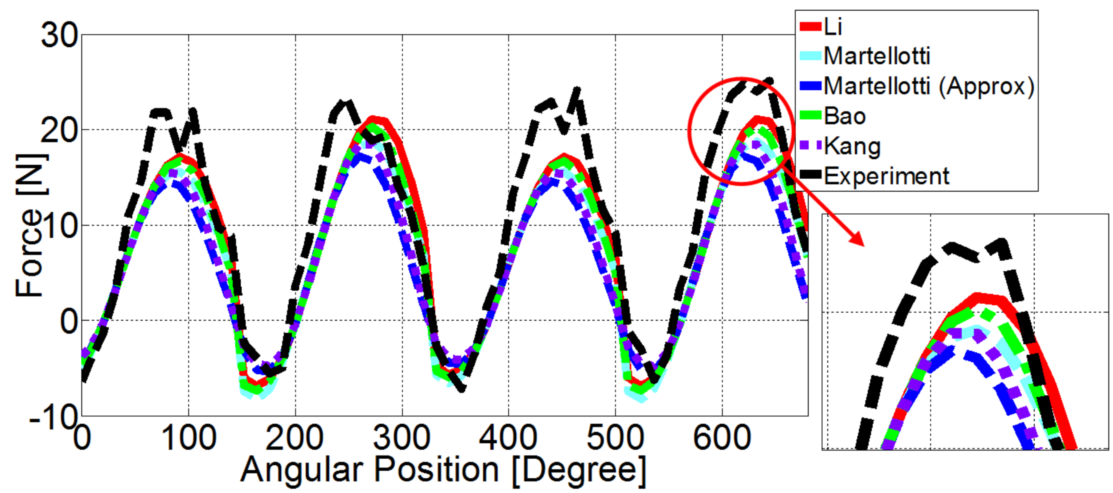

Figure 3-8 - Comparison of force estimation of chip thickness models for the feed per tooth to tool radius ratio 0.5

It can be seen from Figure 3-4 – Figure 3-8 that when feed per tooth to tool radius ratio (t_x/R) is smaller than 0.3, all chip thickness models are giving close results with respect to each other and differences in the estimated forces are becoming more significant when t_x/R is greater than 0.3. Comparing the simulation outputs with experimental measurement results showed that the model proposed by Li gives the closest results to the experimental forces. In order to quantify this statement, an error evaluation is performed in the following section.

3.4 Error Evaluation of Chip Thickness Models

There are some convenient scale dependent accuracy measurement techniques for error evaluations. These measures are useful when comparing different methods on the same set of data scales. One of the most commonly used scale-dependent measurement technique is Root Mean Square Deviation (RMSD), which represents standard deviation of differences between true and estimated values and can be formulated as following:

$$MSE = \frac{1}{n}\sum_{i=1}^{n}\left(\hat{Y}_i - Y_i\right)^2 \qquad RMSD = \sqrt{MSE} \tag{3-9}$$

Here, n is the number of elements, $\hat{Y}$ is the vector of estimates, Y is the vector of true values and MSE is mean squared error of estimations. The RMSD values of all model estimations for five different feed per tooth to tool radius ratios is measured and given below in Figure 3-9.

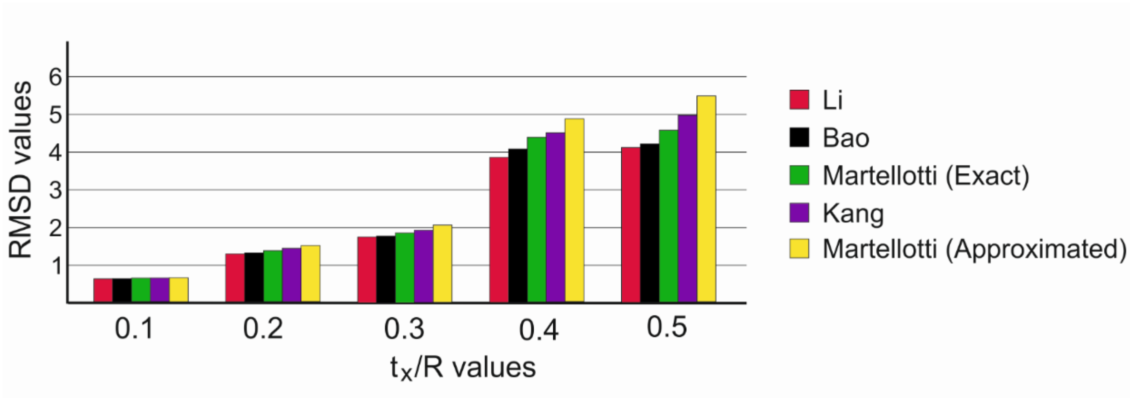

Figure 3-9 - The Root Mean Square Deviation (RMSD) values of the estimated forces at various ratios of feed per tooth to tool radius (t_x/R) for the different chip thickness models used in micro milling modeling

It is seen from Figure 3-9 that for all feed per tooth to tool radius ratios, models developed Kang, Bao and Li give better results than approximated Martellotti's model, which is used for conventional milling simulations. However, the RMSD values of estimated force obtained with an extended form of Martellotti's model given in Equation (3-1) is less than the values of Kang's model. The RMSD values of all models are close to each other when t_x/R is smaller than 0.3, but when t_x/R is greater than 0.3 effect of the chip thickness model in the force model is becoming more significant and from the results it can be seen that utilization of Li's model gives the least error in force prediction.

Another way for determination accuracy of the estimated values is the coefficient of determination denoted as R^2. This coefficient determines how well-estimated data fit the true value. R^2 coefficient varies between $0 \leq R^2 \leq 1$ and converges to 1 when estimation fits true value. The definition of the coefficient of determination is given below in Equation (3-10).

$$SS_R = \sum_{i=1}^{n} (\hat{Y}_i - \bar{Y})^2, \qquad SS_T = \sum_{i=1}^{n} (Y_i - \bar{Y})^2, \qquad R^2 = \frac{SS_R}{SS_T} \qquad (3\text{-}10)$$

Here, n is the number of elements, $\hat{Y}$ is the vector of estimated force, Y is the vector of experimentally measured force in the feed direction, $\bar{Y}$ is the mean value of experimentally measured force in the feed direction, SS_R is the regression sum of squares and SS_T is the total sum of squares. The R^2 values of all model estimations for five different feed per tooth to tool radius ratios is measured and given below in Figure 3-10. Li's chip thickness model showed the highest R^2 values for all t_x/R ratios.

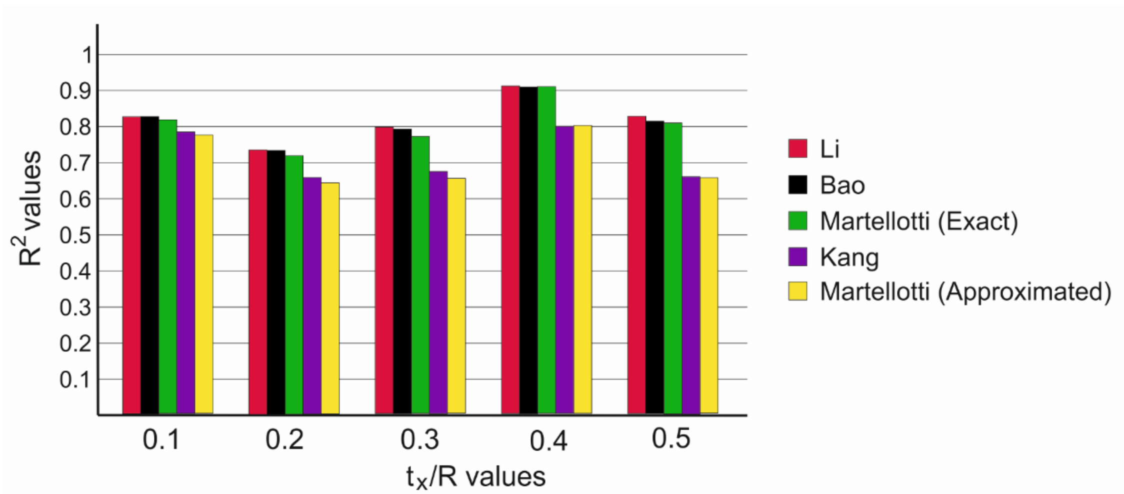

Figure 3-10 - R^2 values of the estimated forces at various ratios of feed per tooth to tool radius (t_x/R) for the different chip thickness models used in micro milling modeling

Presented chip thickness models are evaluated at different feed per tooth to tool radius values by calculating their Root Mean Square Deviation (RMSD) and coefficient of determination (R^2). From the results, it is seen that models developed by Bao, Kang and Li are able to estimate cutting forces in micro milling better than the approximated Martellotti model, which is employed for conventional milling simulations. However, an extended form of Martellotti's model gives more accurate results than approximated form. Results showed that the chip thickness model developed by Li has the least root mean square deviation (RMSD) and the highest coefficient of determination (R^2), which denotes that this model has the better fit with experimental results. The chip thickness model developed by Bao has a high R^2 coefficient as well, but the RMSD values of force estimations with this chip thickness model are higher than in Li's models, which shows that model is making more error in estimating cutting forces for micro milling, especially when feed per tooth to tool radius ratio is higher than 0.3. The chip thickness model developed by Kang gives a better result than approximated Martellotti's model and poorer result than the extended form of Martellotti's model.

In the overall analysis, it is seen that although, in low t_x/R ratios, most of the chip thickness models perform well, cutting force estimations with Li's chip thickness models showed better performance in all t_x/R ratios in force predictions in micro milling when compared the other chip thickness models.

3.5 Summary

In this chapter, the performance of four major different chip thickness models for micro milling exist in the literature is comparatively evaluated. The effects of proposed chip thickness models for prediction of cutting forces are examined via experimental force measurements. The mathematical force prediction model is used to compare the effects of closed-form of chip thickness models on force prediction for different feed per tooth to tool radius ratios by calculating their Root Mean Square Deviation (RMSD) and coefficient of determination (R^2) values. From the conducted comparative evaluation, it is seen that if the feed per tooth to tool diameter ratio (t_x/R) is smaller than 0.3, the RMSD values of all models are close to each other. However, when t_x/R is greater than 0.3, the effects of the chip thickness models in the force model are becoming more significant. In all the validation tests performed for the five different (t_x/R) ratio, the chip thickness model proposed by Li, presented in Equation (3-5), has the least root mean square deviation (RMSD) and the highest coefficient of determination (R^2), which denotes that this model has better fits with the experimental measurements and performed better in the predictions of micro-milling cutting forces.

Chapter 4
MECHANICS OF MICRO MILLING

4.1 Overview

Micro milling is one of the most fundamental manufacturing processes, which is extensively used for manufacturing of complex miniature parts. While the mechanisms of conventional milling are well established, micro milling mechanics are less well understood. Micro mechanical machining techniques bring many advantages to the fabrication of micro sized features. In order to improve machining quality, control and understand cutting process, modeling of the micro milling forces is vital. The most common model to estimate the cutting forces in literature is mechanistic cutting force model in which the cutting force is a linear function of uncut chip thickness area and cutting coefficients. From prior research, it is clear that micro milling is different from conventional machining operations and besides scaling down of the process, presences of specific phenomena were found. In this chapter, a new mathematical modeling of micro cutting process by considering tool edge radius effect and tool run-out is proposed to estimate cutting forces formed during micro end milling. Estimated cutting forces are presented as a function of cutting coefficients in both shearing and ploughing zones. A comprehensive chip thickness model developed by Li for micro milling is used for precise estimation of cutting forces. Ploughing force is modeled as the function of ploughed area and related to the height of elastically recovered material.

4.2 Modeling of Cutting Forces for Micro Milling

Modeling of micro milling process is important to improve the machined part quality and increase the productivity of the process. However, conventional modeling approach cannot be applied to micro milling due to the specific nature of the process. Micro machining is also characterized by a high ration of feed per tooth to tool radius. When the edge radius of the cutting tool is comparable with feed per tooth, the transition between cutting mechanisms occurs. As the result, two cutting mechanisms occur: cutting with chip formation and ploughing without chip formation, are dominant during micro milling process. During ploughing dominant regime, no chip is formed when the chip thickness is below minimum chip thickness and workpiece material is elastically deformed. Therefore, minimum chip thickness can be defined as a critical value of chip thickness below which no chip can be formed stably. The shear dominant cutting regime is active when actual uncut chip thickness is greater than minimum uncut chip thickness, h_{min}. However, if actual uncut chip thickness is less than h_{min} ploughing dominant cutting regime is observed, as shown in Figure 4-1. Minimum chip thickness is calculated as 30% of edge radius of the tool.

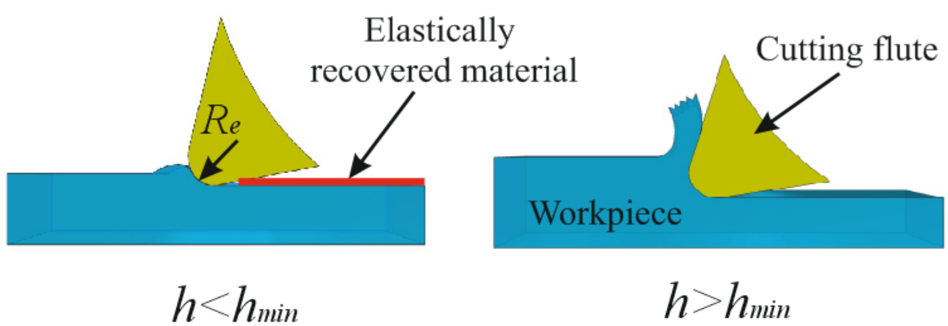

Figure 4-1 – Shear and ploughing dominant cutting regimes

A mechanistic cutting force model is developed to estimate cutting forces during micro milling, considering shearing and ploughing cutting mechanisms. A comprehensive chip thickness model developed by Li is utilized in the developed force prediction model. Cutter run-out was measured as 2 μm and was considered during simulation [68]. The proposed chip thickness model is given below,

$$h = m_i R \cdot \left[1 - \sqrt{1 - \frac{2t_x sin\theta}{R+\frac{Nt_x}{2\pi}cos\theta} - \frac{{t_x}^2\cos(2\theta)}{(R+\frac{Nt_x}{2\pi}cos\theta)^2} + \frac{{t_x}^3\sin\theta\cos^2\theta}{(R+\frac{Nt_x}{2\pi}cos\theta)^3}}\right] + R_i - R_{i-m_i} \quad (4\text{-}1)$$

Here, R_i is rotation radius of an arbitrary element of cutting edge i

$$R_i = \rho\, cos\left[\lambda - \kappa - \frac{2(i-1)\pi}{N}\right] \quad (4\text{-}2)$$

$$\kappa = \frac{ztan\beta}{R} \quad (4\text{-}3)$$

Here, N represents the number of flutes, the radius of the tool is denoted by R, t_x is feed per tooth, ρ is run-out amplitude and λ is run-out angle, β is helix angle, z is axial position of discreet element of cutting edge, m_i means that current tooth i is removing material left by m_i^{th} previous tooth and θ stands for rotational angle.

When the chip thickness is bigger than the critical value ($h>h_{min}$), the cutting mechanism is assumed to be similar to the conventional cutting mechanism that considers the shearing and edge coefficients. The differential cutting forces for shearing dominant regime are estimated like following:

$$\begin{bmatrix} dF_{xs} \\ dF_{ys} \\ dF_{zs} \end{bmatrix} = \begin{bmatrix} \cos(\theta) & \sin(\theta) & 0 \\ -\sin(\theta) & \cos(\theta) & 0 \\ 0 & 0 & 1 \end{bmatrix} \left(\begin{bmatrix} K_{tc}h_\theta dz \\ K_{rc}h_\theta dz \\ K_{ac}h_\theta dz \end{bmatrix} + \begin{bmatrix} K_{te}dz \\ K_{re}dz \\ K_{ae}dz \end{bmatrix} \right) \quad (4\text{-}4)$$

Here, dF_{xs}, dF_{ys} and dF_{zs} represent shearing components of differential x, y and z forces, K_{tc}, K_{rc} and K_{ac} are cutting coefficients, K_{te}, K_{re} and K_{ae} are edge coefficients, dz denotes differential axial depth of cut, h stands for uncut chip thickness.

When the chip thickness is lower than the critical value ($h<h_{min}$), the cutting mechanism is assumed to be ploughing. The differential cutting forces for ploughing dominant regime are estimated like following:

$$\begin{bmatrix} dF_{xp} \\ dF_{yp} \\ dF_{zp} \end{bmatrix} = \begin{bmatrix} \cos(\theta) & \sin(\theta) & 0 \\ -\sin(\theta) & \cos(\theta) & 0 \\ 0 & 0 & 1 \end{bmatrix} \begin{bmatrix} K_{tp} \cdot Ap \cdot dz \\ K_{rp} \cdot Ap \cdot dz \\ K_{ap} \cdot Ap \cdot dz \end{bmatrix} \tag{4-5}$$

Above, dF_{xp} , dF_{yp} and dF_{zp} represent ploughing components of differential x, y and z forces, K_{tp}, K_{rp} and K_{ap} stand for ploughing coefficients and A_p denotes ploughed area, which depends on height of elastically recovered material (h_e), edge radius of the tool (r_e) and clearance angle (ψ_e). The cutting coefficients are modeled according to the procedure described by Altintas [67]. Detailed calculation of ploughed area is presented below [10]:

If $h_{er} \geq r_e(1 - cos\psi_e)$

$$A_p = \frac{1}{2} r_e^2 \left(\alpha_p + \psi_e\right) + \frac{1}{2} r_e l_{AD} - \frac{1}{2} r_e l_{AB} \sin(\alpha_p + \psi_e + \psi_p) \tag{4-6}$$

If $h_{er} < r_e(1 - cos\psi_e)$

$$A_p = \frac{1}{2} r_e^2 \left(\alpha_p + \psi_s - \sin(\alpha_p + \psi_s)\right) \tag{4-7}$$

where ψ_s, α_p are angles and l_{AD}, l_{AB} are magnitudes calculated from geometrical relations:

$$\psi_s = cos^{-1}(1 - \frac{h_{er}}{r_e}) \tag{4-8}$$

$$\alpha_p = cos^{-1}(1 - \frac{h}{r_e}) \tag{4-9}$$

$$l_{AD} = \left(\frac{h_{er} - r_e(1 - cos\psi_e)}{sin\psi_e}\right) \tag{4-10}$$

$$l_{AB} = \sqrt{r_e^2 + l_{AD}^2} \tag{4-11}$$

As the result the total differential forces including shearing and ploughing forces are estimated as following:

$$\begin{bmatrix} dF_x \\ dF_y \\ dF_z \end{bmatrix} = \begin{bmatrix} \cos(\theta) & \sin(\theta) & 0 \\ -\sin(\theta) & \cos(\theta) & 0 \\ 0 & 0 & 1 \end{bmatrix} \left(\begin{bmatrix} K_{tc}h_\theta dz \\ K_{rc}h_\theta dz \\ K_{ac}h_\theta dz \end{bmatrix} + \begin{bmatrix} K_{te}dz \\ K_{re}dz \\ K_{ae}dz \end{bmatrix} + \begin{bmatrix} K_{tp}A_p dz \\ K_{rp}A_p dz \\ K_{ap}A_p dz \end{bmatrix} \right) \tag{4-12}$$

4.3 Force Simulations and Experimental Validations

The proposed mechanistic cutting force model was used as a core program for several applications such as force based feedrate scheduling, tool deflection model, cutting temperature estimation model and distortion estimation model. In all the mentioned applications, the cutting force model was able to predict the trend and magnitude of cutting forces with a very good accuracy.

Experiments are performed on Titanium alloy Ti-6Al-4V using 800 µm diameter two fluted Tungsten Carbide micro end mill (T1) and on Aluminum Alloy Al-7050 using 1500 µm diameter two fluted Tungsten Carbide end mill (T2) on Mori Seiki NMV5000DCG 5-axis CNC milling machine. The cutting force measurements are performed using Kistler 9256C mini dynamometer. The experimental setup used for force measurements is shown below in Figure 4-2.

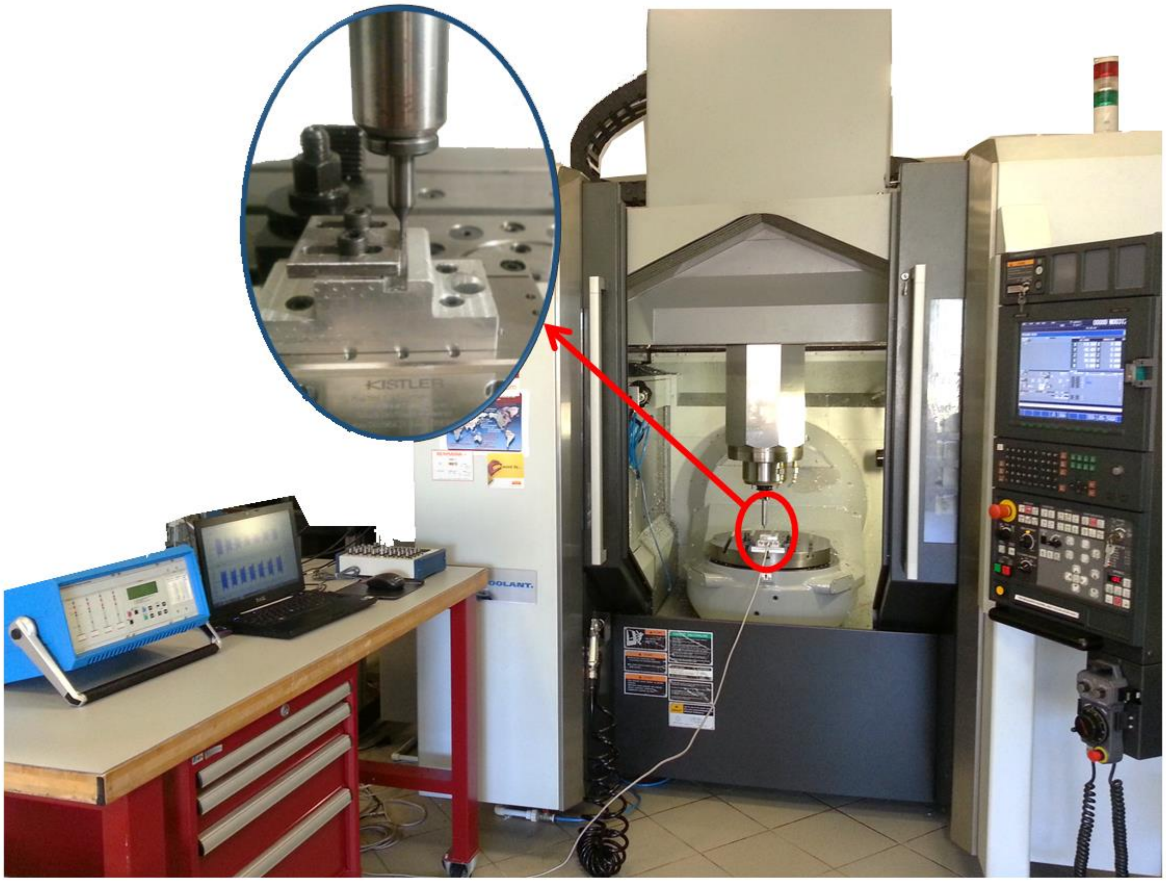

Figure 4-2 – Experimental setup for force measurements

Cutting experiments are performed on Titanium alloy at 10.000 rpm spindle speed and on Aluminum alloy at 20.000 rpm spindle speed at various cutting conditions given in Table 4-1.

Table 4-1 – Cutting conditions for force measurement experiments

	Workpiece	Condition	Axial depth of cut [µm]	Feed per tooth [µm/rev-tooth]
Case 1	Ti-6Al-4V	Down-milling	100	10
Case 2	Ti-6Al-4V	Down-milling	200	5
Case 3	Ti-6Al-4V	Up-milling	200	7
Case 4	Al-7050	Down-milling	500	10
Case 5	Al-7050	Down-milling	500	15

Mechanistic calibration is performed to estimate the cutting constants according to the method proposed by Altintas [67]. The experimental and theoretical forces were synchronized for full immersion, a set of milling experiments at various feed rates and constant axial depth of cut were conducted. Experimentally evaluated average cutting forces can be expressed as a linear function of feed rate and an offset contributed by the edge forces. Ploughing coefficients were obtained from average cutting forces measured at feed per tooth values equal and lower that minimum uncut chip thickness and shearing coefficients were measured from average cutting forces measured at feed per tooth values higher than minimum chip thickness. It is the common identification technique, also was utilized by Malekian et al. [10].

Using a calibrated tool for both shearing and plowing cutting regimes, corresponding cutting coefficients are estimated and given in Table 4-2 and Table 4-3.

Table 4-2 – Cutting coefficients for Ti-6Al-4V with T1 Tungsten Carbide cutting tool

K_{tc} [N/mm^2]	K_{tp} [N/mm^3]	K_{te} [N/mm]	K_{rc} [N/mm^2]	K_{rp} [N/mm^3]	K_{re} [N/mm]	K_{ac} [N/mm^2]	K_{ap} [N/mm^3]	K_{ae} [N/mm]
4264	3263	28	3887	3262	22	199	293	3

Table 4-3 – Cutting coefficients for Al-7050 with T2 Tungsten Carbide cutting tool

K_{tc} [N/mm^2]	K_{tp} [N/mm^3]	K_{te} [N/mm]	K_{rc} [N/mm^2]	K_{rp} [N/mm^3]	K_{re} [N/mm]	K_{ac} [N/mm^2]	K_{ap} [N/mm^3]	K_{ae} [N/mm]
1687	3460	16	2765	3831	14	349	482	13

The total cutting forces during micro milling process are expressed as the sum of differential forces due to shearing and ploughing cutting mechanisms. Run-out of the tool was measured as 2μm and was considered during simulations. Tool properties are given in Table 4-4.

Table 4-4 – Tool and workpiece material properties

Tool diameter (T1)	800 μm
Tool diameter (T2)	1500 μm
Measured helix angle (T1)	25.2°
Measured helix angle (T1)	31.2°
Tool edge radius (T1 and T2)	6 μm
Tool projection length	20 mm

Validation of the force model was performed through experimental force measurements. In Figure 4-3 – Figure 4-7 validation results for several cutting experiments are given and it can be seen that the simulation results are in a good agreement with experimental force measurements.

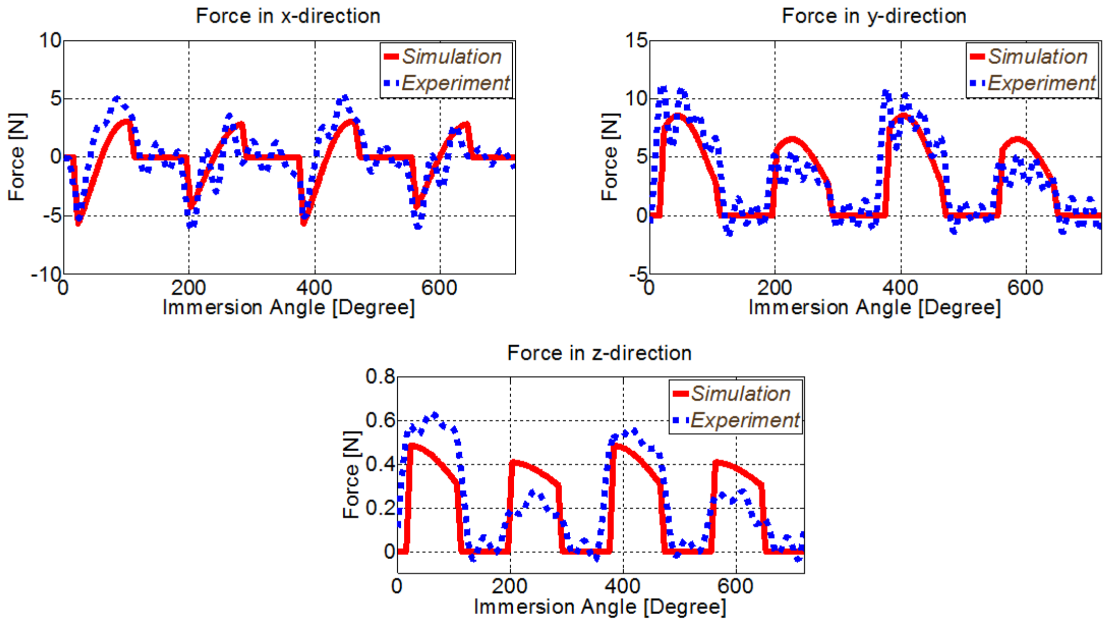

Figure 4-3 – Simulated and experimental forces in x, y and z directions for case 1

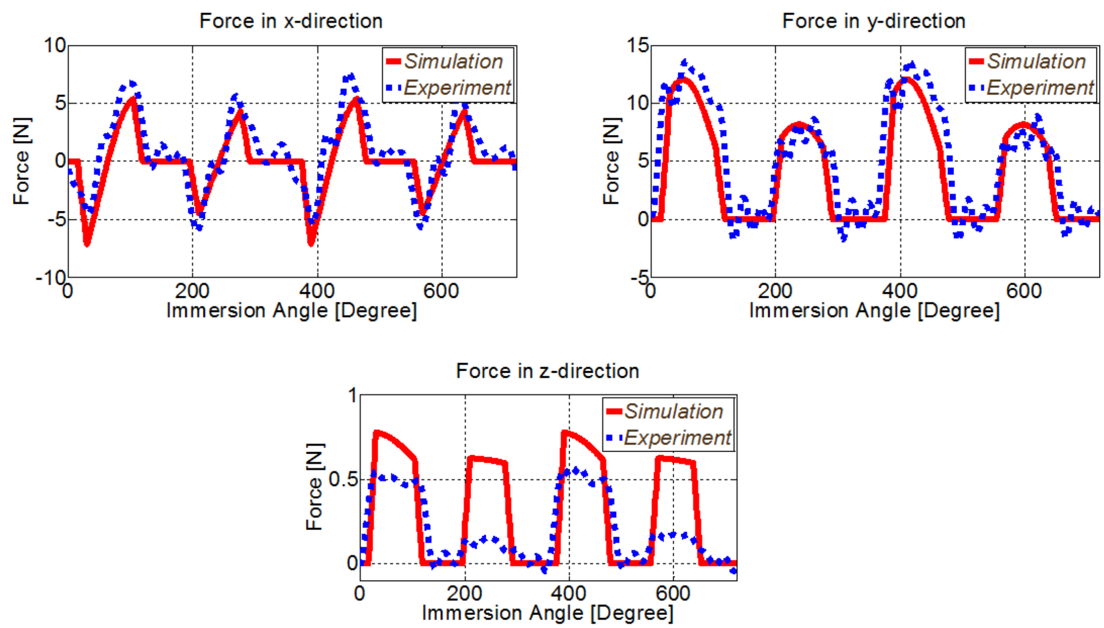

Figure 4-4 – Simulated and experimental forces in x, y and z directions for case 2

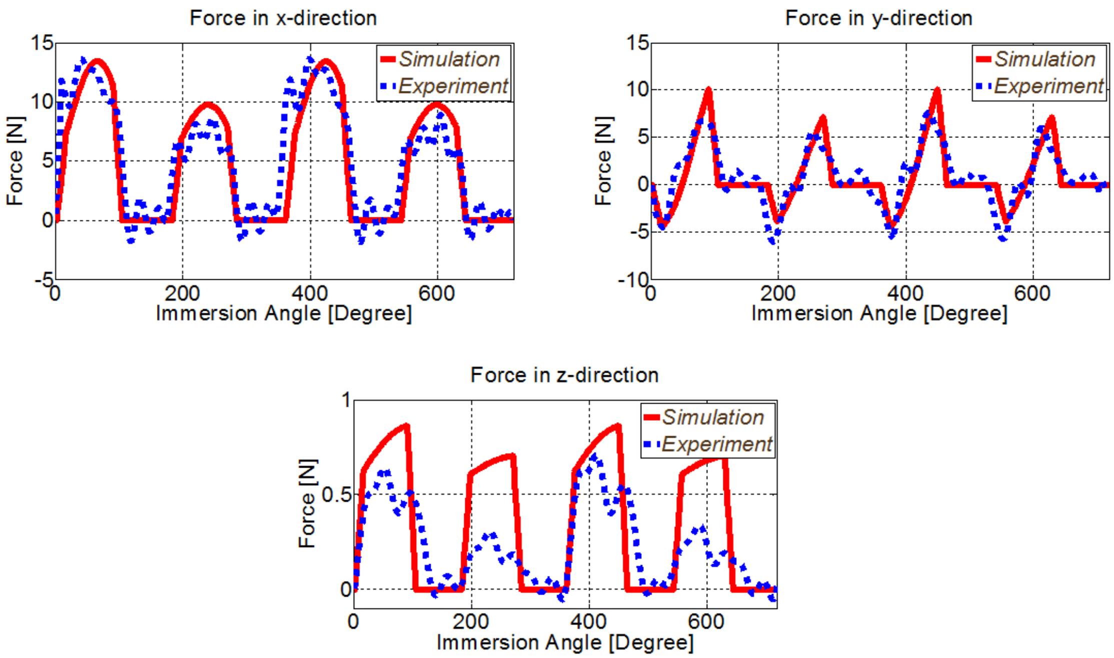

Figure 4-5 – Simulated and experimental forces in x, y and z directions for case 3

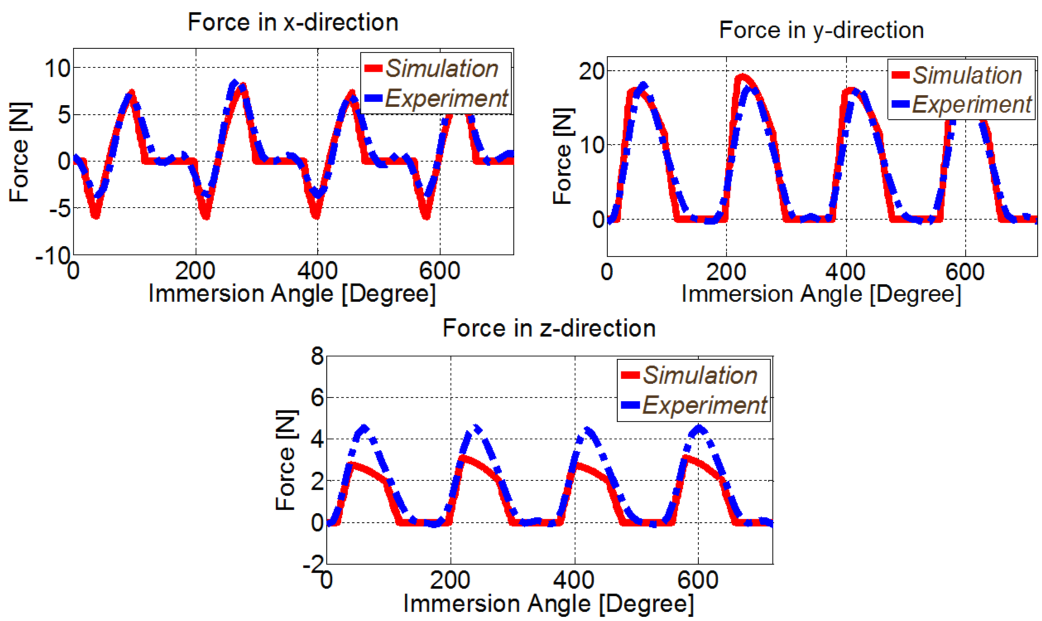

Figure 4-6 – Simulated and experimental forces in x, y and z directions for case 4

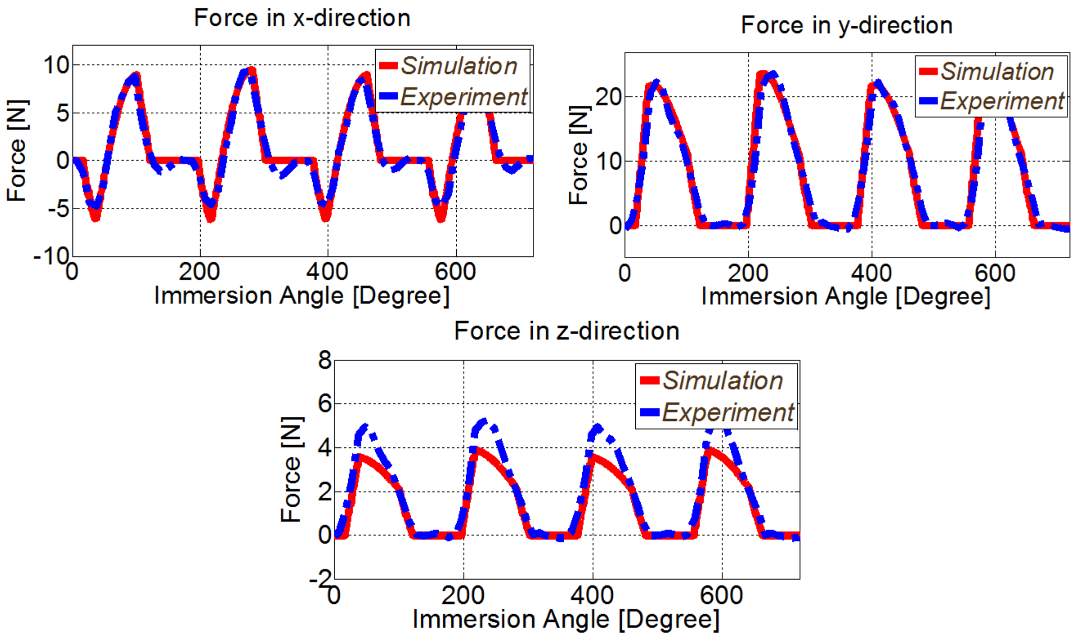

Figure 4-7 – Simulated and experimental forces in x, y and z directions for case 5

4.4 Force Simulations for Freeform Surfaces

Modeling of process kinematics is a key factor to improve machining quality, control and accuracy of machined parts with freeform surfaces. A new methodology for modeling of cutting forces for ball end mill is proposed in this chapter. The ball end mill is discretized to a finite number of flat end mills according to the local radius as shown in Figure 4-8 and forces calculated at each disk are integrated to calculated total cutting force in x and y directions. The cutting force calculation algorithm for flat end mill is described above in Section 4.2. In order to model cutting forces for freeform surfaces accurately, cutter-workpiece engagement should be calculated.

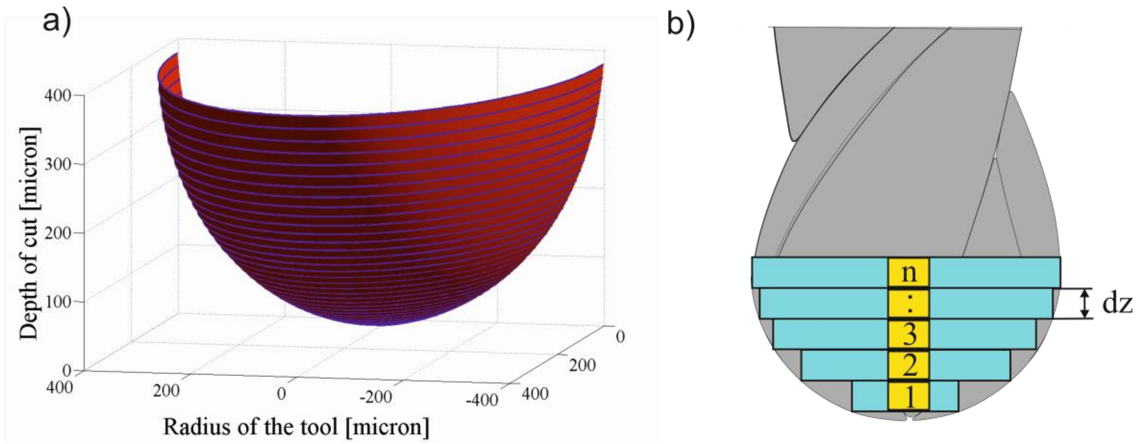

Figure 4-8 – a) Discretization of ball end mill, b) Schematic view of discretization

4.4.1 Cutter-Workpiece Engagement Calculation

Cutter workpiece engagement calculation plays an important role in the modeling of the kinematics of the cutting process. Cutter workpiece calculation method based on solid modeler is employed in proposed algorithm. In this method, the contact surface between tool and workpiece is calculated at each cutter location point. Later, from the cutter location file, swept volume of the tool is calculated and subtracted from a blank workpiece. After subtraction, entrance and exit angles of each discrete cutting disc are calculated. The cutter engagement input for force model is formed from calculated entrance and exit angles. In other words, cutter-workpiece engagement map or entry and exit angles of cutting flute as a function of tool height is considered as a boundary condition for prediction of the cutting forces. A detailed explanation of employed cutter-workpiece engagement model is presented by Yigit et al. [69]. The sample contact region for cutter location point and machined part are shown below in Figure 4-9.

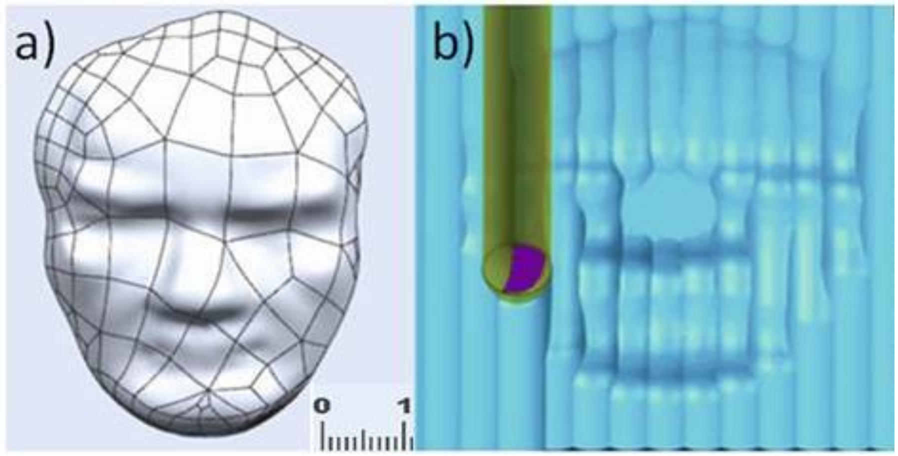

Figure 4-9 – a) CAD model of freeform surface, b) CAM simulation and tool workpiece contact region

4.4.2 Experimental Validation of Force Simulations for Freeform Surfaces

Cutting experiments are performed on Ti-6Al-4V grade Titanium alloy at 10.000 rpm spindle speed with 800 µm diameter ball end mill at the feed per tooth value of 5 microns. Edge radius of the tool is measured using white light interferometer, the average value of edge radius is 4 µm. Run out of the tool is measured as 2 µm and was considered during simulations of cutting forces. The cutting coefficients for Ti-6Al-4V with Tungsten Carbide ball end mill are given in Table 4-5. Cutting forces are simulated for two case studies: a freeform surface of Atatürk sculpture shown in Figure 4-10 and a freeform surface of impeller presented in Figure 4-13.

Table 4-5 – Cutting coefficients for Ti-6Al-4V with Tungsten Carbide ball end mill

	K_{tc} [N/mm²]	K_{tp} [N/mm³]	K_{te} [N/mm]	K_{rc} [N/mm²]	K_{rp} [N/mm³]	K_{re} [N/mm]
Disc 1	1080	4110	3.07	540	2300	1.04
Disc 2	397	3678	0.80	234	1660	0.61
Disc 3	286	1450	0.53	139	1036	0.46
Disc 4	158	850	0.39	95	632	0.24

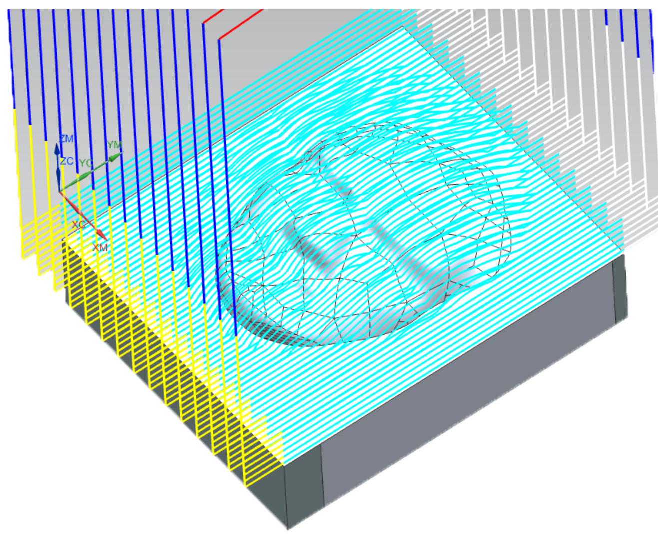

Figure 4-10 – Freeform surface of Atatürk sculpture

The machining is performed in six layers with 15 paths in each layer. Experimental force measurements are performed in order to validate the proposed force model. Estimated and measured forces in *x* and *y* directions for sample 13th path in the second layer are shown in Figure 4-11. The prediction accuracy of the proposed force model can be seen in Figure 4-12.

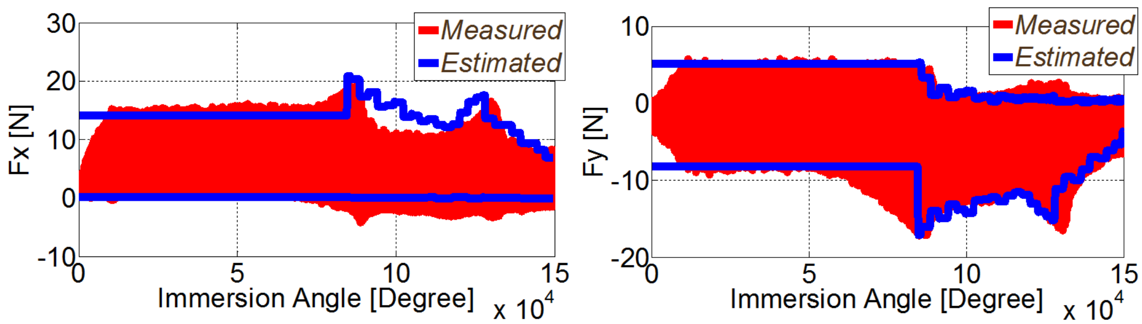

Figure 4-11 – Cutting forces in feed *(x)* and cross-feed *(y)* directions for single path

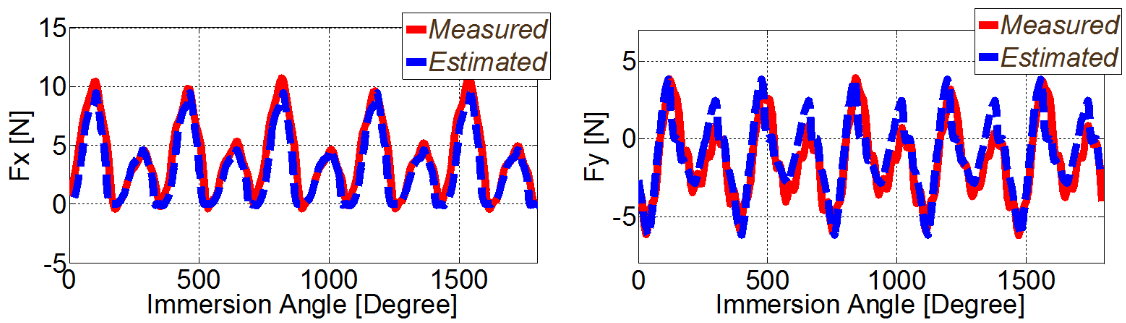

Figure 4-12 – Cutting forces in feed *(x)* and cross-feed *(y)* directions

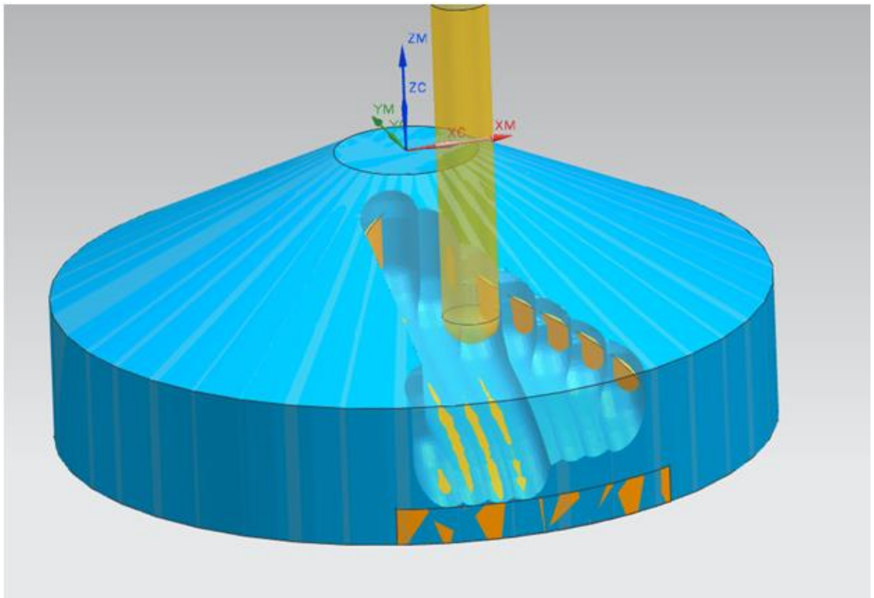

Figure 4-13 – Freeform surface of impeller

The machining of the impeller is performed in five layers with 8 paths in each layer. Experimental force measurements are performed in order to validate the proposed force model. Estimated and measured forces in *x* and *y* directions for sample 3rd path in the 4th layer are shown in Figure 4-14.

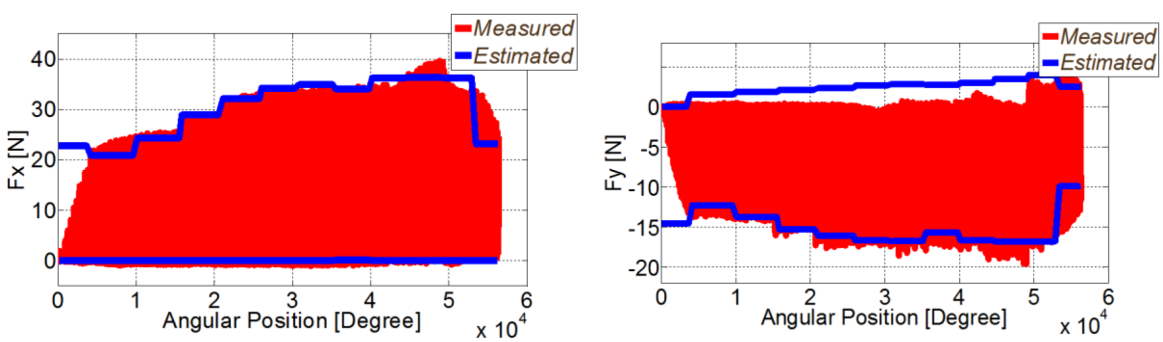

Figure 4-14 – Cutting forces in feed *(x)* and cross-feed *(y)* directions for single path

4.5 Summary

In this chapter, a new analytical model for predicting micro milling cutting forces is presented. The presented cutting force model is a function of cutting force coefficients, micro chip thickness model and tool edge geometry. This model precisely estimates micro milling cutting forces formed by both shearing and ploughing cutting mechanisms. The effect of different parameters like cutting speed, feedrate, axial depth of cut, edge radius and immersion is investigated. It is observed that effect of the edge radius is significant at low feedrates, this phenomenon can be explained by an increase of the ploughing forces. As the feedrate increases, the effect of the edge radius and ploughing forces becomes less significant. It means that manufacturing of micro tools with low edge radius is quite important for micro milling in order to decrease the effect of the ploughing forces. There are some assumptions made for proposed model. The workpiece is assumed to be uniform and rigid and the thermal effects are not considered in the presented model. These assumptions are reasonable for modeling of the micro milling process. Through the sets of the experiments, it was seen that presented force model estimates cutting forces accurately. The estimated cutting forces in X and Y directions for both flat and ball end mill tool geometries showed good agreement with experimental data. The main source of the difference of the estimated cutting forces in Z direction and experimental results is due to the fact that cutting forces acting on the bottom surface of the micro end mill were not considered during the modeling process.

Chapter 5
TOOL DEFLECTION IN MICRO MILLING OPERATION

5.1 Overview

Deflection of the tool is one of the major dimensional error sources during micro milling. The reason for this is low stiffness of micro tool. Due to this reason, cutting parameters during micro milling process should be selected correctly, in order to avoid the undercutting or overcutting issue and manufacture part within desirable tolerances.

So far, deflection models presented in the literature are for conventional milling and are not suitable for precise micro milling operation. Most of the available models consider the cutting force as point load applied to the tip of the tool. This assumption gives a rough estimation for a magnitude of the tool deflection.

In this chapter, a new mathematical model for estimation of instantaneous tool deflections during micro milling using FEM method is presented. Cutting forces for the deflection experiments are predicted from the model presented in Chapter 4 and validated through cutting experiments. Unlike applying the total forces at the tool tip as in the existing models in the literature, the newly presented micro tool deflection model considers cutting forces as distributed loads along cutting flutes in the workpiece tool contact zone. Presented deflection model is validated on Titanium Alloy (Ti-6Al-4V), through micro end milling experiments for a wide range of cutting conditions using laser displacement sensors.

5.2 Modeling Deflection Simulations

Deflection models presented in the literature, consider cutting force as a concentrated load applied to the tool tip. Consequently, these models can only give an approximate value of resulting tool deflections. This is because the cutting force applied on a cutting edge is not a point load, but a distributed load and contact area is a line. In the presented work, cutting force was implemented on the tool as a distributed load along the cutting edge, in order to have more precise modeling of deflection of the tool.

The tool is considered as a cantilever beam supported in the tool holder and modeled as a cylinder with variable cross sections. Due to the flute-groove design of the tool, it is not accurate to consider the radius of the cutter as the nominal radius of the tool section in deflection model. In order to overcome this problem, the equivalent diameter of the tool is determined based on its compliance factor. From calculations of moments of inertia of both solid cylinder and a fluted portion of the tool, effective diameter of a fluted portion of the tool was calculated as 80% of the nominal diameter. The tool is sliced into disks with discrete thickness and forces estimated by force model are applied on each the disk at certain cutter locations.

The tool is modeled as a two-dimensional Timoshenko beam element. Stiffness matrix of an element (K_e) is calculated for a two-dimensional Timoshenko beam element. Figure 5-1 shows a schematic view of Timoshenko beam element with 6 degrees of freedom (translation components as *U1, U2, U4, U5* and rotational components as *U3, U6*). Element nodal coordinates, modulus of elasticity E, shear modulus G, cross section area A, a moment of inertia I and shear correction factor K_s are the inputs for the beam element.

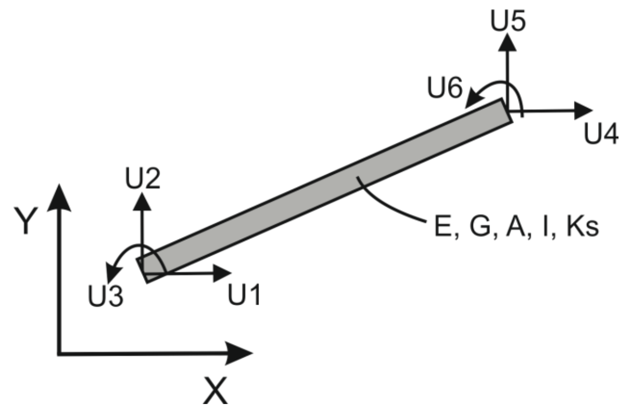

Figure 5-1 – Micro end mill is considered as a discretized Timoshenko beam element with six degrees of freedom

The shear correction factor for Timoshenko beam element is calculated as following:

$$K_s = \frac{5(1+\upsilon)}{6+5\upsilon} \qquad (5\text{-}1)$$

Above, υ is the poison ration of the cutting tool material defined as

$$\upsilon = \frac{E}{2G} - 1 \qquad (5\text{-}2)$$

Where E is modulus of elasticity and G is shear modulus.

The stiffness matrix of an element (K_e) is computed according to

$$K_e = \begin{bmatrix} \frac{EA}{L} & 0 & 0 & \frac{-EA}{L} & 0 & 0 \\ 0 & \frac{12EI}{L^3(1+\mu)} & \frac{6EI}{L^2(1+\mu)} & 0 & \frac{-12EI}{L^3(1+\mu)} & \frac{6EI}{L^2(1+\mu)} \\ 0 & \frac{6EI}{L^2(1+\mu)} & \frac{4EI\left(1+{}^{\mu}/_{4}\right)}{L(1+\mu)} & 0 & \frac{-6EI}{L^2(1+\mu)} & \frac{2EI\left(1-{}^{\mu}/_{2}\right)}{L(1+\mu)} \\ \frac{-EA}{L} & 0 & 0 & \frac{EA}{L} & 0 & 0 \\ 0 & \frac{-12EI}{L^3(1+\mu)} & \frac{-6EI}{L^2(1+\mu)} & 0 & \frac{12EI}{L^3(1+\mu)} & \frac{-6EI}{L^2(1+\mu)} \\ 0 & \frac{6EI}{L^2(1+\mu)} & \frac{2EI\left(1-{}^{\mu}/_{2}\right)}{L(1+\mu)} & 0 & \frac{-6EI}{L^2(1+\mu)} & \frac{4EI\left(1+{}^{\mu}/_{4}\right)}{L(1+\mu)} \end{bmatrix} \quad \textit{(5-3)}$$

$$\mu = \frac{12EI}{L^2GAk_s} \quad \textit{(5-4)}$$

Above L is the element length. The element matrices are assembled to the structure stiffness matrix K, in accordance with the Element Topology Matrix (*ETM*).

The element topology matrix is calculated as

$$ETM = \begin{bmatrix} el_1 & dof_1 & dof_2 & \cdots & dof_{ndof} \\ el_2 & dof_1 & dof_2 & \cdots & dof_{ndof} \\ \vdots & \vdots & \vdots & & \vdots \\ el_{nel} & dof_1 & dof_2 & \cdots & dof_{ndof} \end{bmatrix} \quad \textit{(5-5)}$$

Here, *nel* denotes the number of elements and *ndof* denotes the number of corresponding degrees of freedom. The first column is the element number, and the rest contain the corresponding degrees of freedom. Formed structure stiffness matrix K is as following

$$K = \begin{bmatrix} k_{11} & k_{12} & \vdots & \vdots & & \\ k_{21} & & \vdots & \vdots & & \\ \cdots & \cdots & k_{ii} + k_{ii}{}^{e} & k_{ij} + k_{ij}{}^{e} & \cdots & \cdots \\ \cdots & \cdots & k_{ji} + k_{ji}{}^{e} & k_{jj} + k_{jj}{}^{e} & \cdots & \cdots \\ & & \vdots & \vdots & & \\ & & \vdots & \vdots & & k_{nn} \end{bmatrix} \quad \textit{(5-6)}$$

Here, n is the number of discrete elements on the tool.

After structure stiffness matrix K is formed, displacements and reaction forces are calculated by solving the system of equations.

$$\begin{cases} K \times X_x = F_x \\ K \times X_y = F_y \end{cases} \tag{5-7}$$

F_x and F_y are respectively cutting forces vectors in x and y direction. Those vectors are predicted using the cutting force model introduced in Chapter 4. The micro end mill is modeled as sliced cylinder with variable cross-sections, as shown in Figure 5-2.

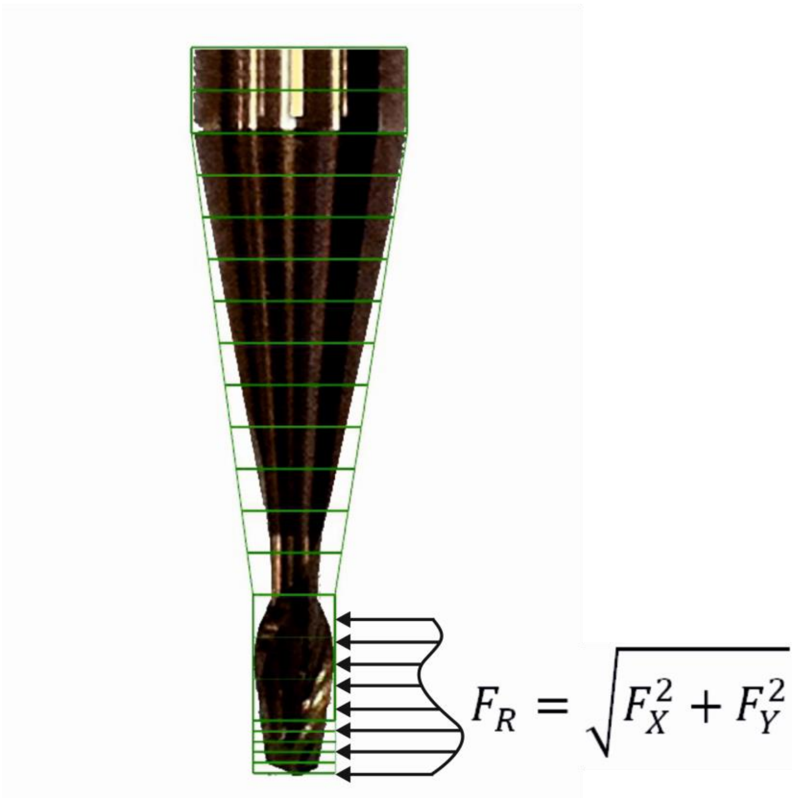

Figure 5-2 – Discretized model of micro end mill

5.3 Deflection Simulations and Experimental Validations

The simulations are validated by performing cutting experiments and measuring instantaneous tool deflection during the cutting process. Experiments are performed on Titanium alloy Ti-6Al-4V using 800 μm diameter two fluted Tungsten Carbide micro end mill on Mori Seiki NMV5000DCG 5-axis CNC milling machine. The tool deflection measurements are performed using a specially designed experimental setup with two laser sensors. The experimental setup used for force measurements is shown below in Figure 5-3 and schematic view of the setup is shown in Figure 5-4.

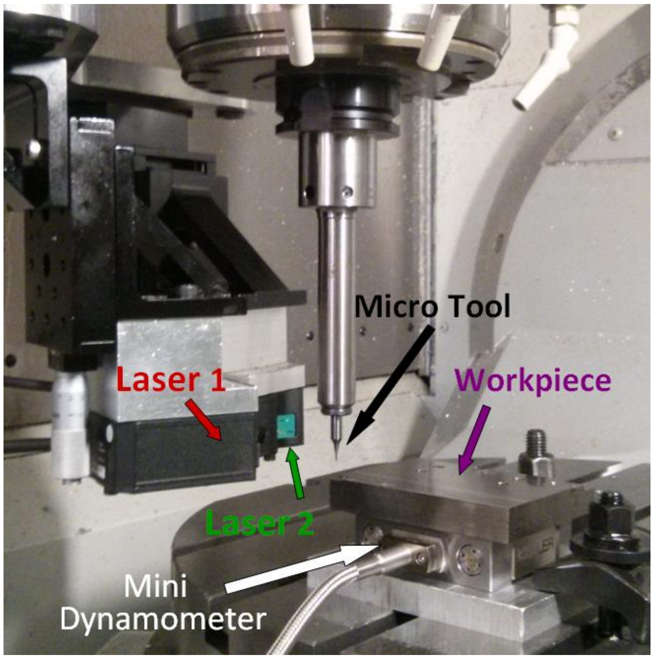

Figure 5-3 – Experimental setup for instantaneous force and deflection measurements in micro milling

A specially designed fixture was used to measure instantaneous tool deflection during the machining. The fixture orients two laser displacement sensor to measure the tool deflection in X and Y directions. Figure 5-5 shows the fixtured assembled on the spindle of CNC machining center.

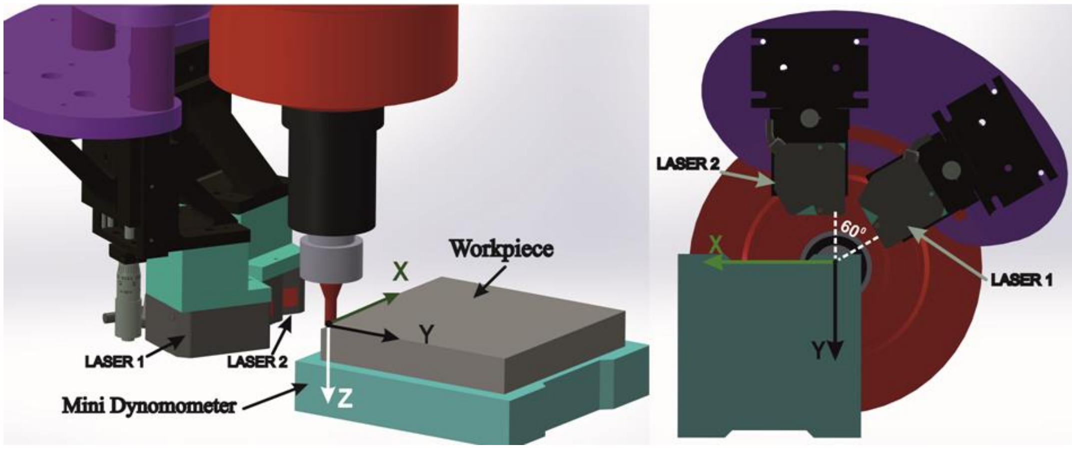

Figure 5-4 – Schematic view of experimental setup

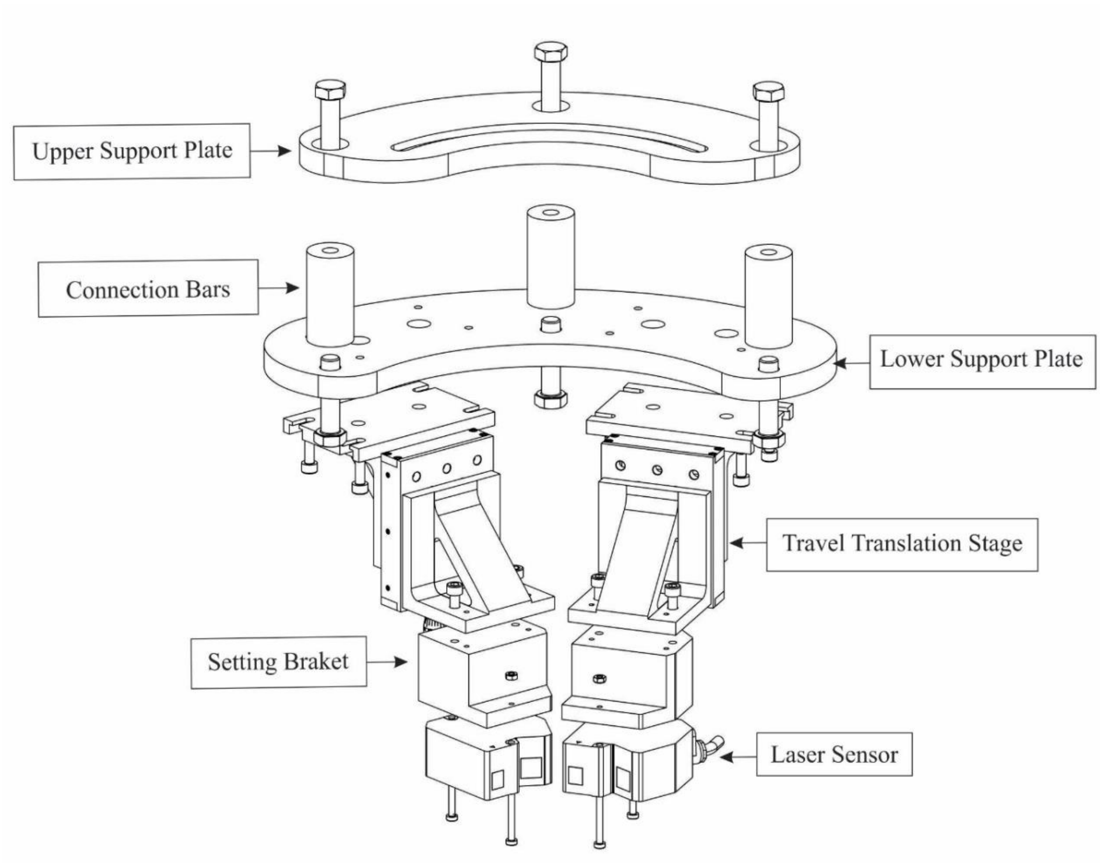

Figure 5-5 – Exploded view of the laser displacement sensor fixture

Cutting experiments were performed on Titanium alloy at 10.000 rpm spindle speed, at various cutting conditions given in Table 5-1. All cutting experiments were performed at half immersion cutting condition in order to measure tool deflection on the tool tip.

Table 5-1 – Cutting conditions for tool deflection measurement experiments

	Condition	Axial depth of cut [μm]	Feed per tooth [μm/rev-tooth]
Case 1	Down-milling	100	5
Case 2	Down-milling	100	7
Case 3	Down-milling	100	10
Case 4	Down-milling	200	5
Case 5	Down-milling	200	7
Case 6	Down-milling	200	10
Case 7	Up-milling	100	5
Case 8	Up-milling	100	7
Case 9	Up-milling	100	10
Case 10	Up-milling	200	5
Case 11	Up-milling	200	7
Case 12	Up-milling	200	10

Validation of the deflection model was also performed through experimental tool deflection measurements. Deflection of the tool was measured at the tool tip using two laser displacement sensors. . In Figure 5-7 – Figure 5-10 validation results for several cutting experiments are given and it can be seen that the simulation results are in a good agreement with experimental force measurements. All force and deflection measurements for cutting conditions presented in Table 5-1 are repeated three times.

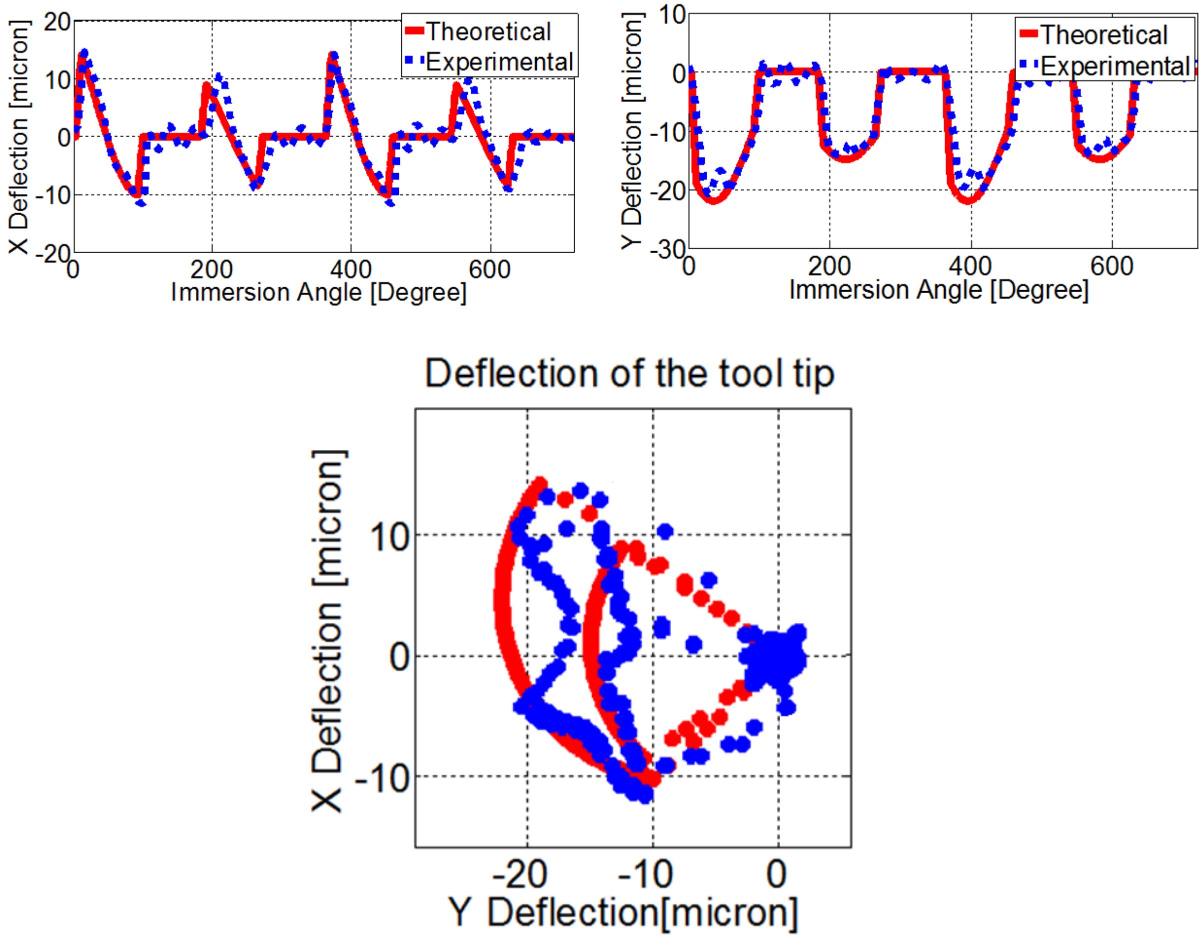

Figure 5-6 – Simulated and experimental deflection values of the tool tip in x and y direction for case 1

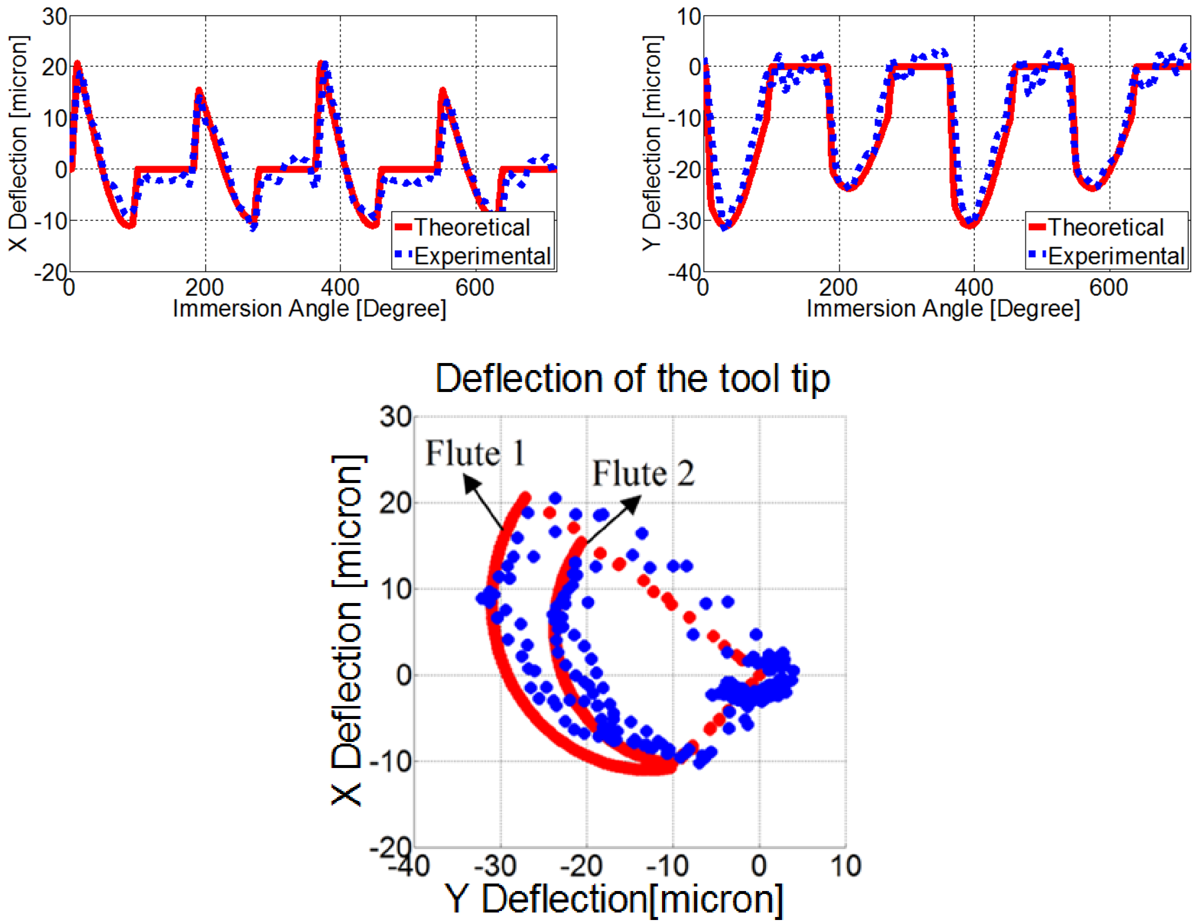

Figure 5-7 – Simulated and experimental deflection values of the tool tip in x and y direction for case 3

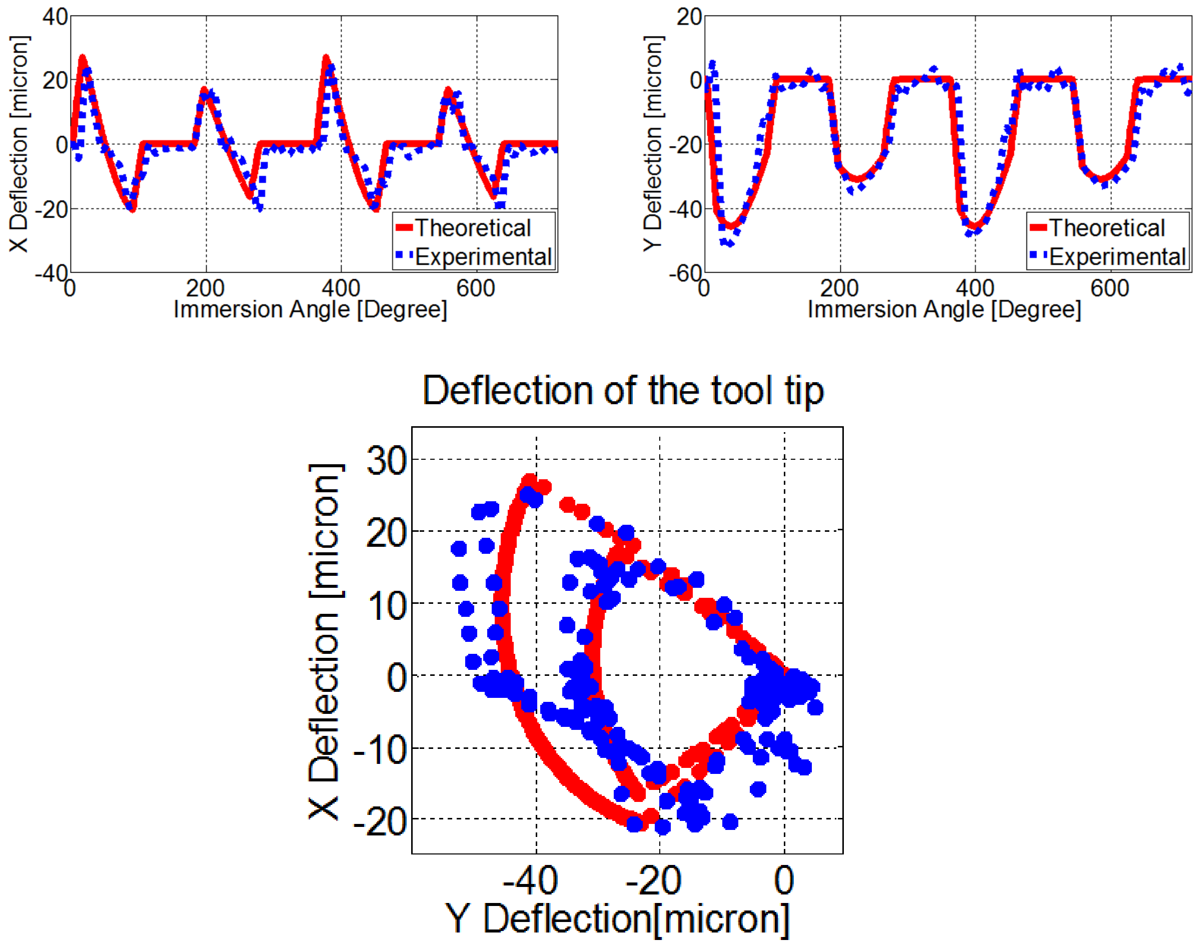

Figure 5-8 – Simulated and experimental deflection values of the tool tip in x and y direction for case 4

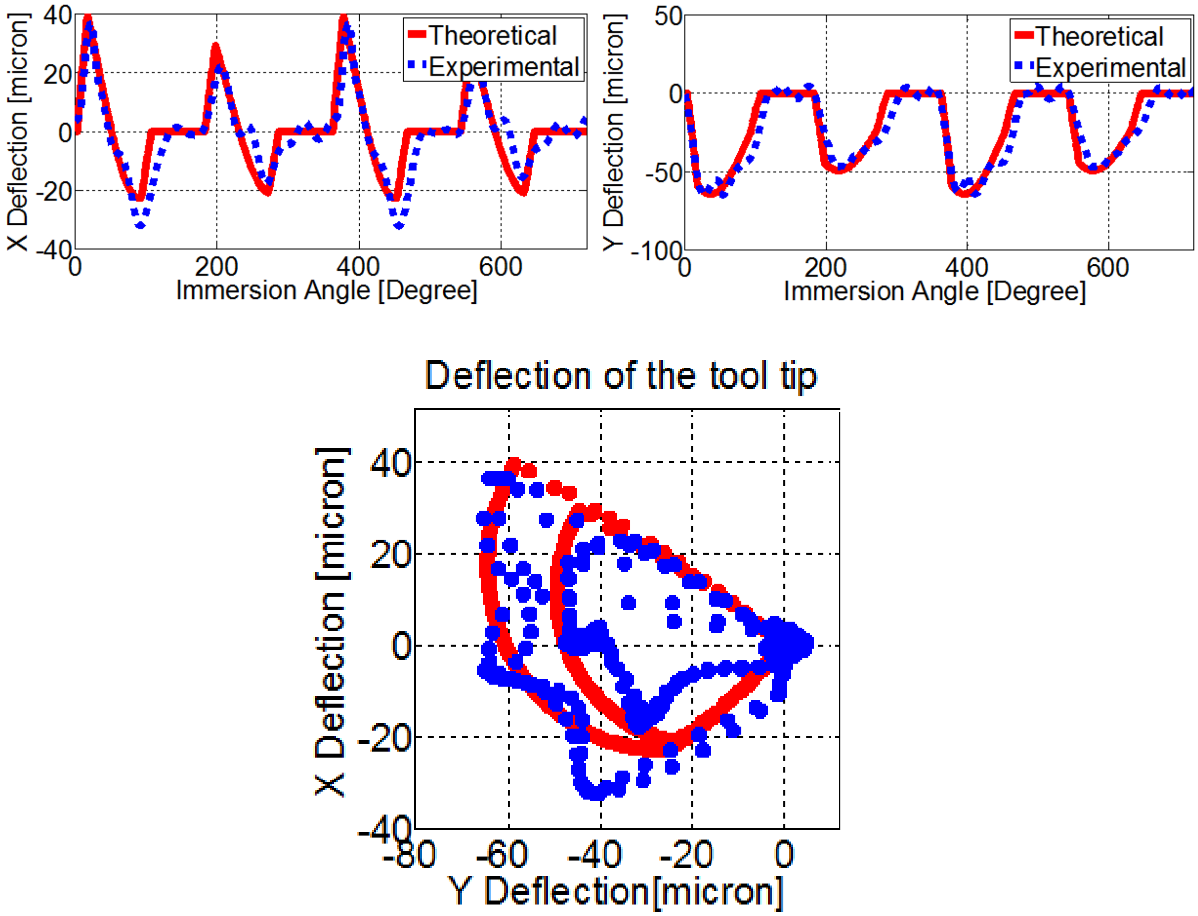

Figure 5-9 – Simulated and experimental deflection values of the tool tip in x and y direction for case 6

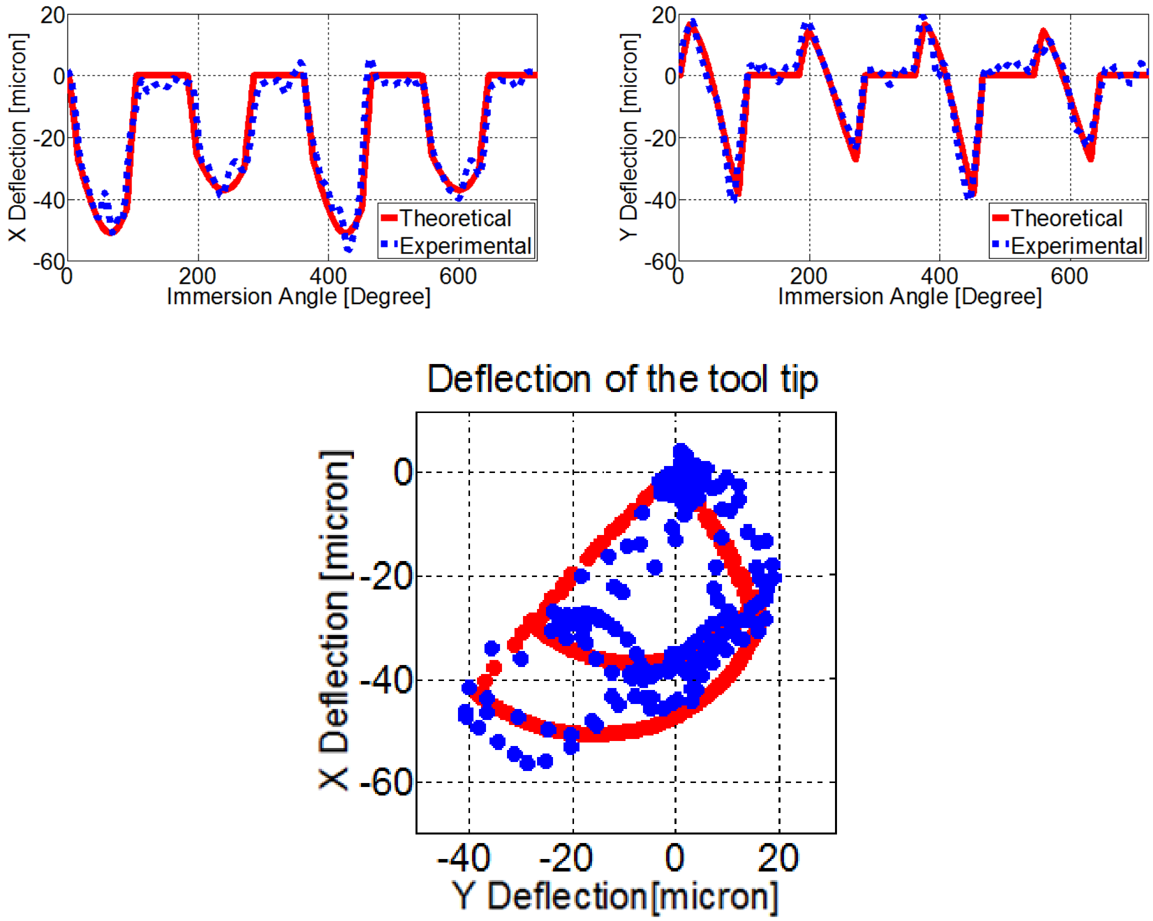

Figure 5-10 – Simulated and experimental deflection values of the tool tip in x and y direction for case 11

In order to validate a presented model, experiments have been performed with same cutting conditions and as it can be seen from Figure 5-11 the results of the experiments show that deflection model accurately estimates tool deflection formed during micro end milling process.

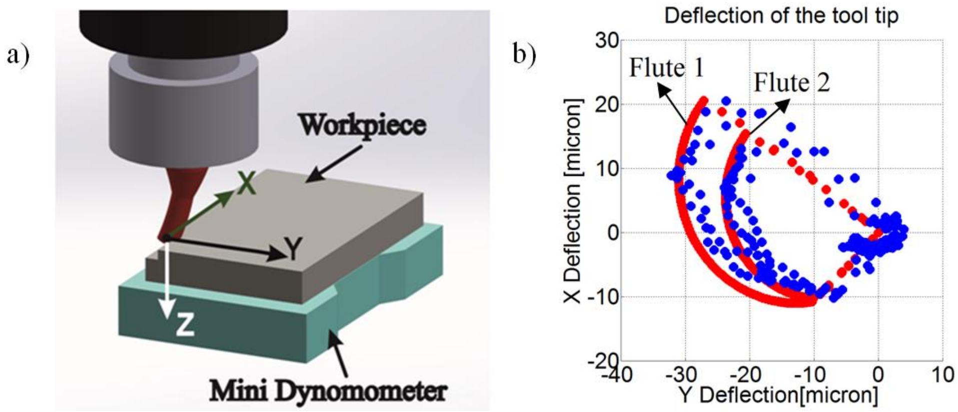

Figure 5-11 – a) Schematic view of deflection of the tool, b) simulated and experimental deflection values of the tool tip for case 3

5.4 Summary

In this paper, a new analytical model for estimating instantaneous deflections during micro milling is presented. This model consists of two parts: cutting force model and deflection model. The instantaneous cutting forces are estimated by force model presented in Chapter 4. The deflections of the micro end mill occurred due to the cutting forces acting on the tool are successfully estimated by presented deflection model. The deflection of the end mill is estimated by employing cantilever beam theory. The micro end mill is assumed as three sectional cylindrical cantilever beam, with effective radius at the fluted portion. Illustrated deflection model precisely estimates instantaneous deflections of micro end mill by applying cutting force to cutting flute portion which is in contact with workpiece material. Specially designed setup with two laser displacement sensors is used to validate deflection model. The experimental validation showed that the tool deflection is very sensitive to machining parameters and accurate measurement of it during milling process requires well-designed setup and fine adjustments. Through the sets of the experiments, it was seen that deflection model showed very good agreement with experimental data.

Chapter 6
FORCE BASED FEEDRATE SCHEDULING

6.1 Overview

Most of the small-sized Titanium parts with freeform geometries are machined using micro ball-end milling before polishing and other surface treatments. As the demand for parts with complex geometries increases, the need for increasing efficiency also increases. Decreasing the cycle time of the machining parts is important for the productivity. One of the potentials to decrease cycle time is the optimization of feedrate during the cutting process. In order to perform a precise and reliable feedrate scheduling algorithm, the kinematics and mechanics of milling process should be modeled. Using a mechanic force model presented in Chapter 4, it is possible to schedule the feedrate off-line. Based on the force model, a feed can be increased at the CL points that force is relatively lower. This idea tremendously leads to lower machining cycle time and higher productivity. In the proposed scheduling algorithm, CL files are extracted from CAM software and engagement map is calculated in a Parasolid solid modeler kernel. Then, by means of developed force model cutting forces are estimated. Estimated cutting forces for each CL are used in feedrate scheduling technique. The proposed algorithm is calculating appropriate feedrate at each CL point in order to keep cutting forces below a known threshold. Finally, it will be shown experimentally that this strategy is able to reduce the cycling time and increase the productivity.

6.2 Force Based Feedrate Scheduling Algorithm

Because of the complex geometry of free-form surfaces, operators tend to select conservative cutting parameters to avoid tool deflections, tool breakage and low surface quality. On the other hand, manufacturing with higher feedrates will result in an increase of productivity. It is possible to increase feedrate while staying in a safe region by considering kinematics of the cutting process. In order to model cutting forces for free form surfaces accurately, cutter-workpiece engagement should be calculated. A detailed explanation of employed cutter-workpiece engagement model developed by Yigit et al. [69] is presented in Section 4.4.1. The freeform surface of Atatürk portrait is employed for feedrate scheduling algorithm validation. The CAD geometry and machined part are shown below in Figure 6-1.

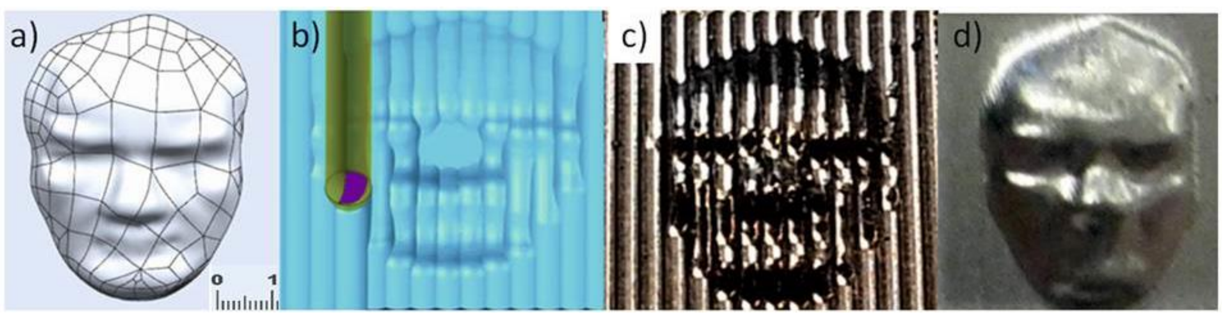

Figure 6-1 – a) CAD model of freeform surface, b) CAM simulation and tool workpiece contact region, c) Machined part after roughing, d) Machined part after finishing

6.2.1 Theory of Feedrate Scheduling Technique

The offline feedrate scheduling model presented here is able to adjust the feedrate values for each CL point based on cutting force model that was introduced in Chapter 4. In micro milling of freeform surfaces because of the fluctuation in the depth of cut and engagement domain, the resultant cutting force is not constant. By determining the cutting forces using above mentioned force model, appropriate feedrate values can be selected to keep the cutting forces below a threshold which is determined by the user. Scheduled feedrate for each CL point can be calculated as following:

$$f_{lim,i} = \left(F_{lim,i} - F_{1,i}\right) * \frac{f_2 - f_1}{F_{2,i} - F_{1,i}} + f_1 \qquad (6\text{-}1)$$

Here, $F_{1,i}$ is estimated resultant force at point i for feed f_1 and $F_{2,i}$ for feed f_2. $F_{lim,i}$ denotes threshold value of resultant cutting force for i^{th}CL point. Scheduled feedrate is calculated from process simulation at different constant feedrates by adjusting resultant cutting force at each CL point as shown in Figure 6-2.

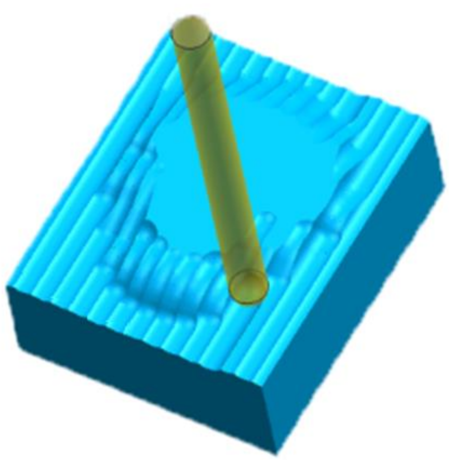

```
.
.
.
N1970 X5.141 Y2.379 Z-.506 F115.
N1971 X5.141 Y2.449 Z-.471 F122.
N1972 X5.141 Y2.519 Z-.435 F148.
N1973 X5.141 Y2.589 Z-.401 F134.
N1974 X5.141 Y2.659 Z-.372 F163.
N1975 X5.141 Y2.729 Z-.347 F150.
N1976 X5.141 Y2.799 Z-.325 F146.
N1977 X5.141 Y2.869 Z-.304 F179.
N1978 X5.141 Y2.939 Z-.287 F178.
N1979 X5.141 Y3.009 Z-.276 F189.
.
.
.
```

Figure 6-2 – A sample of NC code with scheduled feedrate for 13th path of second layer

6.3 Simulation Results and Validation

Experiments were performed on Mori Seiki NMV5000DCG 5-axis CNC milling machine using 800 μm diameter two fluted Tungsten Carbide micro ball-end mill. A freeform geometry was machined on Ti-6Al-4V grade 5 titanium alloy workpiece and cutting forces were measured with a table type mini dynamometer. The experimental setup and freeform part geometry used for validation of proposed models are shown in Figure 6-3 and Figure 6-4.Cutting conditions and tool specifications are presented in Table 6-1 and cutting coefficients for Ti-6Al-4V with tungsten carbide ball-end mill are presented in Table 6-2**.**

Figure 6-3 – Experimental setup

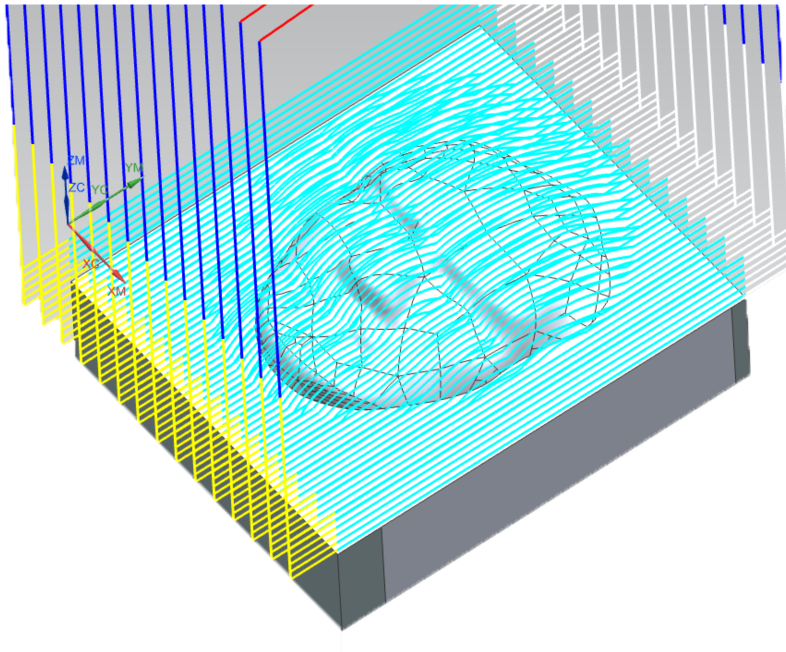

Figure 6-4 – Cutting tool path for entire sculptured geometry

Table 6-1 – Cutting conditions and tool specifications

Tool Diameter	800 [μm]
Number of flutes	2
Measured run-out	2 [μm]
Edge radius	4 [μm]
Spindle Speed	10000 rpm
Feedrate	100 mm/min
Step over	0.4 mm

Cutting tool path for the entire sculptured surface with the size of 6 mm x 7mm is shown in Figure 6-4. The machining was performed in six layers with 15 paths in each layer. Experimental force measurements are performed in order to validate the proposed force model. Estimated and measured forces in *x* and *y* directions for sample 13th path in the second layer are shown in Figure 6-5. The prediction accuracy of the proposed force model can be seen in Figure 6-6.

Table 6-2 – Cutting coefficients for Ti-6Al-4V with Tungsten Carbide ball end mill

	K_{tc} $[N/mm^2]$	K_{tp} $[N/mm^3]$	K_{te} $[N/mm]$	K_{rc} $[N/mm^2]$	K_{rp} $[N/mm^3]$	K_{re} $[N/mm]$
Disc 1	1080	4110	3.07	540	2300	1.04
Disc 2	397	3678	0.80	234	1660	0.61
Disc 3	286	1450	0.53	139	1036	0.46
Disc 4	158	850	0.39	95	632	0.24

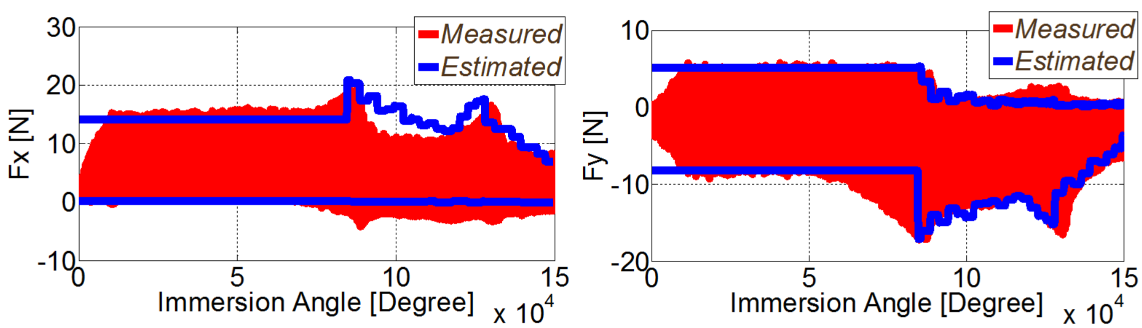

Figure 6-5 – Cutting forces in feed *(x)* and cross-feed *(y)* directions for single path

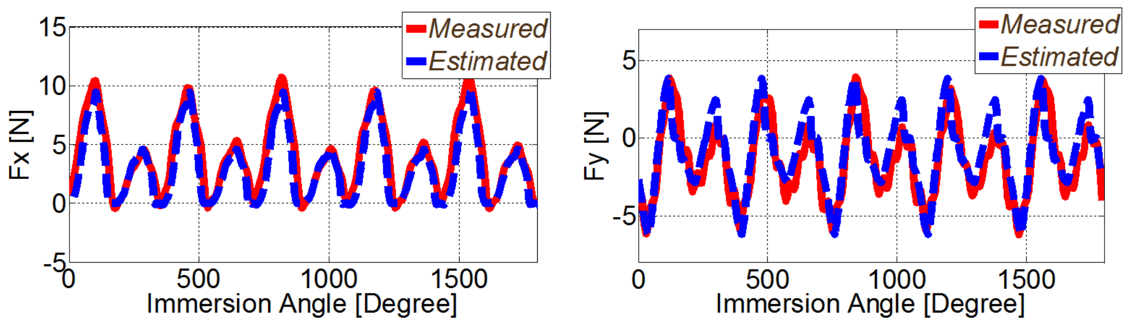

Figure 6-6 – Cutting forces in feed *(x)* and cross-feed *(y)* directions

The feedrate scheduling technique was validated through comparison of the set target value of resultant force with experiments for scheduling implemented case. Experiments were performed on the freeform surface. The feedrate scheduling algorithm calculates appropriate feedrate value for each CL point according to the selected threshold value of resultant cutting force. The threshold cutting force is the limitation for the resultant cutting force was set as $F_{lim} = 30\ N$ which is the maximum resultant cutting force for unscheduled milling.

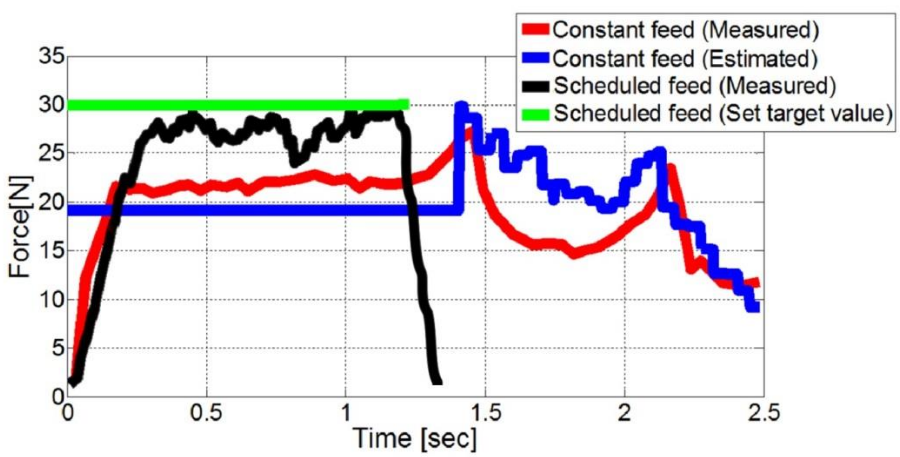

Figure 6-7 – Resultant cutting force magnitudes along tool path for the constant and scheduled feedrate cases

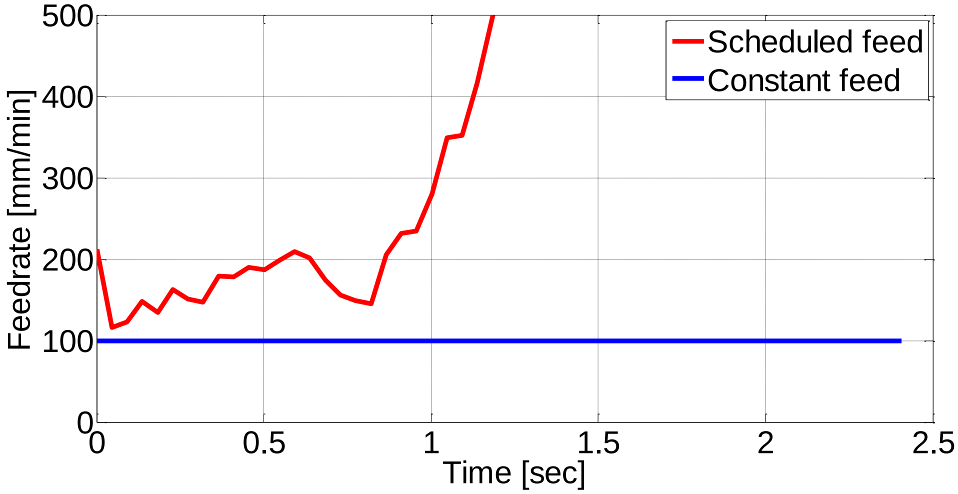

Figure 6-8 – Illustration of the scheduled and constant feedrate values

Figure 6-7 and Figure 6-8 show that if the feedrate is kept constant along the simple tool path, the resultant cutting force magnitudes are varying. In the constantan feedrate case, the time to complete one roughing path across the freeform part is 2.5 seconds. While in the case when the FFS technique is implemented in roughing by varying the feedrate according to the algorithm, the machining time decreases to 1.23 seconds in one tool path across the freeform surface. In the FFS case, the resultant cutting forces were also kept below 30 N, without exceeding the set target value. This example demonstrates that implementation of the forced based feedrate scheduling technique has a potential to decrease the cycle time in the micro milling of freeform surfaces.

6.4 Summary

In this section, an offline force based feedrate scheduling algorithm for rough cutting of parts with complex freeform surface geometries is proposed. This model consists of two parts: cutting force model and feedrate scheduling model. The cutting force model accurately estimates cutting forces during micro milling of parts with freeform surface geometries. By employing estimated forces proposed feedrate scheduling technique calculates appropriate feedrate at each CL point according to selected force threshold. The proposed technique drastically decreases cycle time for an entire cutting process. Since choosing conservative feedrates is one of the main obstacles in improving machining performance, developed model is considered to shorten machining time and increase productivity. Through the sets of the experiments, it was seen that feed rate scheduling model simulation results are in a good agreement with experiments. The force based feedrate scheduling technique considers the physics of cutting process and it is far beyond of nowadays geometry-based CAM technology and can be integrated with next generation CAM software in order to enhance machining performance.

Chapter 7
THERMAL MODELING OF MICRO MILLING

7.1 Overview

Thermal simulation of the micro machining is important since the heat generated during the metal cutting process directly affects material properties of the tool and the workpiece, deflection of the tool, geometrical tolerances and residual stresses produced in manufactured parts. Accordingly, modeling of temperature becomes essential for machining alloys with difficult thermo-mechanical properties like Ti-6Al-4V.

This article presents an analysis of micro end milling of titanium alloy using finite element modelling and experimental validations. In this work, energy formed in the primary zone and friction energy created at the chip - tool interface is estimated using analytical thermo-mechanical model. A finite element model of micro milling process was developed in multi-physics simulation software. The temperature distribution in the tool and the workpiece is estimated using the heat generated in primary and secondary deformation zones, originally calculated in the mechanical model. The cutting process was simulated as the time-dependent heat transfer model. Simulation results are validated through temperature measurement experiments on the workpiece using a specially designed set-up with thermocouples.

7.2 Shearing and Frictional Heat Generations

In order to develop a thermal model, mechanical model of micro milling process is required for the estimations of heat generation due to the shear and friction in the primary and secondary zones. A mathematical model of micro milling mechanics, including the shearing and ploughing, is used to predict the three-orthogonal cutting force components. Details of the micro milling mechanics and cutting force modeling can be found in the previously presented Chapter 4. The cutting force predictions from this mechanic model are employed as the inputs to the thermal model presented in this chapter.

In presented thermal modeling approach, it is assumed that the main heat inputs are generated in the primary and secondary deformation zones and modeled as instantaneous heat sources in the shear plane and on the chip-tool contact surface. Heat generated in the primary deformation zone due to the shearing is predicted as the following;

$$P_s(\theta) = V_s \cdot F_s(\theta) = \frac{V \cdot \tau_s \cdot a \cdot h(\theta) \cdot cos(\alpha_n)}{\cos(\phi_n - \alpha_n) \cdot \sin(\phi_c)} \qquad (7\text{-}1)$$

Here, P_s, V_s, V, F_s, τ_s, h, a, α_n, ϕ_n, ϕ_c and θ represent the shearing power, shear velocity, cutting velocity, shear force on shear plane, average shear flow stress, uncut chip thickness, depth of cut, normal rake angle, normal shear angle, shear angle and immersion angle, respectively.

Frictional power generated in the secondary deformation zone can be determined as

$$P_f(\theta) = V_c \cdot F_u = \frac{V \cdot F_R \cdot sin(\phi_n) \cdot sin(\beta_a)}{\cos(\phi_n - \alpha_n)} \qquad (7\text{-}2)$$

Here, P_f, V_c, F_u, F_R and β_a are friction power, chip velocity, friction force on the rake face, planar resultant cutting force and friction angle, respectively. Cutting forces, velocities acting on a differential cutting edge along the micro milling tool and related angels are presented in Figure 7-1.

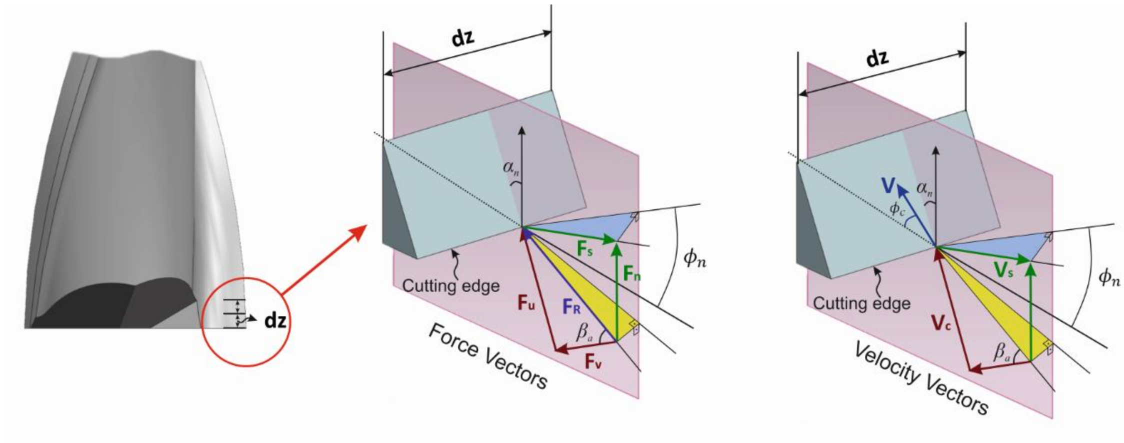

Figure 7-1 – Force and velocity components acting on cutting edge

The chip contact length and shear plane length were estimated by the following equations [46]:

$$l_c(\theta) \approx \frac{2 * h(\theta) * \sin(\phi_n + \beta_n - \alpha_n)}{\cos(\beta_n) * \sin(\phi_n)} \tag{7-3}$$

$$l_{sh}(\theta) \approx \frac{h(\theta)}{\sin(\phi_c)} \tag{7-4}$$

Where, l_c, l_{sh} and β_n are chip contact length, shear plane length and normal friction angle, respectively. Estimated shearing and frictional heat by the above equations are employed as the heat input sources to the shearing and frictional zones in the thermal simulations of the micro milling. Calculated frictional power is applied to tool-chip contact interface and calculated shearing power is applied to the shear plane. Both contact planes are also updated with geometry. It means that for the specified immersion angle, for instance, $\theta=30^0$, workpiece geometry is updated so that tool is at $\theta=30^0$ immersion, Frictional power $P_f(30)$ and shearing power $P_s(30)$ are calculated and applied to tool-chip contact zone $l_c(30)$ and shear plane $l_{sh}(30)$. Detailed explanation on heat application zones is shown in Figure 7-2.

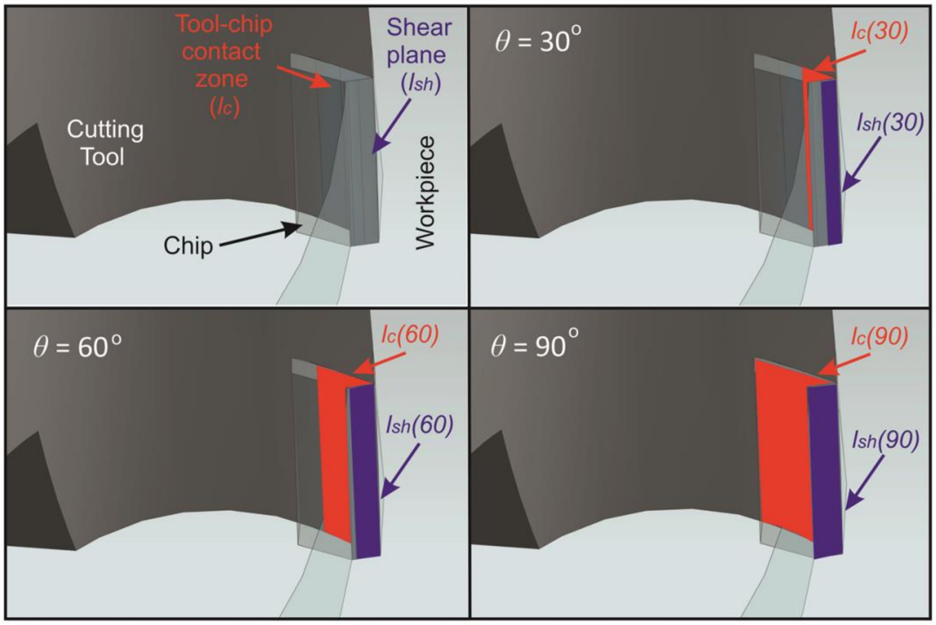

Figure 7-2 – Heat source application zones

7.3 Temperature Modeling

A finite element model of micro milling process is developed in the multi-physics Comsol software. The temperature distribution on the tool and the workpiece is estimated using the heat generated in primary and secondary deformation zones, originally calculated in the mechanical model. The cutting process is simulated as the time-dependent heat transfer model. Instantaneous tool and workpiece temperature fields are simulated for slot milling. A variable mesh density was implemented for the simulations. Simulations of the micro-milling process for full immersion cutting, shown in Figure 7-3, consist of a workpiece with chip geometry meshed with 150,000 tetrahedral elements and a micro end-mill meshed with 90,000 tetrahedral elements. The cutting region is meshed with extra fine mesh in order to obtain accurate temperature distributions.

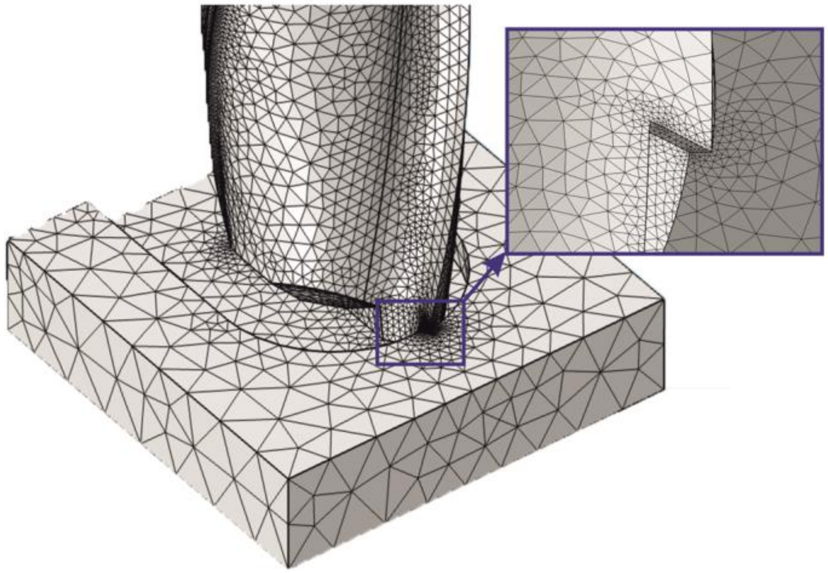

Figure 7-3 – Finite element model of micro milling

Convective cooling is applied to the outer surface of the tool and workpiece. According to Ozerdem [70], convection heat transfer coefficients for the stationary workpiece and cutting tool rotating at 10.000 rpm are assumed as h_w=10 W/m^2 ^{o}C and h_t=100 W/m^2 ^{o}C, respectively. Temperature-dependent thermo-physical properties of Ti-6Al-4V and Tungsten Carbide materials shown in Figure 7-4 are implemented. The friction and shear angles are assumed to be constant through whole immersion and calculated according to [67] as $\beta_a = 19.1 + 029\alpha_r$ and $\phi_c = {}^{\pi}/_{4} - \beta_a + \alpha_r$, respectively. The temperature simulations and experimental measurements are performed for the cutting conditions given in Table 7-1. Properties of the cutting tool and workpiece used in simulations are presented in Table 7-2.

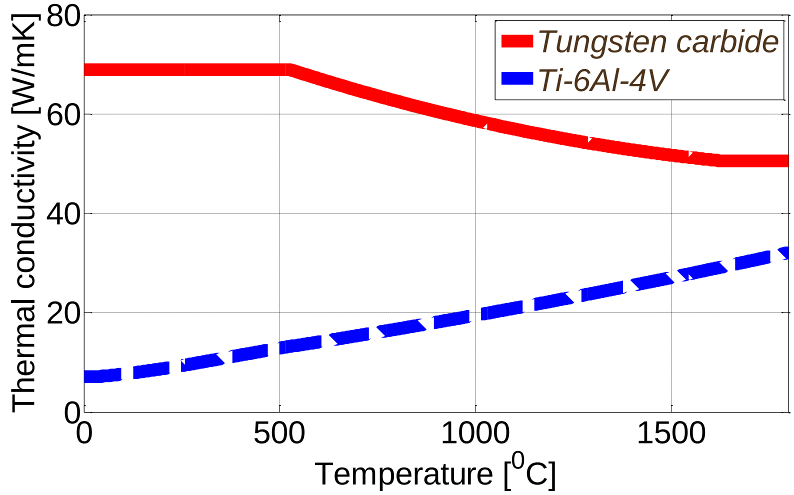

Figure 7-4 – Temperature dependent thermo-physical properties of Ti-6Al-4V and Tungsten Carbide materials

Table 7-1 – Cutting conditions for temperature simulations and cutting experiments

	Axial depth of cut [µm]	Feed-per-tooth [µm/rev-tooth]	Estimated planar resultant cutting force [N]	Measured planar resultant cutting force [N]	Chip tool contact length [µm]
Case 1	100	5	6.5	7.2	13.2
Case 2	100	10	9.4	10.5	26.4
Case 3	100	15	12.3	13.0	39.5
Case 4	150	5	9.8	10.2	13.2
Case 5	150	10	14.1	14.9	26.4
Case 6	150	15	18.4	19.1	39.5

Table 7-2 – Tool and workpiece properties

Tool Diameter	800 μm
Rake angle	8°
Edge radius of the tool	6 μm
Cutting speed	25.1 m/min
Shear stress of Ti-6Al-4V	613 MPa
Shear angle	32°
Friction angle	21°
Density of Ti-6Al-4V	4430 kg/m^3

Figure 7-5 shows the estimated frictional and shearing power. The computation time to complete 180^0 rotation of the micro end mill in the FE simulation on a computer with 8 GB RAM and 2.50 GHz CPU was approximately 54 minutes. Temperature fields in micro milling can be obtained at any immersion angles as shown in Figure 7-6.

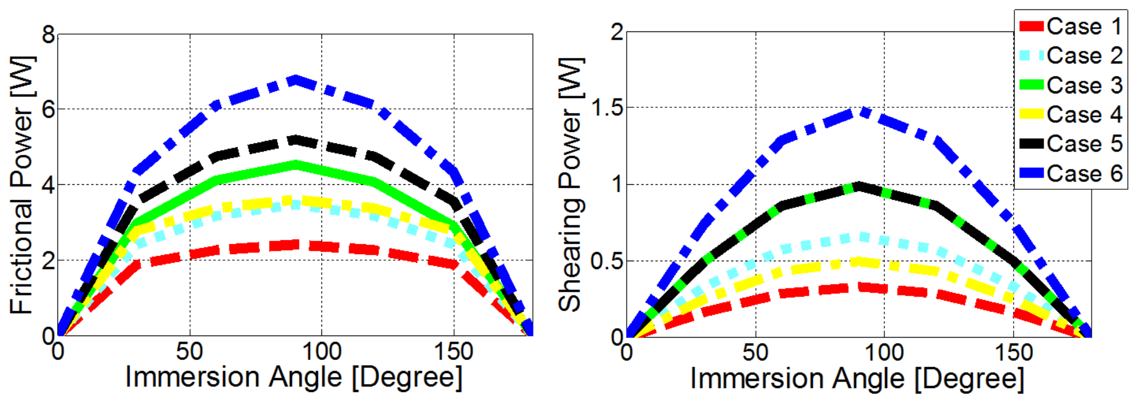

Figure 7-5 – Estimated frictional and shearing power

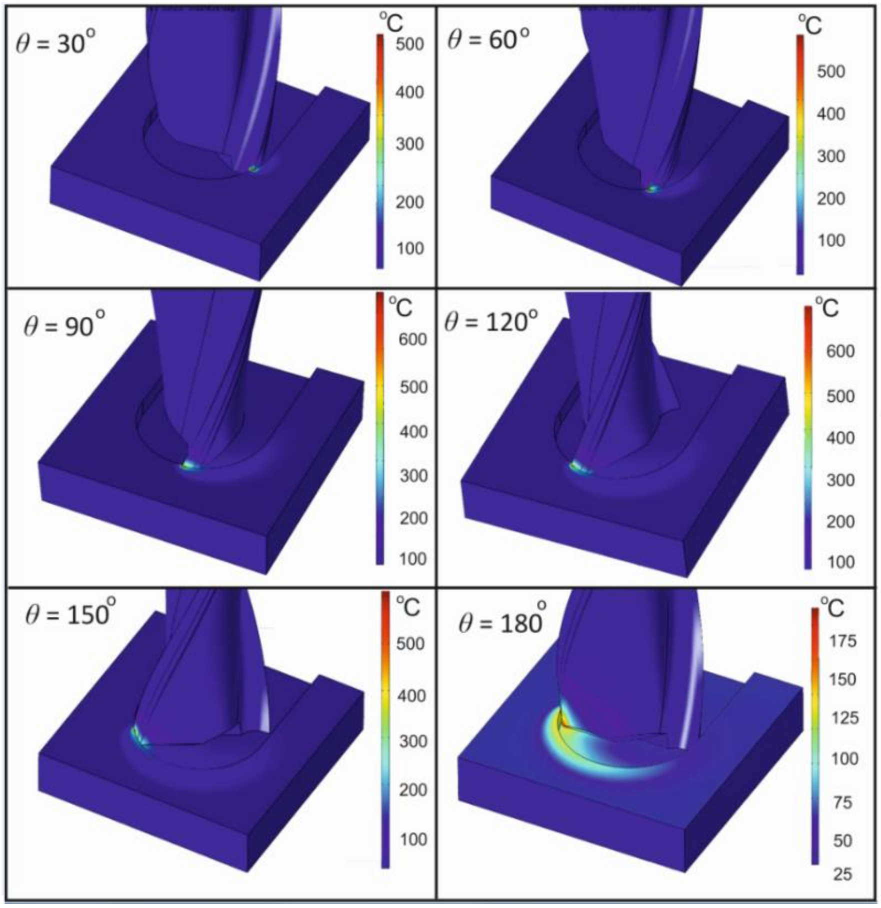

Figure 7-6 – An illustration of the temperature fields at various immersion angles

7.4 Experimental Setup and Validation

Experiments are performed on Titanium alloy Ti-6Al-4V grade 5 using 800 μm diameter two fluted Tungsten Carbide micro end mill on Mori Seiki NMV5000DCG 5-axis CNC milling machine. Force and temperature measurements are performed using Kistler 9256C Mini dynamometer and the specially designed setup is shown in Figure 7-7.

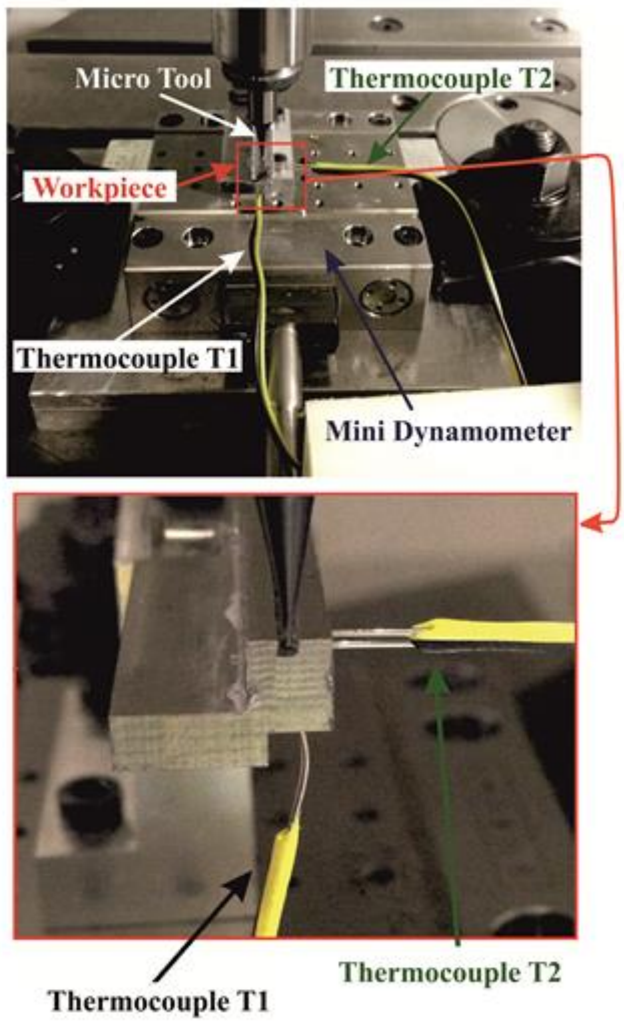

Figure 7-7 – An illustration of the experimental setup

Schematic view of the experimental setup is shown in Figure 7-8. Two K-type thermocouples with 130 µm diameter and 0.15 s response time are placed in certain positions to measure the temperature at the exit point (T2) of engagement and bottom point (T1). The distance between thermocouple T1 and cutting flute is set to 25 µm and the distance between thermocouple T2 and cutting flute is set to 15 µm. MX-2 thermal compound with high thermal conductivity and low thermal resistance is used to minimize temperature loss.

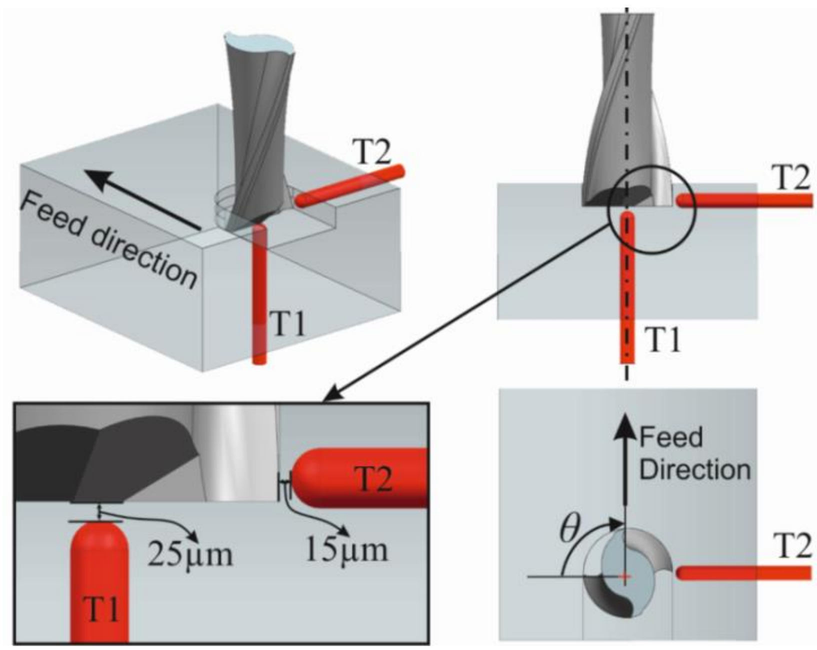

Figure 7-8 – Schematic view of the temperature measurement setup

Simulations are validated by experiments performed on titanium alloy at 10.000 rpm spindle speed (cutting speed of 25.1 m/min), at various cutting conditions given in Table 7-1. The temperature results of the simulations are evaluated at the same positions as that of thermocouples in the setup. The comparison of simulation results and workpiece temperatures measured experimentally at T1 and T2 points are shown in Figure 7-9 – Figure 7-14.

The temperature graphs show temperature measurement from a specific point for entire cutting operation and it can be seen from the signal that it gives peak when the cutting flute is passing by the thermocouple.

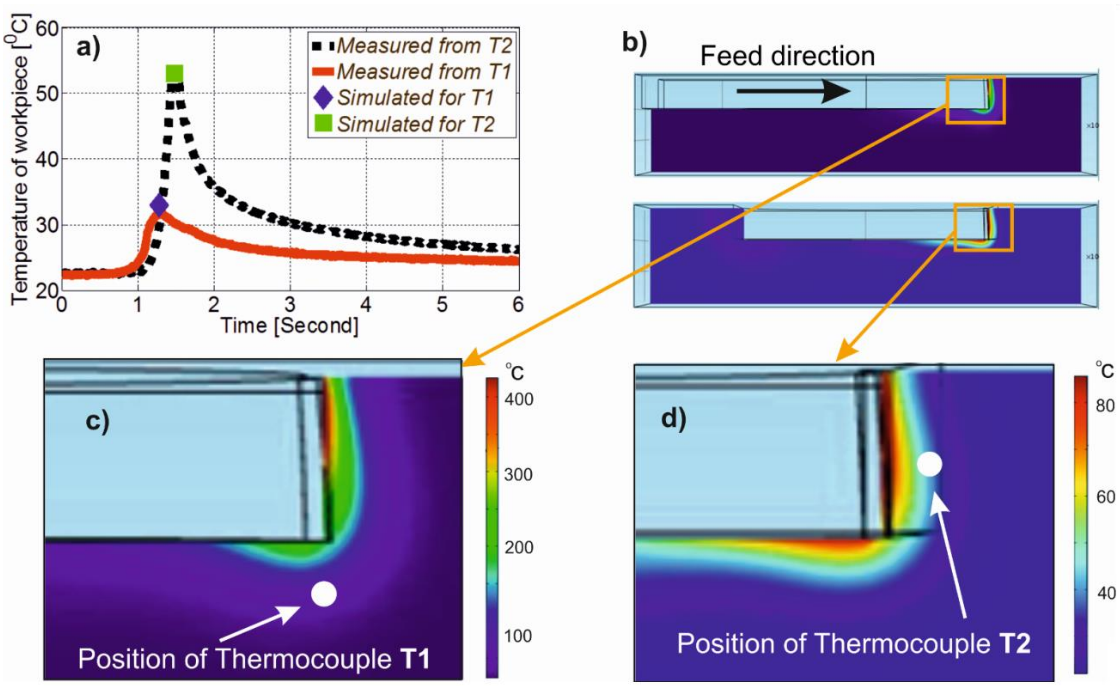

Figure 7-9 – a) Experimentally measured temperature for Case 1; b) Simulated temperature for Case 1; c) Temperature distribution field at $\theta = 90^o$; d) Temperature distribution field at $\theta = 180^o$.

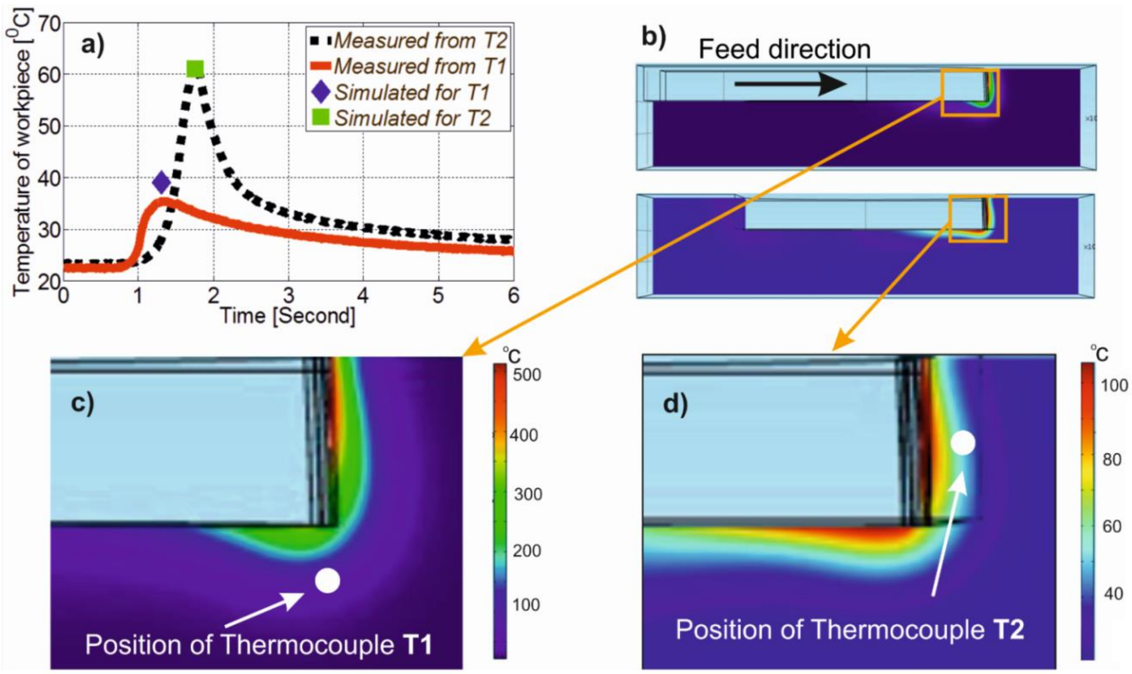

Figure 7-10 – a) Experimentally measured temperature for Case 2; b) Simulated temperature for Case 2; c) Temperature distribution field at $\theta = 90^o$; d) Temperature distribution field at $\theta = 180^o$.

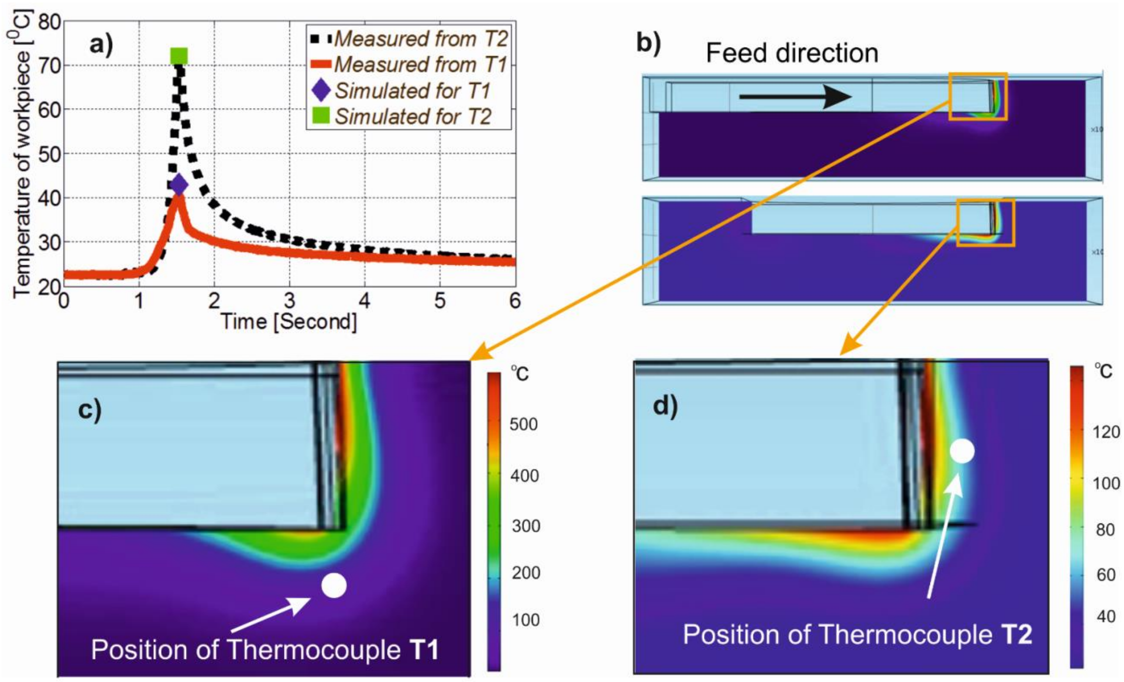

Figure 7-11 – a) Experimentally measured temperature for Case 3; b) Simulated temperature for Case 3; c) Temperature distribution field at $\theta = 90^o$; d) Temperature distribution field at $\theta = 180^o$.

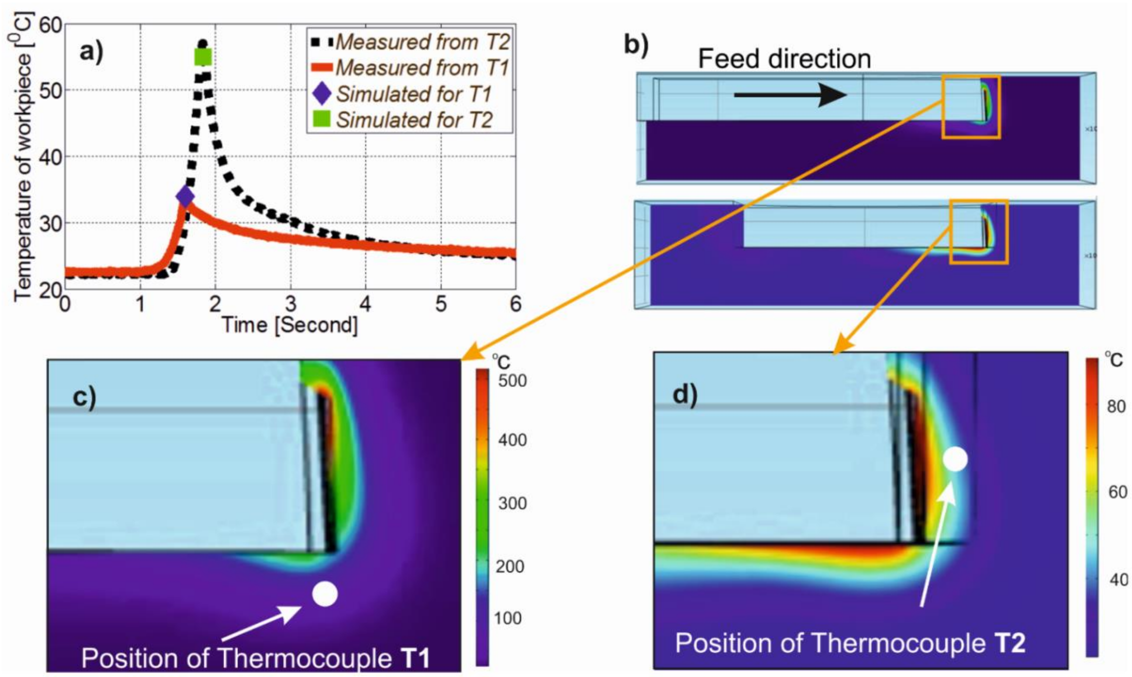

Figure 7-12 – a) Experimentally measured temperature for Case 4; b) Simulated temperature for Case 4; c) Temperature distribution field at $\theta = 90^o$; d) Temperature distribution field at $\theta = 180^o$.

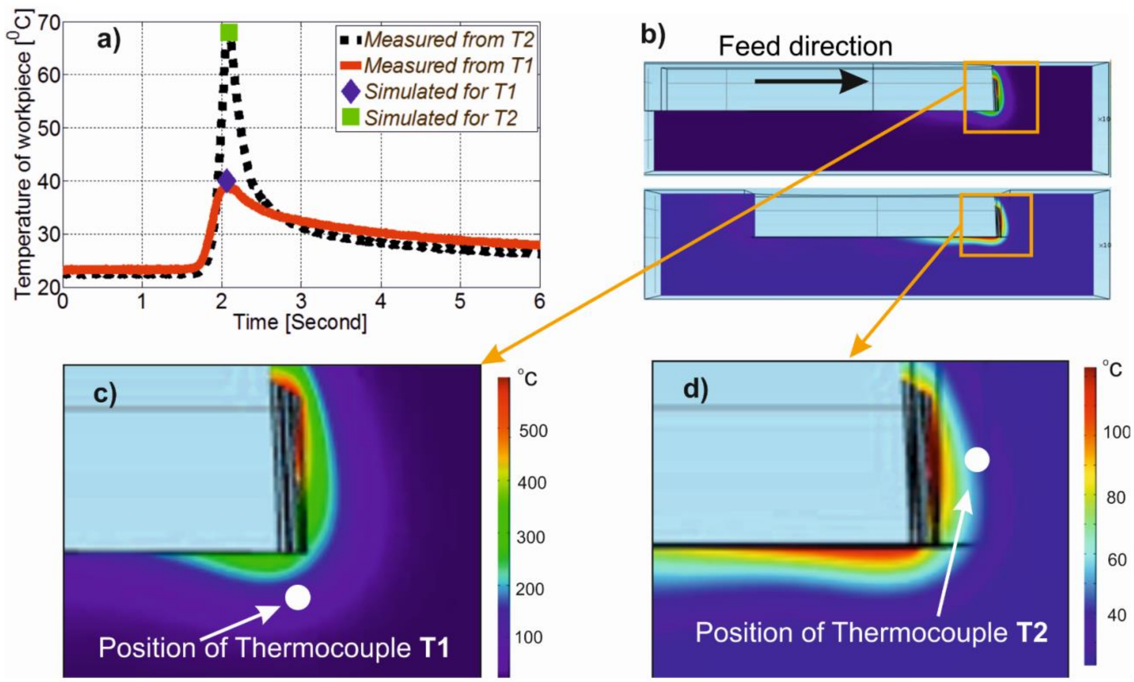

Figure 7-13 – a) Experimentally measured temperature for Case 5; b) Simulated temperature for Case 5; c) Temperature distribution field at $\theta = 90^o$; d) Temperature distribution field at $\theta = 180^o$.

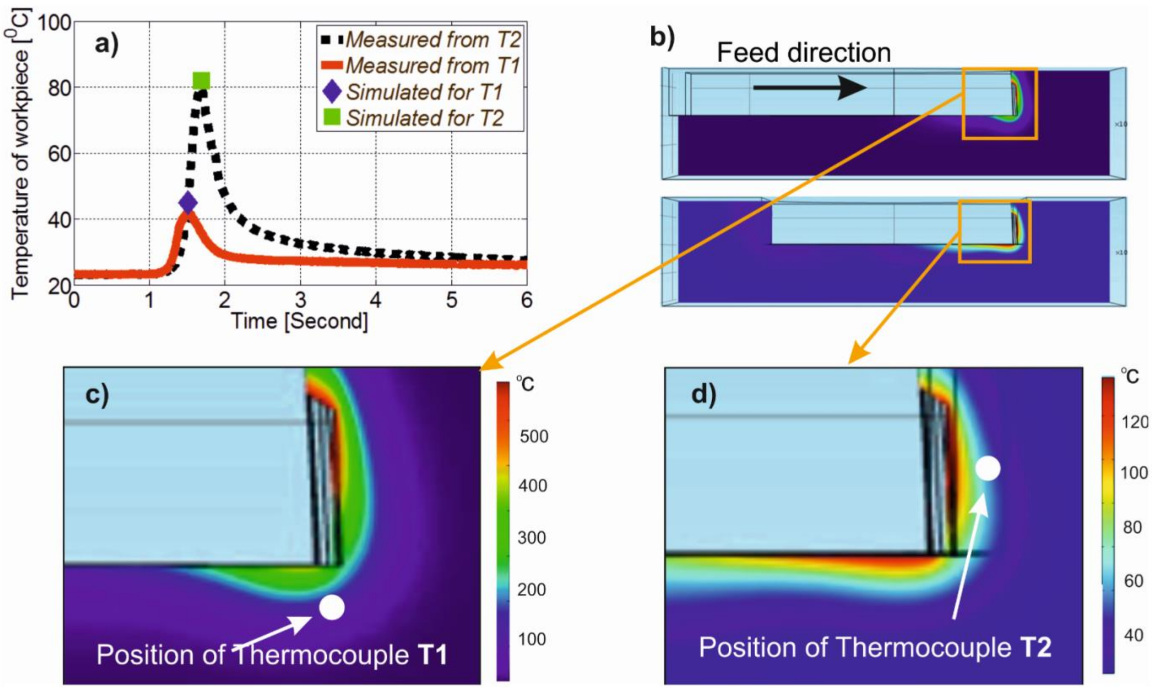

Figure 7-14 – a) Experimentally measured temperature for Case 6; b) Simulated temperature for Case 6; c) Temperature distribution field at $\theta = 90^o$; d) Temperature distribution field at $\theta = 180^o$.

Table 7-3 – Experimental and simulation results

	Temperature point	Simulation [℃]	Experimental [℃]	Simulated maximum temperature of the workpiece at $\theta = 90^o$ [℃]	Simulated maximum temperature of the workpiece at $\theta = 180^o$ [℃]
Case 1	T1	33	31.6	454	87
	T2	53	54.7		
Case 2	T1	39	35.3	518	110
	T2	61	61.5		
Case 3	T1	43	40.4	607	145
	T2	72	71.1		
Case 4	T1	34	32.8	523	96
	T2	55	57.0		
Case 5	T1	40	38.9	590	132
	T2	68	67.8		
Case 6	T1	45	41.9	655	164
	T2	82	79.5		

In order to investigate temperature during micro milling, fast response thermocouples placed at 15 μm and 25 μm distance from cutting zone were used. Considering the complexities of modeling of the micro milling process, it can be observed from Figure 7-9 – Figure 7-15 and Table 7-3 that the simulated temperatures are predicted with less than 12% error. The simulated maximum temperature of the workpiece presented in Figure 7-15-a also maintains the expected trend. Simulated temperature increases with chip load and at $\theta = 90^o$ when the chip load is maximum reaches its peak value. From simulation and experimental results, it was observed that the temperature is increasing with increasing feed and depth of cut.

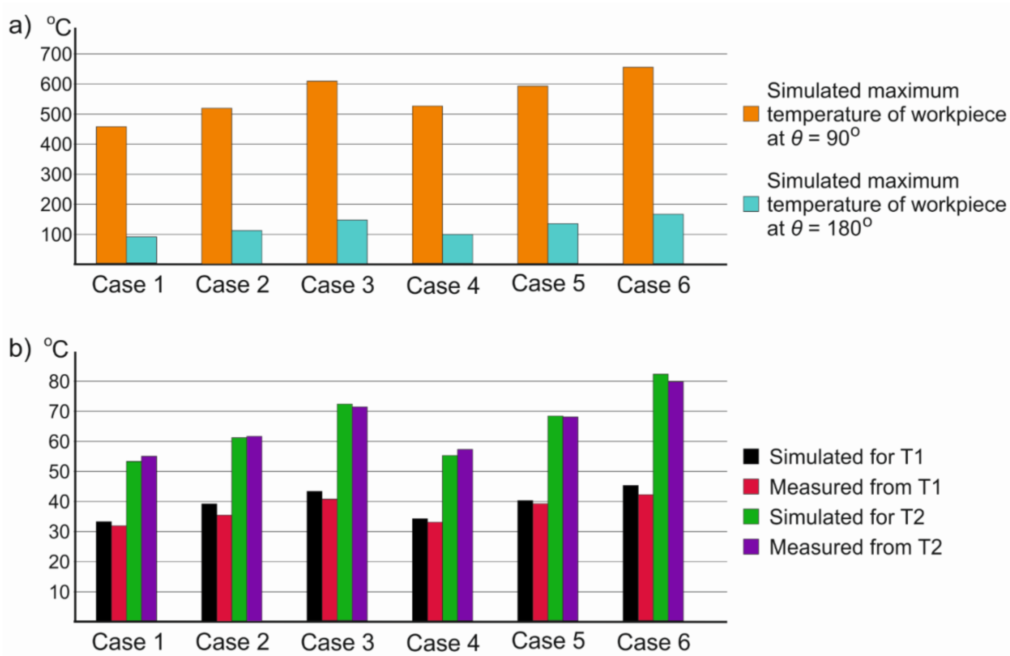

Figure 7-15 – a) Simulated maximum temperatures of the workpiece at $\theta = 90^{o}$ and $\theta = 180^{o}$; b) Experimental and simulation results at T1 and T2 points.

7.5 Summary

This chapter presents an analysis for micro milling of titanium alloy using finite element modelling and experimental approaches. The developed model uses semi-analytical approach to calculate the heat generated due to cutting process in the primary and secondary deformation zones. Using estimated heat inputs developed finite element model predicts tool and workpiece temperature fields in the micro milling process of Ti-6Al-4V under various cutting conditions. Estimated temperatures are validated by temperature measurements with thermocouples at the certain points in the micro milling experiments. Results showed that temperatures proposed by the thermal model are predicted with less than 12% difference for validated cases.

Chapter 8
MACHINING INDUCED DISTORTIONS

8.1 Overview

Nowadays, there are significant demands of hi-tech industries for high-performance micro milling of complex parts with freeform geometries. The performance of micro milling is highly dependent on the accuracy of the manufactured parts. By considering the mechanics of the process, it is possible to estimate the geometrical accuracy of manufactured part. In order to fulfill desired geometrical accuracy while machining a workpiece with thin wall geometry it is essential to model machining-induced distortions. Simulation of the machining-induced distortions is important since it directly affects the accuracy of manufactured micro parts. Due to this reason, it is crucial to predict distortions of the thin wall and develop strategies to prevent geometrical errors.

This chapter presents an investigation of micro milling induced distortions of thin wall workpiece made of Titanium alloy using finite element modeling approach. The factors affecting distortions – thermal and mechanical effects are considered in proposed model. The results from the previous developed thermal and force models are used as inputs for the distortion simulations. The effects of the cutting parameters, forces and cutting temperatures are investigated in proposed model. The model is validated through micro milling experiments and White Light Interferometer (WLI) measurements.

8.2 Modeling of Micro Milling Induced Distortions

Nowadays, manufacturing micro parts within tight tolerances is becoming more essential. Distortions are one of the major concerns while manufacturing micro parts with thin walls. Due to this reason it is important to estimate the amount of distortions and develop strategies to prevent them. In order to develop a model that simulates machining-induced distortions, it is necessary to have a clear understanding of mechanics and thermal aspects of the cutting process.

A finite element model for simulation of distortions is developed in multi-physics Comsol software. A combined effect of cutting force acting on the thin wall and temperature on the workpiece generated during cutting is applied to the thin wall as an input for simulation of distortion. The process is simulated as a time-dependent multi-physics problem consisting of structural mechanics and heat transfer. The elastoplastic material model with isotropic tangent modulus is employed in distortion simulations [71]. The workpiece is loaded with moving heat source and mechanical load at each axial depth of cut for a time period equal to the machining time. Later, thermal and mechanical loads are removed and workpiece undergoes elastic recovery, as the result total plastic deformation after machining is obtained for 12 different cutting conditions. The cutting conditions for experiments, cutting force acting on the thin wall ($\theta \approx 180^o$) and cutting temperatures during micro milling are given in Table 8-1. The tool and workpiece properties used in simulations are given in Table 8-2.

Table 8-1 – Cutting conditions for distortion simulations and cutting experiments

	Cutting speed [m/min]	Spindle speed [rpm]	Axial depth of cut [µm]	Feed rate [mm/min]	Feed rate [µm/rev-tooth]	Temperature of the workpiece [°C]
Case 1	25	10.000	50	100	5	60
Case 2	25	10.000	50	200	10	88
Case 3	25	10.000	100	100	5	85
Case 4	25	10.000	100	200	10	106
Case 5	25	10.000	150	100	5	90
Case 6	25	10.000	150	200	10	123
Case 7	50	20.000	50	200	5	72
Case 8	50	20.000	50	400	10	108
Case 9	50	20.000	100	200	5	110
Case 10	50	20.000	100	400	10	140
Case 11	50	20.000	150	200	5	120
Case 12	50	20.000	150	400	10	167

Table 8-2 – Tool and workpiece properties

Tool Diameter	800 µm
Rake angle	8°
Density of Ti-6Al-4V	4430 kg/m^3
Shear stress of Ti-6Al-4V	613 MPa
Young’s modulus of Ti-6Al-4V	110 GPa
Poisson’s ratio	0.34
Initial yield stress of Ti-6Al-4V	880 MPa
Isotropic tangent modulus of Ti-6Al-4V	1.25 GPa

In all cases cutting is full immersion, the length of the workpiece is 10 mm, the total depth of cut is 2 mm and thickness of the machined thin wall is 100 µm. At each axial depth of cut cutting forces acting on the thin wall are calculated from the force model presented in Chapter 4, where forces are calculated from Equation (8-1) as following:

$$\begin{bmatrix} dF_x \\ dF_y \\ dF_z \end{bmatrix} = \begin{bmatrix} \cos(\theta) & \sin(\theta) & 0 \\ -\sin(\theta) & \cos(\theta) & 0 \\ 0 & 0 & 1 \end{bmatrix} \left(\begin{bmatrix} K_{tc} h_\theta dz \\ K_{rc} h_\theta dz \\ K_{ac} h_\theta dz \end{bmatrix} + \begin{bmatrix} K_{te} dz \\ K_{re} dz \\ K_{ae} dz \end{bmatrix} + \begin{bmatrix} K_{tp} A_p dz \\ K_{rp} A_p dz \\ K_{ap} A_p dz \end{bmatrix} \right) \tag{8-1}$$

The temperature calculated from the thermal model is applied to the workpiece to cutting region via moving heat source. The temperature is calculated by the hybrid analytical a finite element temperature model presented in Chapter 7, where shearing and frictional heat formed during cutting is calculated from Equations (8-2) and (8-3) as following:

$$P_s(\theta) = V_s \cdot F_s(\theta) = \frac{V \cdot \tau_s \cdot a \cdot h(\theta) \cdot cos(\alpha_n)}{\cos(\phi_n - \alpha_n) \cdot \sin(\phi_c)} \tag{8-2}$$

$$P_f(\theta) = V_c \cdot F_u(\theta) = \frac{V \cdot F_R(\theta) \cdot sin(\phi_n) \cdot sin(\beta_a)}{\cos(\phi_n - \alpha_n)} \tag{8-3}$$

Here, P_s, P_f, V_s, V_c, V, F_s, F_u, F_R, τ_s, h, a, α_n, β_a, ϕ_n, ϕ_c and θ represent the shearing power, are friction power, shear velocity, chip velocity, cutting velocity, shear force on shear plane, friction force on the rake face, planar resultant cutting force, average shear flow stress, uncut chip thickness, depth of cut, normal rake angle, friction angle, normal shear angle, shear angle and immersion angle, respectively. Later analytically calculated shearing and frictional heat is applied to shear plane and tool chip interface and temperature distribution on tool and workpiece is calculated. As the result, temperature formed on the workpiece ($\theta \approx 180^o$ for our particular case) employed in distortion estimation model. The cutting force acting on the thin wall is calculated and applied in the model as an equivalent force (F_{eq}). The geometry of the workpiece and FE model is presented below in Figure 8-1.

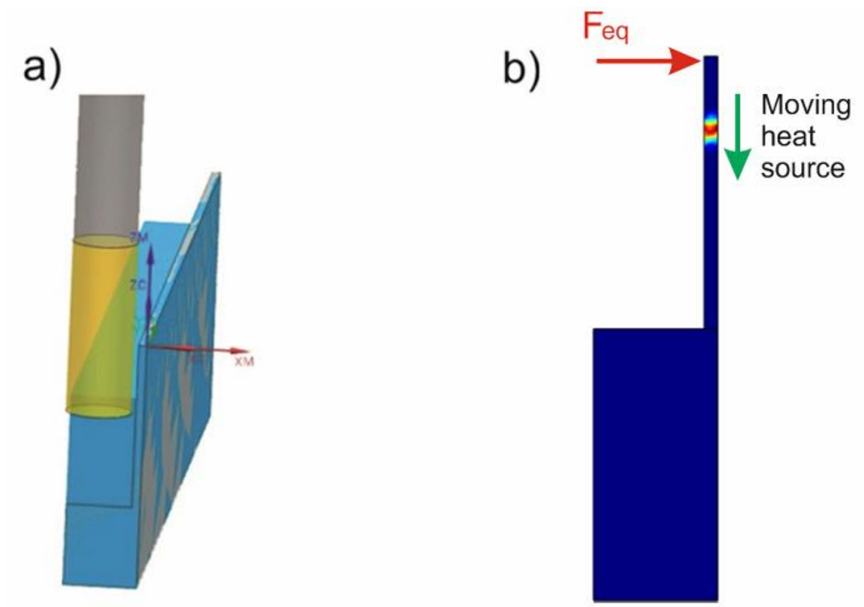

Figure 8-1 – a) CAM model of the workpiece; b) FE model of the distortion simulation.

The finite element model is meshed with extra fine mesh in order to obtain accurate distortion results. The minimum element size is 3 μm. The convective cooling is applied to the outer surface of the workpiece, the heat transfer coefficient for stationary workpiece is assumed to be h_w = 10 [W/m^2·^{o}C]. Temperature-dependent thermo-physical properties of Ti-6Al-4V material, shown in Equation (8-4), are implemented.

$$k_{Ti6Al4V}(T) = \begin{cases} 0.15 + 0.07 \cdot T - 2.88 \cdot 10^{-4} \cdot T^2 + 3.68 \cdot 10^{-7} \cdot T^3, & 0 < T \leq 311 \\ 8.11 - 0.14 \cdot T + 4.46 \cdot 10^{-5} \cdot T^2 - 2.27 \cdot 10^{-8} \cdot T^3, & 311 < T \leq 811 \end{cases} \quad (8\text{-}4)$$

The temperature distribution in the workpiece is calculated according to time-dependent heat transfer equation in solid bodies, shown in Equation (8-5).

$$\rho C_p \frac{\partial T}{\partial t} + k \nabla T = Q \quad (8\text{-}5)$$

Here, Q and ∇T are heat source and temperature gradient, ρ, k and C_p are material properties, which represent material density, thermal conductivity and heat capacity at constant pressure. Later temperature coupling is used to add temperature distribution calculated in the heat transfer module as an input to the solid mechanics module. At the same time thermal expansion is added to the model under linear elastoplastic material and calculated from Equation (8-6) as following:

$$\epsilon_{th} = \alpha \vartriangle T \tag{8-6}$$

Here, ϵ_{th} is a thermal expansion and α is the coefficient of thermal expansion. With addition of the thermal expansion, thermal stresses are included to the interface.

On the final stage, the results from mechanical loading and thermal expansion are combined in structural mechanics, where linear elastoplastic material model is used to calculate workpiece distortions. The elastic strain is calculated from linear elastic constitutive model and small plastic strains decomposition is used, since Ti-6Al-4V material does not have hyperelastic characteristics. As the result, the total strain is

$$d\varepsilon = d\varepsilon_e + d\varepsilon_p \tag{8-7}$$

where, elastic strain $d\varepsilon_e$ is fully recoverable and plastic strain $d\varepsilon_p$ cannot be recovered and calculated from following flow rule:

$$d\varepsilon_p = d\lambda \frac{\partial f}{\partial \sigma} \tag{8-8}$$

The von-Mises stress criterion is used to define the limit of elastic regime and an isotropic hardening parameter $d\lambda$ described by isotropic tangent modulus is employed to define hardening model.

As the result, thermal and mechanical loads are removed and workpiece undergoes elastic recovery and total plastic deformation after machining is obtained for 12 different cutting conditions.

8.3 Experimental Setup and Validation

Experiments are performed on Titanium alloy Ti-6Al-4V grade 5 using 800 μm diameter two fluted Tungsten Carbide micro end mill on Mori Seiki NMV5000DCG 5-axis CNC milling machine. Force measurements are performed using Kistler 9256C mini dynamometer and distortion measurements are performed by Keyence LK – 030 laser sensor and later by White Light Interferometer. The specially designed setup is shown in Figure 8-2.

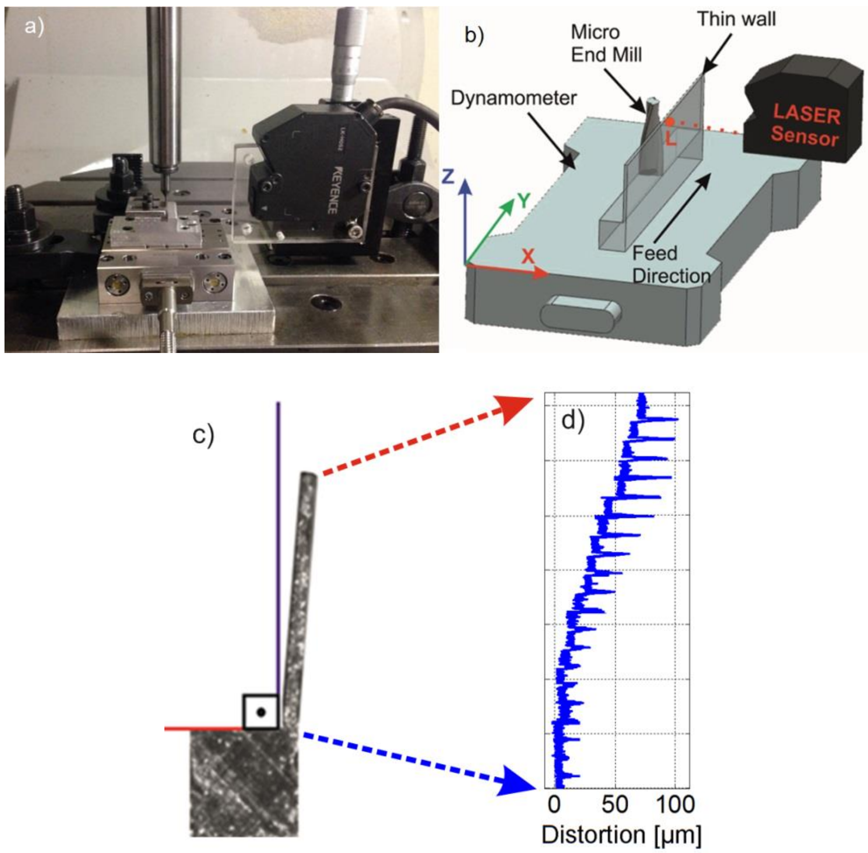

Figure 8-2 – a) Experimental setup, b) an illustration of the experimental setup, c) Microscope view of distorted part, d) Laser measurement of Case 10

The distortion of the workpiece was measured by laser sensor during a machining operation. Laser measurement data provides extremely important information about cutting process. As it is seen from Figure 8-3 laser measurement data contains information about total plastic deformation and amount of elastic deformation during cutting process. On top of the plastic deformation peaks in the data correspond to elastic deformation during cutting of the thin wall. The number of peaks equals to a number of cutting passes and FFT frequency analysis of the peak showed that tool pathing frequencies are dominant, which means that peaks occur due to the interaction of the tool and workpiece.

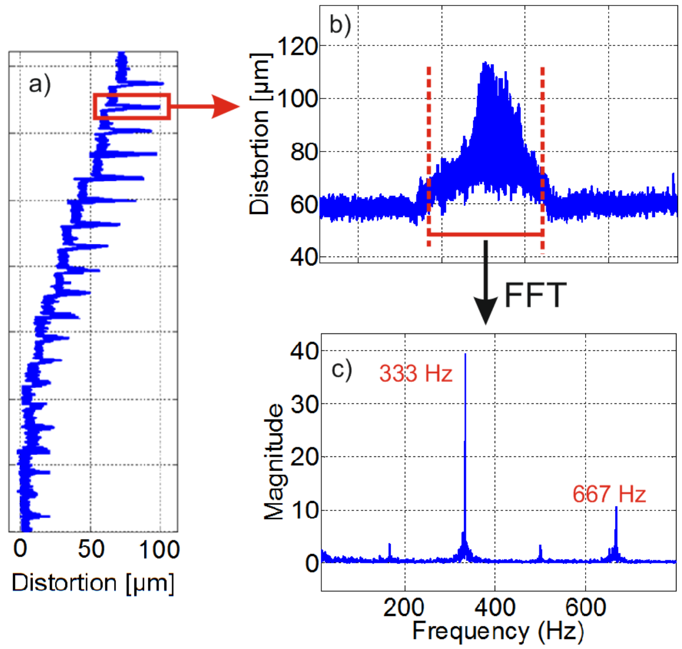

Figure 8-3 – a) Laser measurement of Case 10, b) Zoomed peak, c) FFT analysis of peak

Later distortion is verified by white light interferometer measurement. The WLI measurement was performed on the back side of a machined surface. The simulation and experimental results for some cases with different cutting conditions are presented below in Figure 8-4 –Figure 8-8 and Table 8-3.

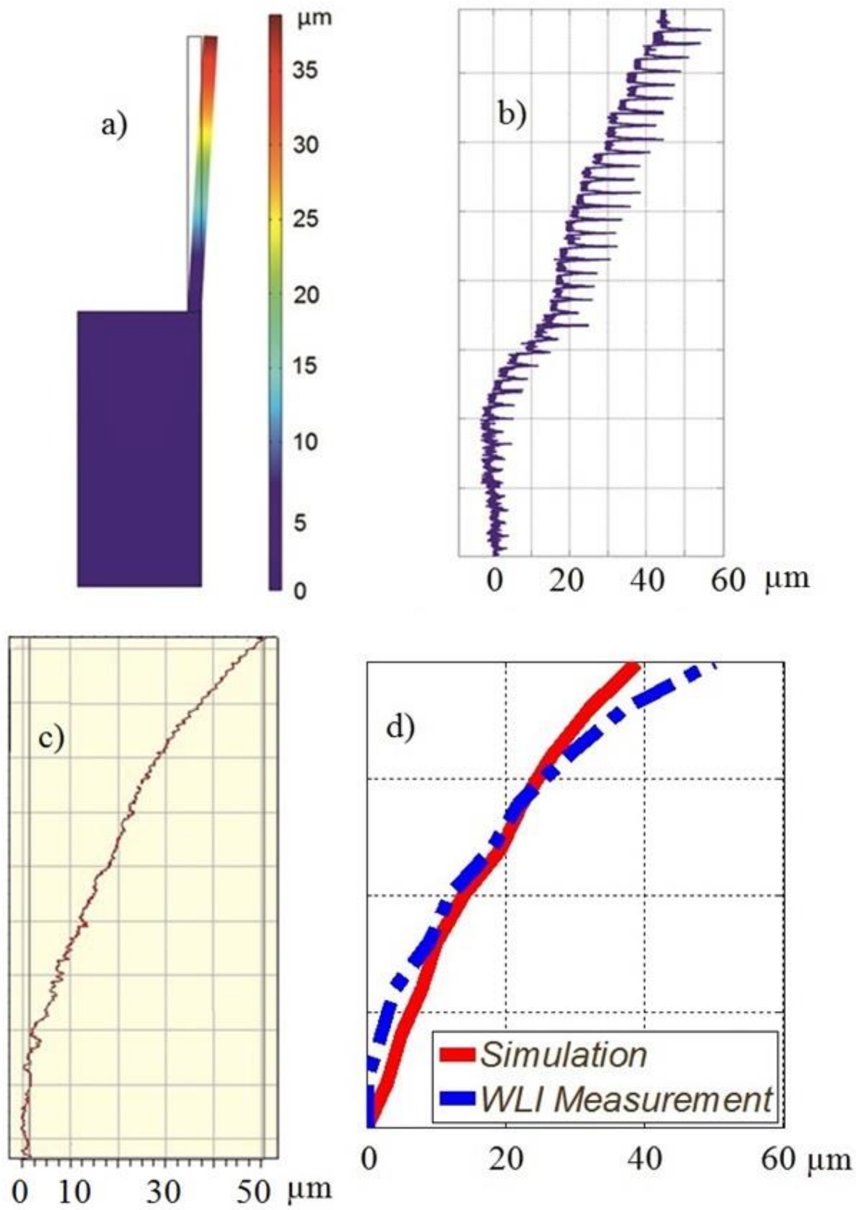

Figure 8-4 – Simulation and experimental results for Case 2: a) FEM distortion simulation, b) Laser distortion measurement, c) WLI distortion measurement, d) Comparison of simulation and WLI distortion measurement.

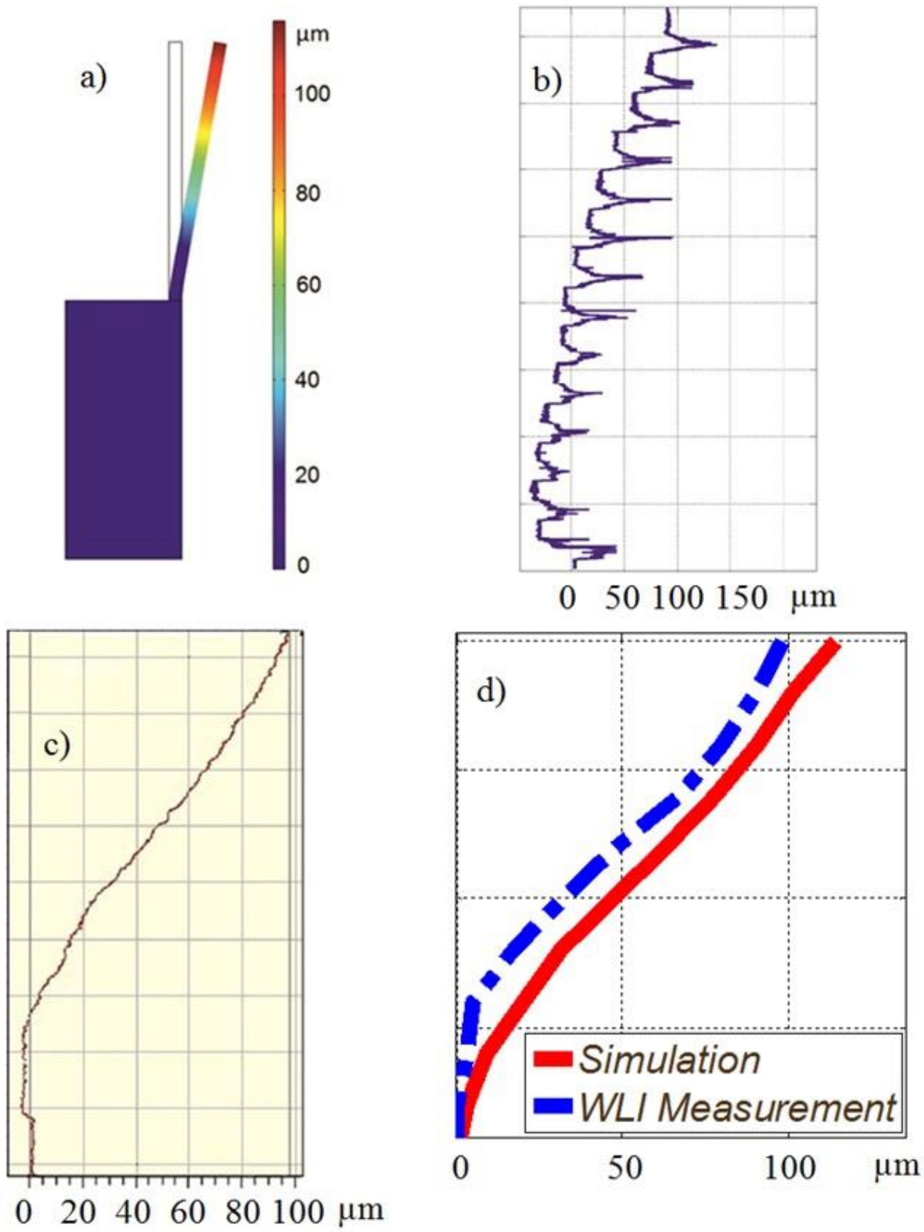

Figure 8-5 – Simulation and experimental results for Case 5: a) FEM distortion simulation, b) Laser distortion measurement, c) WLI distortion measurement, d) Comparison of simulation and WLI distortion measurement.

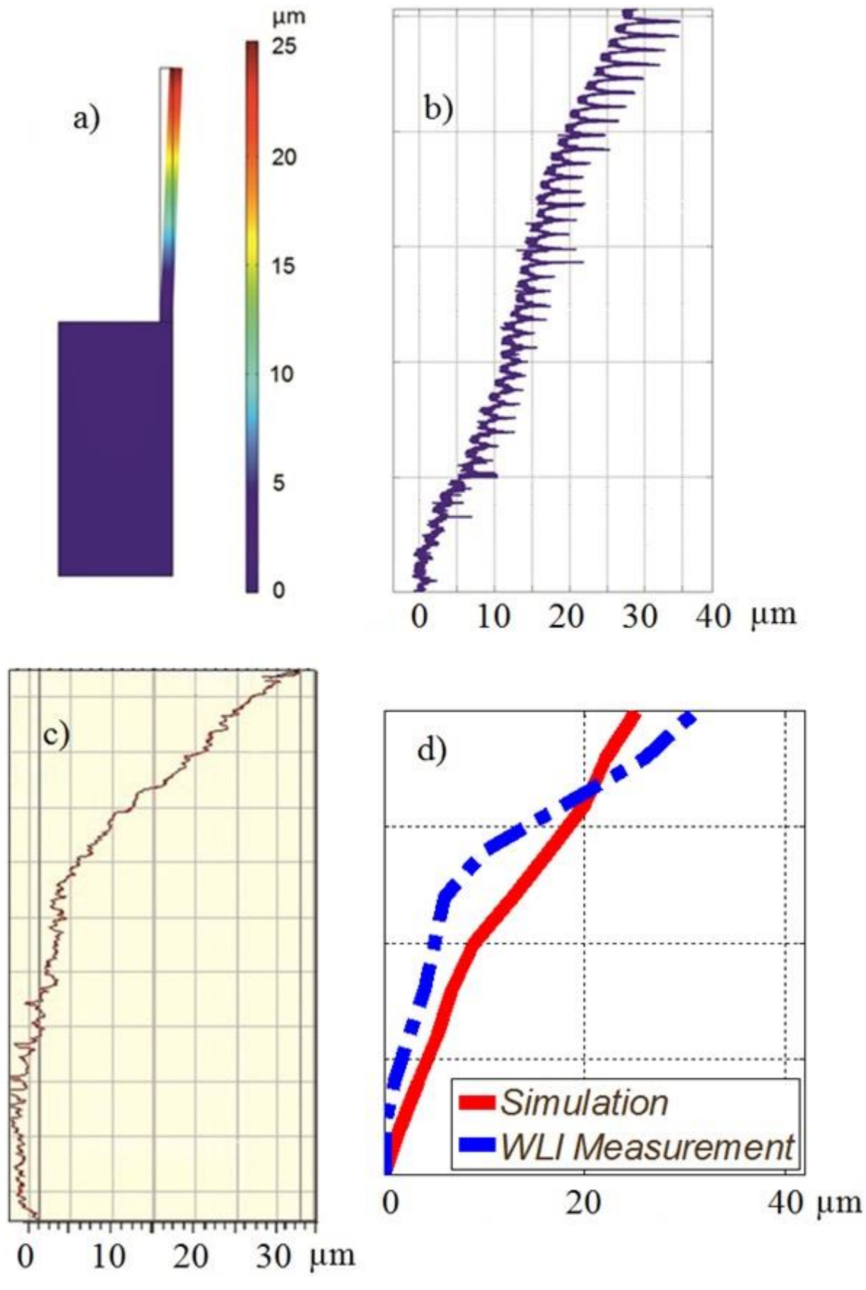

Figure 8-6 – Simulation and experimental results for Case 7: a) FEM distortion simulation, b) Laser distortion measurement, c) WLI distortion measurement, d) Comparison of simulation and WLI distortion measurement.

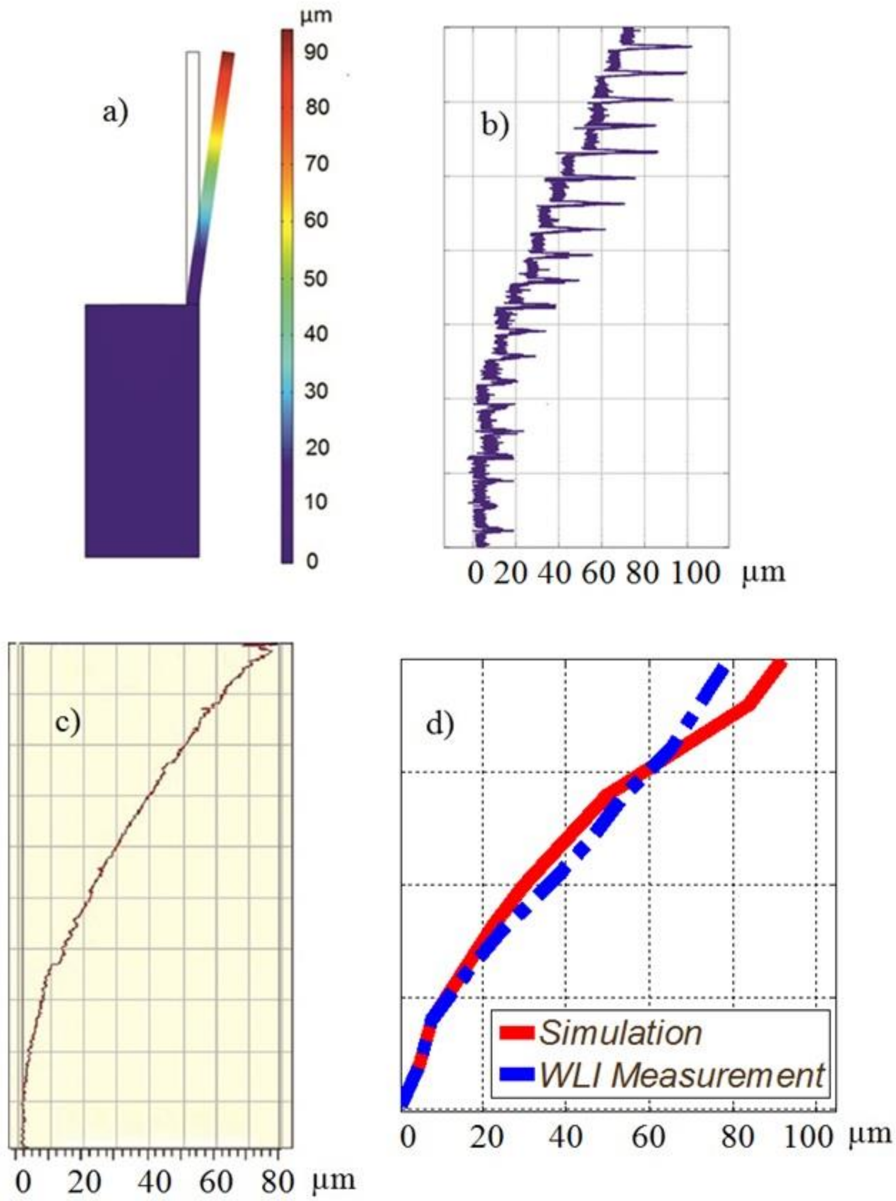

Figure 8-7 – Simulation and experimental results for Case 10: a) FEM distortion simulation, b) Laser distortion measurement, c) WLI distortion measurement, d) Comparison of simulation and WLI distortion measurement.

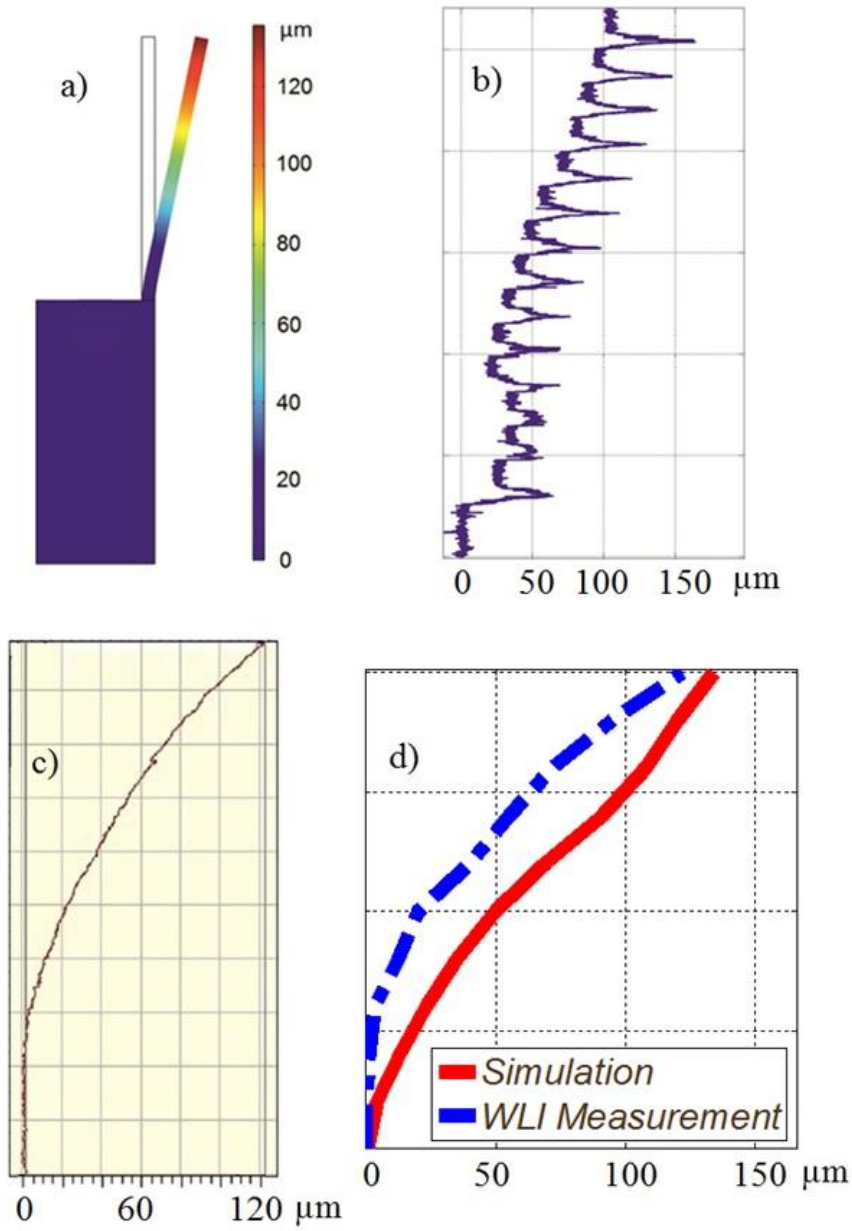

Figure 8-8 – Simulation and experimental results for Case 12: a) FEM distortion simulation, b) Laser distortion measurement, c) WLI distortion measurement, d) Comparison of simulation and WLI distortion measurement.

Table 8-3 – Experimental and simulation results

	Simulated Distortion [μm]	WLI Measured Distortion [μm]	Laser Measured Distortion [μm]
Case 1	22.2	29	27
Case 2	38.7	50	45
Case 3	48.8	58	55
Case 4	76.1	79	73
Case 5	115.2	97	95
Case 6	155.1	135	130
Case 7	25.2	32	28
Case 8	43.8	44	36
Case 9	56.6	68	62
Case 10	92.3	79	76
Case 11	104.6	100	93
Case 12	134.9	122	114

From Figure 8-4 – Figure 8-8 it is seen that the both experimental validations: laser measurement and WLI measurement give approximately the same result. From online laser measurements, it is also seen that during machining process thin wall undergoes elastic deformation, which are represented by peaks on the laser measurement data. A number of peaks is exactly equal to a number of cuts for each case. The FFT of the signal also showed that peaks occurred at tool passing frequencies, which means that they occurred due to forced vibration and stand for elastic deformation of the thin wall during machining. The results showed that both temperature and cutting force have a direct influence on the amount of deformation.

From the simulation and experimental results, it is observed that amount of distortions increases with increasing force and temperature generated during the micro milling process. The simulated distortions of the workpiece are estimated with less than 20% difference. Considering complexities of micro milling process from Figure 8-9 it is seen that simulated distortions of the thin wall are in a good agreement with experimental results.

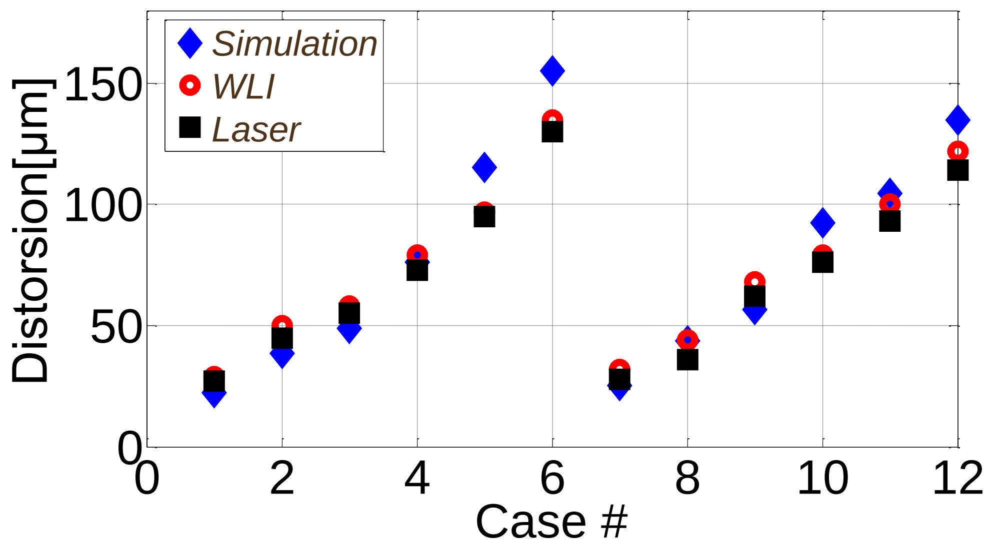

Figure 8-9 – Simulation results and experimentally measured distortions

8.4 Summary

This chapter presents an investigation of micro milling induced distortions of titanium workpiece, relating them to thermal and mechanical loads. The distortion and dimensional instability in machined parts is a function of the residual stresses, which are strongly related to the thermal and mechanical loads induced by manufacturing processes. Before machining, the workpiece has internal stress balance, this balance is formed during material production processes. During machining, a portion of the workpiece is removed and an imbalance in internal stresses occurs. Thus, the part deforms to maintain an internal stress balance. The developed model employed a finite element modeling approach to estimate distortions of the thin wall. Temperature and cutting force calculated by previously developed thermal and mechanical models of micro milling are used as an input for presented model. The combined effect of the temperature and cutting forces is applied to the thin wall and the distortions formed on the Titanium workpiece are estimated. Thin wall is machined in several paths. Each process step affects the initial stress state of the following process step. The simulation results are validated by an online laser measurement setup and later by White Light Interferometer measurements. Results showed that distortions estimated by the presented model are predicted with maximum 20% difference for validated cases and are in a good agreement with experimental results.

BIBLIOGRAPHY

[1] Altintas Y, Kersting P, Biermann D, Budak E, Denkena B, Lazoglu I. (2014),"Virtual process systems for part machining operations", *CIRP Annals - Manufacturing Technology*, 63, 585–605.

[2] Martellotti M. (1941),"An Analysis of Milling Process", *ASME Journal of Manufacturing Science and Engineering*, 63, 677–700.

[3] Bao W. (2000),"Modeling micro-end-milling operations. Part I: analytical cutting force model", *International Journal of Machine Tools and Manufacture*, 40, 2155–73.

[4] Bao WY, Tansel IN. (2000),"Modeling micro end milling operations . Part II : Tool run-out", *International Journal of Machine Tools and Manufacture*, 40, 2175–92.

[5] Li HZ, Liu K, Li XP. (2001),"A new method for determining the undeformed chip thickness in milling", *Journal of Materials Processing Technology*, 113, 378–84.

[6] Li XP, Li HZ. (2004),"Theoretical modelling of cutting forces in helical end milling with cutter runout", *International Journal of Mechanical Sciences*, 46, 1399–414.

[7] Kang YH, Zheng CM. (2013),"Mathematical modelling of chip thickness in micro-end- milling: A Fourier modelling", *Applied Mathematical Modelling*, 37, 4208–23.

[8] Kim J-D, Kim DS. (1995),"Theoretical analysis of micro-cutting characteristics in ultra-precision machining", *Journal of Materials Processing Technology*, 49, 387–98.

[9] Jin X, Altintas Y. (2012),"Prediction of micro-milling forces with finite element method", *Journal of Materials Processing Technology*, 212, 542–52.

[10] Malekian M, Park SS, Jun MBG. (2009),"Modeling of dynamic micro-milling cutting forces", *International Journal of Machine Tools & Manufacture*, 49, 586–98.

[11] Wang J, Zheng CM. (2002),"An analytical force model with shearing and ploughing mechanisms for end milling", *International Journal of Machine Tools and Manufacture*, 42, 761–71.

[12] Lucca D, Seo Y, Komanduri R. (1993),"Effect of Tool Edge Geometry on Energy Dissipation in Ultraprecision Machining", *CIRP Annals - Manufacturing Technology*, 42, 83–6.

[13] Vogler M, Kapoor S, DeVor R. (2004),"On the Modeling and Analysis of Machining Performance in Micro-End milling, Part II: Cutting Force Prediction", *Trans ASME Journal of Manufacturing Science and Engineering*, 126, 695–705.

[14] Liu K, Li XP, Rahman M. (2003),"Characteristics of high speed micro-cutting of tungsten carbide", *Journal of Materials Processing Technology*, 140, 352–7.

[15] Son SM, Lim HS, Ahn JH. (2005),"Effects of the friction coefficient on the minimum cutting thickness in micro cutting", *International Journal of Machine Tools and Manufacture*, 45, 529–35.

[16] Waldorf DJ, DeVor R, Kapoor S. (1998),"Slip-Line Field for Ploughing During Orthogonal Cutting", *Trans ASME Journal of Manufacturing Science and Engineering*, 120, 693–8.

[17] Jun MBG, Liu X, DeVor RE, Kapoor SG. (2006),"Investigation of the Dynamics of Microend Milling—Part I: Model Development", *Journal of Manufacturing Science and Engineering*, 128, 893–900.

[18] Fang N. (2003),"Slip-line modeling of machining with a rounded-edge tool—Part I: new model and theory", *Journal of the Mechanics and Physics of Solids*, 51, 715–42.

[19] Fang N, Jawahir IS. (2002),"An Analytical Predictive Model and Experimental Validation for Machining with Grooved Tools Incorporating the Effects of Strains, Strain-rates, and Temperatures", *CIRP Annals - Manufacturing Technology*, 51, 83–6.

[20] Rodríguez P, Labarga JE. (2013),"A new model for the prediction of cutting forces in micro-end-milling operations", *Journal of Materials Processing Technology*, 213, 261–8.

[21] Park SS, Malekian M. (2009),"Mechanistic modeling and accurate measurement of micro end milling forces", *CIRP Annals - Manufacturing Technology*, 58, 49–52.

[22] Jing X, Li H, Wang J, Tian Y. (2014),"Modelling the cutting forces in micro-end-milling using a hybrid approach", *The International Journal of Advanced Manufacturing Technology*, 73, 1647–56.

[23] Çelebi C, Özlü E, Budak E. (2013),"Modeling and experimental investigation of edge hone and flank contact effects in metal cutting", *Procedia CIRP*, 8, 194–9.

[24] Kim GM, Kim BH, Chu CN. (2003),"Estimation of cutter deflection and form error in ball-end milling processes", *International Journal of Machine Tools and Manufacture*, 43, 917–24.

[25] Dépincé P, Hascoët JY. (2006),"Active integration of tool deflection effects in end milling. Part 2. Compensation of tool deflection", *International Journal of Machine Tools and Manufacture*, 46, 945–56.

[26] Kaymakci M, Lazoglu I. (2008),"Tool Path Selection Strategies for Complex Sculptured Surface Machining", *Machining Science and Technology*, 12, 119–32.

[27] Larue a., Altintas Y. (2005),"Simulation of flank milling processes", *International Journal of Machine Tools and Manufacture*, 45, 549–59.

[28] Larue a., Anselmetti B. (2003),"Deviation of a machined surface in flank milling", *International Journal of Machine Tools and Manufacture*, 43, 129–38.

[29] Ryu SH, Lee HS, Chu CN. (2003),"The form error prediction in side wall machining considering tool deflection", *International Journal of Machine Tools and Manufacture*, 43, 1405–11.

[30] Ratchev S, Liu S, Huang W, Becker a. a. (2004),"Milling error prediction and compensation in machining of low-rigidity parts", *International Journal of Machine Tools and Manufacture*, 44, 1629–41.

[31] Rao VS, Rao PVM. (2006),"Tool deflection compensation in peripheral milling of curved geometries", *International Journal of Machine Tools and Manufacture*, 46, 2036–43.

[32] Zeroudi N, Fontaine M. (2015),"Prediction of tool deflection and tool path compensation in ball-end milling", *Journal of Intelligent Manufacturing*, 26, 425–45.

[33] Rodríguez P, Labarga JE. (2014),"Tool deflection model for micromilling processes", *The International Journal of Advanced Manufacturing Technology*, 76, 199–207.

[34] Lekkala R, Bajpai V, Singh RK, Joshi SS. (2011),"Characterization and modeling of burr formation in micro-end milling", *Precision Engineering*, 35, 625–37.

[35] Aurich JC, Dornfeld D, Arrazola PJ, Franke V, Leitz L, Min S. (2009),"Burrs—Analysis, control and removal", *CIRP Annals - Manufacturing Technology*, 58, 519–42.

[36] Piquard R, D’Acunto a., Laheurte P, Dudzinski D. (2014),"Micro-end milling of NiTi biomedical alloys, burr formation and phase transformation", *Precision Engineering*, 38, 356–64.

[37] Merdol SD, Altintas Y. (2008),"Virtual cutting and optimization of three-axis milling processes", *International Journal of Machine Tools and Manufacture*, 48, 1063–71.

[38] Erdim H, Lazoglu I, Ozturk B. (2006),"Feedrate scheduling strategies for free-form surfaces", *International Journal of Machine Tools and Manufacture*, 46, 747–57.

[39] Ko JH, Cho D-W. (2004),"Feed rate scheduling model considering transverse rupture strength of a tool for 3D ball-end milling", *International Journal of Machine Tools and Manufacture*, 44, 1047–59.

[40] Layegh K. SE, Erdim H, Lazoglu I. (2012),"Offline Force Control and Feedrate Scheduling for Complex Free Form Surfaces in 5-Axis Milling", *Procedia CIRP*, 1, 96–101.

[41] Altintas Y, Erkorkmaz K. (2003),"Feedrate Optimization for Spline Interpolation In High Speed Machine Tools", *CIRP Annals - Manufacturing Technology*, 52, 297–302.

[42] Sun Y, Jia Z, Ren F, Guo D. (2008),"Adaptive feedrate scheduling for NC machining along curvilinear paths with improved kinematic and geometric properties", *International Journal of Advanced Manufacturing Technology*, 36, 60–8.

[43] Erkorkmaz K, Layegh SE, Lazoglu I, Erdim H. (2013),"Feedrate optimization for freeform milling considering constraints from the feed drive system and process mechanics", *CIRP Annals - Manufacturing Technology*, 62, 395–8.

[44] Komanduri R, Hou ZB. (2001),"Thermal modeling of the metal cutting process Part III : temperature rise distribution due to the combined effects of shear plane heat source and the tool chip interface frictional heat source", *International Journal of Mechanical Sciences*, 43, 89–107.

[45] Molinari A, Moufki A. (2005),"A new thermomechanical model of cutting applied to turning operations. Part I. Theory", *International Journal of Machine Tools and Manufacture*, 45, 166–80.

[46] Lazoglu I, Altintas Y. (2002),"Prediction of tool and chip temperature in continuous and interrupted machining", *International Journal of Machine Tools and Manufacture*, 42, 1011–22.

[47] Ulutan D, Lazoglu I, Dinc C. (2009),"Three-dimensional temperature predictions in machining processes using finite difference method", *Journal of Materials Processing Technology*, 209, 1111–21.

[48] Lazoglu I, Islam C. (2012),"Modeling of 3D temperature fields for oblique machining", *CIRP Annals - Manufacturing Technology*, 61, 127–30.

[49] Lazoglu I, Bugdayci B. (2014),"Thermal modelling of end milling", *CIRP Annals - Manufacturing Technology*, 63, 113–6.

[50] Lin S, Peng F, Wen J, Liu Y, Yan R. (2013),"An investigation of workpiece temperature variation in end milling considering flank rubbing effect", *International Journal of Machine Tools and Manufacture*, 73, 71–86.

[51] Yang K, Liang Y, Zheng K, Bai Q, Chen W. (2010),"Tool edge radius effect on cutting temperature in micro-end-milling process", *The International Journal of Advanced Manufacturing Technology*, 52, 905–12.

[52] Richardson DJ, Keavey MA, Dailami F. (2006),"Modelling of cutting induced workpiece temperatures for dry milling", *International Journal of Machine Tools and Manufacture*, 46, 1139–45.

[53] Wissmiller DL, Pfefferkorn FE. (2009),"Micro end mill tool temperature measurement and prediction", *Journal of Manufacturing Processes*, 11, 45–53.

[54] Ozel T, Thepsonthi T, Ulutan D, Kaftanoglu B. (2011),"Experiments and finite element simulations on micro-milling of Ti–6Al–4V alloy with uncoated and CBN coated micro-tools", *CIRP Annals - Manufacturing Technology*, 60, 85–8.

[55] Chen G, Ren C, Zhang P, Cui K, Li Y. (2013),"Measurement and finite element simulation of micro-cutting temperatures of tool tip and workpiece", *International Journal of Machine Tools and Manufacture*, 75, 16–26.

[56] Pittalà GM, Monno M. (2011),"A new approach to the prediction of temperature of the workpiece of face milling operations of Ti-6Al-4V", *Applied Thermal Engineering*, 31, 173–80.

[57] Molinari A, Cheriguene R, Miguelez H. (2012),"Contact variables and thermal effects at the tool–chip interface in orthogonal cutting", *International Journal of Solids and Structures*, 49, 3774–96.

[58] Kim K, Lee W, Sin H. (1999),"A finite element analysis for the characteristics of temperature and stress in micro-machining considering the size effect", *International Journal of Machine Tools & Manufacture*, 39, 1507–24.

[59] Islam C, Lazoglu I, Altintas Y. (2016),"A Three-Dimensional Transient Thermal Model for Machining", *American Society of Mechanical Engineers (ASME), Journal of Manufacturing Science and Engineering*, 138, 021003–1/021003–17.

[60] Jawahir IS, Brinksmeier E, M'Saoubi R, Aspinwall DK, Outeiro JC, Meyer D, Umbrello D, Jayal AD. (2011),"Surface integrity in material removal processes: Recent advances", *CIRP Annals - Manufacturing Technology*, 60, 603–26.

[61] Denkena B, Boehnke D, León L. (2008),"Machining induced residual stress in structural aluminum parts", *Production Engineering*, 2, 247–53.

[62] Lazoglu I, Ulutan D, Alaca BE, Engin S, Kaftanoglu B. (2008),"An enhanced analytical model for residual stress prediction in machining", *CIRP Annals - Manufacturing Technology*, 57, 81–4.

[63] Arrazola P, Kortabarria A, Madariaga A, Esnaola J, Fernandez E, Cappellini C, Ulutan D, Özel T. (2014),"On the machining induced residual stresses in IN718 nickel-based alloy: Experiments and predictions with finite element simulation", *Simulation Modelling Practice and Theory*, 41, 87–103.

[64] Smith S, Dvorak D. (1998),"Tool path strategies for high speed milling aluminum workpieces with thin webs", *Mechatronics*, 8, 291–300.

[65] Wang J, Ibaraki S, Matsubara A, Shida K, Yamada T. (2015),"FEM-Based Simulation for Workpiece Deformation in Thin-Wall Milling", *International Journal of Automation Technology*, 9, 122–8.

[66] Schulze V, Arrazola P, Zanger F, Osterried J. (2013),"Simulation of distortion due to machining of thin-walled components", *Procedia CIRP*, 8, 45–50.

[67] Altintas Y. (2012),"Manufacturing Automation, Metal Cutting Mechanics, Machine Tool Vibrations and CNC Design", *Cambridge University Press*, 2nd edition.

[68] Kline W, DeVor RE. (1983),"The effect of runout on cutting geometry and forces in end milling.", *International Journal of Machine Tool Design and Research*, 23, 123–40.

[69] Yigit I, Layegh K. SE, Lazoglu I. (2015),"A solid modeler based engagement model for 5-axis ball end milling", *15th CIRP Conference on Modeling of Machining Operations Accepted for publication*,

[70] Ozerdem B. (2000),"Measurement of convective heat transfer coefficient for a horizontal cylinder rotating in quiescent air", *International Communications in Heat and Mass Transfer*, 27, 389–95.

[71] Ziaja W. (2009),"Finite element modelling of the fracture behaviour of surface treated Ti-6Al-4V alloy", *Computational Materials Science and Surface Engineering*, 1, 53–60.